THE PROCEEDINGS OF THE PHYSICAL SOCIETY

Section A

VOL. 65, PART 2 1 February 1952 No. 386 A

Einstein's Unified Field Theory

BY BEHRAM KURŞUNOĞLU
Fitzwilliam House, Cambridge

Communicated by J. Hamilton; *MS. received* 4*th May* 1951, *and in amended form* 2*nd October* 1951

ABSTRACT. In this paper it is shown that, under certain assumptions about the metric of the space-time, energy momentum tensor of the total field, when Einstein's field equations are satisfied, vanishes identically.

A new version of the unified field theory is suggested, and it is indicated briefly that a genuine energy momentum tensor exists which is conserved and has a structure similar to that of general relativity.

From the form of the energy momentum tensor and from the field equations of the proposed theory it is concluded that the law of force for a charged mass particle moving in a gravitational and electromagnetic field would have the expected form.

In his recent letter Infeld (1950) states that Einstein's theory (1950 a) gives no interaction of a moving charged mass particle with the electromagnetic field. It seems that Infeld's assumptions about the identification of symmetric and antisymmetric parts $a_{\alpha\beta}$ and $\phi_{\alpha\beta}$ of the field variables $g_{\alpha\beta}$ with the gravitational and electromagnetic fields, respectively, cannot be true even at sufficiently large distances from the centre of the particle. In a unified field theory matter is accounted for by an electromagnetic field, therefore it is necessary first to define a metric that represents space–time structure. Once a metric is obtained, one finds the matter tensor that corresponds to this metric which follows from the Hamiltonian derivatives of the Lagrangian with respect to the metric. This is the usual procedure adopted in all classical field theories (Maxwell's classical electrodynamics, Born–Infeld electrodynamics (1934), general relativity).

Thus, if $m_{\alpha\beta}$ is the metric of the space–time, then the matter tensor is given by

$$-\mathfrak{T}^{\alpha\beta}=\frac{\partial\mathfrak{L}}{\partial m_{\alpha\beta}}-\frac{\partial}{\partial x^{\gamma}}\frac{\partial\mathfrak{L}}{\partial m_{\alpha\beta,\gamma}}. \qquad \ldots\ldots(1)$$

In Einstein's theory there is no obvious way for the choice of a metric; at least in its present form it does not render itself to such a treatment. But one is inclined, in comparison with the matter tensor and the metric of general relativity, to choose $b^{\alpha\beta}=\mathfrak{g}^{\underline{\alpha\beta}}/\surd(-\mathrm{Det}\,\mathfrak{g}^{\underline{\alpha\beta}})$, to represent the required metric. If this is granted, then, by taking the non-invariant form of the Lagrangian (Schrödinger 1948) of the total field, i.e. $\mathfrak{R}=\mathfrak{g}^{\alpha\beta}\mathfrak{R}_{\alpha\beta}$ where $\mathfrak{R}_{\alpha\beta}=\Gamma^{\gamma}_{\alpha\beta}\Gamma^{\nu}_{\underline{\gamma\nu}}-\Gamma^{\mu}_{\alpha\nu}\Gamma^{\nu}_{\mu\beta}$, it can easily be shown that

$$\delta\mathfrak{R}=-\mathfrak{R}_{\alpha\beta}\delta\mathfrak{g}^{\alpha\beta}+\mathfrak{R}^{\gamma}_{\alpha\beta}\delta\mathfrak{g}^{\alpha\beta}_{\ \ ,\gamma}, \qquad \ldots\ldots(2)$$

where $\mathfrak{R}^{\gamma}_{\alpha\beta}=\Gamma^{\ \gamma}_{\alpha\beta}-\delta^{\gamma}_{\beta}\Gamma^{\nu}_{\underline{\alpha\nu}}$.

From (2) it follows that

$$\mathfrak{T}^{\varrho\sigma}=\frac{\partial\mathfrak{B}}{\partial b_{\varrho\sigma}}-\frac{\partial}{\partial x^{\gamma}}\frac{\partial\mathfrak{B}}{\partial b_{\varrho\sigma,\gamma}}=-\tfrac{1}{2}\sqrt{(-b)}(b^{\alpha\varrho}b^{\beta\sigma}+b^{\beta\varrho}b^{\alpha\sigma}-b^{\varrho\sigma}b^{\alpha\beta})R_{\underline{\alpha\beta}}+\tfrac{1}{4}b^{\varrho\sigma}\mathfrak{g}^{\underset{\vee}{\alpha\beta}}R_{\underset{\vee}{\alpha\beta}} \qquad \ldots\ldots(3)$$

where $b_{\alpha\mu}b^{\alpha\nu}=\delta^{\nu}_{\mu}$ and $\mathrm{Det}|b_{\alpha\beta}|=b=\mathrm{Det}|\mathfrak{g}^{\underline{\alpha\beta}}|$.

On raising the indices of $R_{\underline{\alpha\beta}}$ by $b^{\alpha\beta}$, (3) may be written as

$$\mathfrak{T}^{\varrho\sigma}=-\sqrt{(-b)}(R^{\underline{\varrho\sigma}}-\tfrac{1}{2}b^{\varrho\sigma}b^{\mu\nu}R_{\underline{\mu\nu}})+\tfrac{1}{4}b^{\varrho\sigma}\mathfrak{g}^{\alpha\beta}R_{\underset{\vee}{\alpha\beta}}. \qquad \ldots\ldots(4)$$

Now, when the field equations $R_{\alpha\beta}=0$ are used in (3) we obtain

$$\mathfrak{T}^{\varrho\sigma}\equiv 0. \qquad \ldots\ldots(5)$$

From (4) it is obvious that what vanishes identically is the matter tensor of the field. If we were to look for the conservation laws (Schrödinger 1948) of the total field the result comes out to be

$$\tfrac{1}{2}(\mathfrak{B}\delta^{\mu}_{\nu}-\mathfrak{g}^{\varrho\sigma}{}_{,\nu}\mathfrak{B}^{\mu}_{\varrho\sigma})_{,\nu}=0. \qquad \ldots\ldots(6)$$

Thus the conservation of energy-momentum for the field is expressed only in terms of a pseudo quantity, and it does not contain a tensor term. On the other hand, it is an experimental fact that energy and momentum are not pseudo quantities, and (6) is not an acceptable representation of matter. Therefore we may safely state that the actual energy momentum tensor is a missing one in Einstein's theory. A similar result as in (3) follows, when one assumes $a_{\alpha\beta}$ to be the metric of the space–time as was done by Infeld.

The above results indicate in a simple manner that a genuine energy-momentum tensor does not exist corresponding to the metrics $b_{\alpha\beta}$ and $a_{\alpha\beta}$, i.e. there is no source to create these 'potentials'. Therefore it is not surprising if one does not find the expected interaction of the moving particle with the electromagnetic field. An attempt to find the equation of motion in a unified field theory with the similar method of Einstein, Infeld and Hoffman (1938), can only be made after a metric and the corresponding energy tensor are obtained. It is not sufficient to associate various field quantities in an *a priori* manner with different fields, if one is not sure of the existence of the sources that create these fields.

Now, we may draw two conclusions from the above considerations:

(i) If Einstein's theory is to be maintained, then the above assumptions which seem most natural in deriving an energy-momentum tensor for the total field have to be abandoned.

(ii) That (1) is true finds confirmation also from Infeld's result, since he assumes $a_{\alpha\beta}$, as in our second alternative, to represent the gravitational field.

A unified field theory free at least from the deficiencies indicated briefly above is in the process of publication. For the sake of comparison we give the field equations of the new theory:

$$R_{\underline{\alpha\beta}}=p^{2}(a_{\alpha\beta}-b_{\alpha\beta}) \qquad \ldots\ldots(7)$$

$$R_{\underset{\smile}{\alpha\beta},\gamma}+R_{\underset{\smile}{\beta\gamma},\alpha}+R_{\underset{\smile}{\gamma\alpha},\beta}=P^{2}I_{\alpha\beta\gamma} \qquad \ldots\ldots(8)$$

$$\mathfrak{g}^{\underset{+\,-}{\alpha\beta}}{}_{;\gamma}=0 \qquad \ldots\ldots(9)$$

$$\Gamma_{\alpha}=0,\quad (\mathfrak{g}^{\underset{\smile}{\alpha\beta}}{}_{,\beta}=0) \qquad \ldots\ldots(10)$$

where $I_{\alpha\beta\gamma}=\phi_{\alpha\beta,\gamma}+\phi_{\beta\gamma,\alpha}+\phi_{\gamma\alpha,\beta}$ (current density), and p has the dimension (length)$^{-1}$. The conservation laws of the total field are given by

$$\mathfrak{T}^{\beta}_{\gamma,\beta}=0, \qquad \ldots\ldots(11)$$

where

$$-\mathfrak{T}^{\beta}_{\gamma}=(\mathfrak{g}^{\underline{\alpha\beta}}R_{\underline{\alpha\gamma}}-\tfrac{1}{2}\delta^{\beta}_{\gamma}\mathfrak{g}^{\underline{\mu\nu}}R_{\mu\nu})+(\mathfrak{g}^{\underset{\smile}{\alpha\beta}}R_{\underset{\smile}{\alpha\gamma}}-\tfrac{1}{2}\delta^{\beta}_{\gamma}\mathfrak{g}^{\underset{\smile}{\mu\nu}}R_{\underset{\smile}{\mu\nu}})+\tfrac{1}{2}(\mathfrak{g}^{\varrho\sigma}{}_{,\gamma}\mathfrak{B}^{\beta}_{\varrho\sigma}-\delta^{\beta}_{\gamma}\mathfrak{B}). \qquad \ldots\ldots(12)$$

The expression (12) in the absence of the antisymmetric field reduces to the usual mixed energy tensor (pseudo + tensor density) of general relativity. When the field equations (7) are used (12) leads to

$$\begin{aligned}-\mathfrak{T}^{\beta}_{\gamma}=p^{2}[(\mathfrak{g}^{\underset{\smile}{\beta\mu}}\phi_{\gamma\mu}-\tfrac{1}{2}\delta^{\beta}_{\gamma}\mathfrak{g}^{\underset{\smile}{\mu\nu}}\phi_{\mu\nu})+\delta^{\beta}_{\gamma}\{\sqrt{(-g)}-\sqrt{(-b)}\}]\\ +(\mathfrak{g}^{\underset{\smile}{\alpha\beta}}R_{\underset{\smile}{\alpha\gamma}}-\tfrac{1}{2}\delta^{\beta}_{\gamma}\mathfrak{g}^{\underset{\smile}{\mu\nu}}R_{\underset{\smile}{\mu\nu}})+\tfrac{1}{2}(\mathfrak{g}^{\varrho\sigma}{}_{,\gamma}\mathfrak{B}^{\beta}_{\varrho\sigma}-\delta^{\beta}_{\gamma}\mathfrak{B}),\end{aligned} \qquad \ldots\ldots(13)$$

where we used the expression for $\mathfrak{g}^{\underline{\alpha\beta}}$ given as

$$\mathfrak{g}^{\underline{\alpha\beta}}=a^{\alpha\beta}\sqrt{(-g)}-\mathfrak{g}^{\underset{\smile}{\alpha\mu}}\phi^{\beta}{}_{.\mu}.$$

The expression in square brackets in (13), when the cubes of the ϕ's are neglected, becomes $\tfrac{1}{4}\delta^{\beta}_{\gamma}\phi^{\mu\nu}\phi_{\mu\nu}-\phi^{\beta\mu}\phi_{\gamma\mu}(=T^{\beta}_{\gamma}$ say). The place of the matter tensor of the general relativity is taken in this theory by an electromagnetic energy tensor. If Einstein's field equations are used in (12), then (11) reduces to (6). The right-hand side of the equations (7), with the same approximation for the ϕ's reduce to $T_{\alpha\beta}$. The fact that we have a Maxwell's energy tensor on the right-hand side of our field equations is sufficiently convincing for us to expect a correct law of force (Lorentz force) for a charged mass particle moving in a gravitational and electromagnetic field. The same was already proved by Infeld and Wallace (1940) in general relativity.

The details for the derivation of our field equations and conservation laws from the Bianchi–Einstein identities for non-symmetric field (1950 b) as well as from a variational principle with a Lagrangian $\mathfrak{L}=\mathfrak{g}^{\alpha\beta}R_{\alpha\beta}+2p^{2}[\sqrt{(-b)}-\sqrt{(-g)}]$ will appear elsewhere.

REFERENCES

Born, M., and Infeld, L., 1934, *Proc. Roy. Soc.* A, **144**, 425–451.

Einstein, A., 1950 a, *The Meaning of Relativity* (London : Methuen) ; 1950 b, *Canad. J. Math.*, **2**, 120.

Einstein, A., Infeld, L., and Hoffman, B., 1938, *Ann. Math.*, **39**, 65.

Infeld, L., 1950, *Nature, Lond.*, **166**, 1075.

Infeld, L., and Wallace, P. R., 1940, *Phys. Rev.*, **57**, 797.

Schrödinger, E., 1948, *Proc. Roy. Irish Acad.*, **52** A.I., 7.

The Two-Body Scattering Problem with Non-Central Forces I—Non-Relativistic

By G. J. KYNCH

Department of Mathematical Physics, The University, Birmingham

MS. received 6th July 1951

ABSTRACT. A perturbation theory is developed for the two-body problem so that central and non-central forces can be treated in a consistent manner. A phase matrix $S(r)$ is introduced which satisfies a first-order Riccati equation. The asymptotic value of S occurs in the formula for the cross section, and for a special choice of functions is the Heisenberg matrix of the problem. The formalism leads to a simple comparison of neutron–proton and proton–proton scattering, an analysis of the degree of separation of the simultaneous equations which occur, and of the most suitable choice of $S(r)$ for calculation.

§ 1. INTRODUCTION

The object of this paper is to expound a consistent method of treating two-body scattering problems which can be used with tensor forces as well as central forces and leads directly to the values of the phases required in the calculation of cross sections. The method is a new type of perturbation theory for degenerate states which is a generalization of a well-known equation. In the present paper we apply it to neutron–proton and proton–proton scattering with and without tensor forces; in the following paper (Kynch 1952) it is applied to the relativistic one-body and two-body problems.

The radial wave function of a particle in an S state, acted on by a central force, can be written $u=A\sin(kr+\delta)$, where A and δ are functions of r, which tend to constant values as r tends to ∞, provided the correct condition on A and δ is applied. The function can also be written $u=(u_1+u_2S)a$, where $u=\sin kr$, $u=\cos kr$ and $S=\tan\delta(r)$. Our choice of condition on A and δ is such that $dS/dr=V(r)(u_1+u_2S)^2$, where $V(r)$ is proportional to the potential. This procedure can also be carried through for other states.

To determine the scattering cross section we need the asymptotic value of $\delta=\delta(\infty)$ as $r\to\infty$. This is found by integrating the equation with the condition $S=0$ at $r=0$. The two-body problem with central forces can be dealt with in the same way.

When there are spin–orbit or tensor forces the two-body radial functions for a given total angular momentum J, M satisfy a set of three simultaneous equations. To obtain scattering cross sections it is necessary to determine the asymptotic forms of the three independent solutions of these equations. This we achieve by expressing the radial wave functions in the same form as before, where $S(r)$ is now a square matrix whose elements satisfy a set of equations similar in form to that of the single S with central forces. These equations are independent of the amplitudes $A(r)$.

As a means of calculating phases these have the advantage of being first-order equations. They readily lend themselves to approximations, and to expansions in powers of the energy. Such an expansion leads in fact to linear equations for all but the lowest order term. They also enable us to link together a number of odd results previously obtained. Thus a relation between n–p and p–p scattering with the same nuclear potential was obtained by Chew and Goldberger (1949) for S states in the approximation where the coulomb term is small near the origin. It is now seen to apply to all states, even when tensor forces are present.

Our equation can be modified so that $\delta(r)$ rather than $S=\tan\delta(r)$ is calculated. For attractive central forces it is a monotonic increasing function of r. This modification is very desirable when there are bound states, as $\delta(r)$ then passes through the value $\frac{1}{2}\pi$ and sometimes higher angles where S diverges.

Owing to the general method of approach we are able to attempt to find the best method of formulating the calculation with tensor forces in order to obtain as directly as possible the matrix needed in the scattering problem. It would seem that there is no especially favoured method when angular distributions are required.

Heisenberg (1943) has introduced into quantum mechanics a scattering matrix $S_H=e^{2i\delta}$. By a suitable choice of the free wave functions u_1 and u_2 our method gives a differential equation for a phase-matrix $S(r)$ with the property that $S_H=\lim_{r\to\infty} S(r)$. The meaning of $S(r)$ for other values of r is that it is the Heisenberg S-matrix if the potential were cut off at this distance. In fact $S(r)$ is more general than S_H since it determines the potential as well as being determined by it.

To find the energies of bound states it is possible to consider the analytical continuation of $S_H=S(\infty)$ in k-space, where k^2 is the energy. A more direct method based on our equations is to replace u_1 and u_2 by solutions for negative energies $-h_0^2$ and choose k_0 so that the wave function has the correct asymptotic behaviour. If $u_1 \sim \exp - k_0 r$ and $u_2 \sim \exp k_0 r$ then the necessary condition is $\lim_{r\to\infty} S(r) \exp 2k_0 r = 0$. This is stronger than the condition $S(\infty)=0$, which is known to be unsatisfactory. For potentials whose solutions are known analytically the method is not very good, but this might be expected from the method of splitting up the wave function.

§ 2. PERTURBATION THEORY FOR THE PHASE FUNCTION

Given two independent solutions $u_1(r)$ and $u_2(r)$ of the differential equation

$$\frac{d}{dr}\left\{p(r)\frac{du}{dr}\right\} + q(r)u = 0 \qquad \ldots\ldots(1)$$

we wish to find the asymptotic solution of the equation

$$\frac{d}{dr}\left\{p\frac{du}{dr}\right\} + qu = Vu \qquad \ldots\ldots(2)$$

which is regular at the origin, i.e. $u=0$ when $r=0$. In the applications it is also true that $\lim_{r\to\infty} rV(r) = 0$.

The required solution of eqn. (2) can be written

$$u = (u_1 + u_2 S)a, \qquad \ldots\ldots(3)$$

where the phase function $S(r)$ and the amplitude $a(r)$ both tend to constant values as $r \to \infty$.

We impose the condition

$$u_1 \frac{da}{dr} + u_2 \frac{d}{dr}(Sa) = 0 \qquad \ldots\ldots(4)$$

so that

$$\frac{du}{dr} = \left(\frac{du_1}{dr} + \frac{du_2}{dr} S\right) a \qquad \ldots\ldots(5)$$

and substitute into eqn. (2). Using eqn. (1) and the Wronskian relation deduced from it, that

$$p\left(u_1 \frac{du_2}{dr} - u_2 \frac{du_1}{dr}\right) = \alpha, \qquad \ldots\ldots(6)$$

where α is a constant, we can eliminate the derivatives of u_1, u_2 and a, leaving

$$\alpha \frac{dS}{dr} a = (u_1 + Su_2)V(u_1 + u_2 S)a. \qquad \ldots\ldots(7)$$

This equation is independent of $a(r)$, so that an equation is obtained for $S(r)$:*

$$\alpha(dS/dr) = (u_1 + Su_2)V(u_1 + u_2 S). \qquad \ldots\ldots(8)$$

This generalized Riccati-type equation for the function $S(r)$ can be solved numerically, or otherwise, and forms the basis of our subsequent discussion.

A slightly more general form for u,

$$u = (u_1 S_1 + u_2 S_2)A, \qquad \ldots\ldots(9)$$

leads to the equation

$$\alpha\left(S_1 \frac{dS_2}{dr} - S_2 \frac{dS_1}{dr}\right) = V(u_1 S_1 + u_2 S_2)^2, \qquad \ldots\ldots(10)$$

where $a = S_1 A$ and $S_2 = SS_1$.

---

* Some trivial details are included in the derivation, and the order of the symbols has been maintained, so that the same equations can be used formally to solve a set of simultaneous equations in § 5, where the symbols represent matrices.

§3. NEUTRON–PROTON SCATTERING WITH CENTRAL FORCES

The scattering is determined by the asymptotic values of the phases δ in the regular solution $u \sim \sin(kr - \frac{1}{2}L\pi + \delta)$ of the Schrödinger equation

$$\frac{d^2u}{dr^2} + \left(k^2 - \frac{L(L+1)}{r^2}\right)u = -v(r)u. \qquad \ldots\ldots(11)$$

Following the method just described, we use for u_1 and u_2 two solutions of this equation with $V(r)=0$. If we choose the solutions $u_1 = j_L(kr) \sim \sin(kr - \frac{1}{2}L\pi)$, $u_2 = n_L(kr) \sim \cos(kr - \frac{1}{2}L\pi)$, then $S(r) \to \tan\delta$ as $r \to \infty$. The equation for S is

$$k\,dS/dr = v(r)(j_L + Sn_L)^2. \qquad \ldots\ldots(12)$$

Alternatively, by writing $S = \tan\delta(r)$ (or $S_1 = \cos\delta(r)$, $S_2 = \sin\delta(r)$ in (10)), we find*

$$\left.\begin{aligned} &k\,d\delta/dr = v(j_L\cos\delta + n_L\sin\delta)^2, \\ \text{i.e.}\quad &k\delta(r) = \int_0^r v(j_L\cos\delta + n_L\sin\delta)^2 dr. \end{aligned}\right\} \qquad \ldots\ldots(13)$$

The integral form uses the result that both $S(r)$ and $\delta(r)$ are zero at the origin, and tend to zero so rapidly as to overcome the singularity in the irregular solution $n_L(kr) \propto r^{-L}$ near the origin.

Both these equations show that $\delta(r)$ and $S(r)$ are monotonic increasing functions of r. The second is more convenient for numerical work when the phase is large. For S states in particular, where there is a bound state, δ exceeds $\frac{1}{2}\pi$, so that $S(r)$ must diverge for a finite value of r. Born approximation corresponds to neglecting Sn_L in comparison with j_L.

An expansion in powers of the energy $\lambda = k^{-1}\tan\delta(r) = \lambda_0 + \lambda_1 k^2 + \lambda_2 k^4 + \ldots$ leads to the equation for λ_0, $d\lambda_0/dr = v(r)(1 + r\lambda_0)^2$. The other terms $\lambda_1, \lambda_2, \ldots$ satisfy linear first-order equations. Such an expansion is not possible if $\delta(r)$ exceeds $\frac{1}{2}\pi$ and a subterfuge is necessary, which is to write $\lambda = \tan\eta(r)$ and expand $\eta(r)$ in powers of k^2.

§4. PROTON–PROTON SCATTERING

For proton–proton scattering the wave equation with the coulomb term is

$$\frac{d^2u}{dr^2} + \left(k^2 - \frac{L(L+1)}{r^2} - \frac{2}{ra}\right)u = -Vu, \qquad \ldots\ldots(14)$$

where $a = (2\hbar/Me^2)$ is the coulomb length. In addition to the coulomb scattering, there is an anomalous scattering, due to the nuclear forces V, which is expressed in terms of an extra phase factor δ.

In applying eqn. (8) we shall treat the nuclear potential as the perturbation, and use coulomb wave functions for u_1 and u_2. If we choose for u_1 and u_2 the functions defined by Yost, Wheeler and Breit (1936)† the asymptotic form of u is given by

$$u = (G_L + SF_L)a \sim \frac{a(\infty)}{\sin\delta}\sin\{kr - \tfrac{1}{2}L\pi - \eta\log 2kr + 2\arg[\delta + \Gamma(i\eta + L + 1)]\},$$

where $ka = (1/\eta)$ and $S = \cot\delta$. $\qquad \ldots\ldots(15)$

The equation for S is similar in form to that for n–p scattering, and only involves the nuclear potential, but the functions $u_1 = G_L$ and $u_2 = F_L$ are completely different.

---

* This particular equation was derived by Dr. Krook four years ago. It has since been published by Bergmann (1950).

† In this section we use the notation of these authors.

A comparison of n–p and p–p scattering on the basis of our equation would be simpler if we could choose functions which behaved near the origin, where V is large, in much the same way as $j_L(kr)$ and $n_L(kr)$. Now there are solutions of the coulomb equation which go over to $j_L(kr)$ and $n_L(kr)$ in the absence of the coulomb force. From the equations of Yost, Wheeler and Breit (1937) we find $F_L=(2L+1)C_L{}^2\phi(kr)$; $G_L=\psi+\phi\{q-p\log 2\eta+p\log r/a\}$, where p and q are functions of k^2, and $C_L{}^2$ is defined by them. The functions ϕ and ψ can be expanded in power series $\phi=(kr)^{L+1}+$ higher powers, $\psi=(kr)^{-L}+$ higher powers. The combinations of these which we are seeking are $j_L^c=\phi/\{1.3\ldots(2L+1)\}$, $n_L^c=1.3\ldots.(2L-1)\{\psi+p\phi\log(r/a)\}$. Expressing F_L and G_L in terms of these we obtain $u=(j_L^c+n_L^c S')a'$, where

$$1/S' = 1^2.3^2\ldots(2L-1)^2(2L+1)\{(2L+1)C_L{}^2\cot\delta+q-p\log(2\eta)\}, \qquad \ldots\ldots(16)$$

so that

$$k\,dS'/dr=V(r)(j_L^c+n_L^c S')^2. \qquad \ldots\ldots(17)$$

We shall not discuss this equation in the detail in which we discussed the equations of the previous section. Everything said in the previous section applies in this section without modification.

We continue our comparison of n–p and p–p scattering by assuming that the nuclear forces are the same, as in the charge-independent hypothesis. Eqns. (17) and (12) would then differ only in the use of j_L^c and n_L^c in the former and j_L and n_L in the latter. Now these two pairs of functions have similar series expansions and behave in approximately the same way near the origin where the potential is large, so that the function $S'(\infty)$ defined here* is almost identical with $\tan\delta(\infty)$ of the n–p problem. This result was obtained by Chew and Goldberger (1949) for S states. This independent derivation shows that it applies to all states, and it is shown later to be true even when tensor forces are present.

A condition for this approximation can very simply be found, although it tends to underestimate the degree of equality. The wave equation (15) can be expressed as an equation with no coulomb term but an effective angular momentum ν where $\nu(\nu+1)=L(L+1)+2r/a$, i.e. $\nu-L=2r/(\nu+L+1)<2r/(2L+1)$. If we can neglect $d\nu/dr$ then we can replace $j_L^c(kr)$ by $j_\nu(kr)$ and $n_L^c(kr)$ by $n_\nu(kr)$ in the equation for S'. The equality of S' for p–p interaction and $\tan\delta$ for the n–p interaction then requires that $\nu-L$ is small within the range of the nuclear force, i.e. that the coulomb term can be neglected inside this range. If the range is r_0 then we require $2r_0/\{a(2L+1)\}\ll 1$. For a meson potential

$$\frac{2r_0}{a}=\frac{2\hbar}{\mu c}\frac{Me^2}{2\hbar^2}=\frac{M}{\mu}\left(\frac{e^2}{\hbar c}\right)\simeq\frac{1}{22},$$

so that this condition is quite well satisfied.

§ 5. PERTURBATION OF A SET OF SIMULTANEOUS EQUATIONS

Consider a set of n simultaneous equations of the second order for n independent functions $u_1, u_2 \ldots . u_n$, of the type

$$\frac{d}{dr}\left(p\frac{du_i}{dr}\right)+q_i u_i=\sum_j V_{ij}u_j \qquad (i=1, 2, \ldots . n) \qquad \ldots\ldots(18)$$

such that $u_i=0$ $(i=1, 2, \ldots . n)$ when $r=0$. Any solution can be expressed as a linear combination of n independent solutions.

---

* The function S' was first introduced by Landau and Smorodinski (1944).

Let $(u_1)_i$ and $(u_2)_i$ be distinct solutions of the ith equation, when all $V_{ij}=0$. Then we shall show that any solution $u(r)$ of eqn. (18) can be written

$$u_i=\{(u_1)_i+\Sigma_j(u_2)_jS_{ji}(r)\}a_i(r), \qquad \ldots\ldots(19)$$

where the functions $S_{ij}(r)$ are independent of the particular solution chosen.

It is convenient to use a matrix notation. The solution $u_i(r)$ and $a_i(r)$ are written as $(n\times 1)$ column matrices; the $(u_1)_i$, $(u_2)_i$ and also the q_i in (18) as the diagonal elements of a square $(n\times n)$ matrix; and V_{ij} and S_{ij} as square matrices. Equations (18) and (19) then become elements of the matrix equation

$$\frac{d}{dr}\left(p\frac{du}{dr}\right)+qu=Vu \qquad \ldots\ldots(20)$$

and $u=(u_1+u_2S)a$. These are similar in form to eqns. (2) and (3), and to prove our statement (19) we carry through formally the process described in §2. All the equations (3)–(9) still apply, provided the quantities in them are regarded as matrix quantities. As already noted, the order of the terms in these equations has been maintained throughout. Eqn. (9) is

$$\alpha a\, dS/dr=(u_1+Su_2)V(u_1+u_2S)a. \qquad \ldots\ldots(21)$$

We now assert that this equation is independent of the functions $a(r)$, so that S is determined by the matrix equation

$$\alpha\, dS/dr=(u_1+Su_2)V(u_1+u_2S), \qquad \ldots\ldots(22)$$

which is identical in form to eqn. (10).

The proof of this is simple. We assume real solutions. Since the system of equations (18) is self-adjoint, it follows that S is symmetric,

$$S'=S, \qquad \ldots\ldots(23)$$

where $S'_{ij}=S_{ji}$ is the transpose of S. Thus S contains $\frac{1}{2}n(n+1)$ independent functions. Assuming that u satisfies eqns. (20), it is possible to impose $\frac{1}{2}n(n+1)$ conditions upon these functions, provided that they are self-consistent and consistent with eqns. (20). Now it is clear that eqns. (21) impose just this number of conditions upon $S(r)$ and that these are consistent with the original equations on account of the method of derivation. Hence the transition from (9) to (23) is justified.

This result is particularly relevant to the scattering problem where the asymptotic values of $a(r)$ are given by the problem.

Before we apply the analysis to nuclear problems we shall discuss some alternatives. The first is that a more convenient form can sometimes be obtained by the substitutions $a=S_1A$ and $S_2=SS_1$ so that $u=(u_1S_1+u_2S_2)a$ by choosing S_1 suitably. The second is that u_1 and u_2 need not be real, and they can be chosen so that S is unitary. This point is discussed in §7.

Amongst the remaining variations the most promising seems to be one which tries to diagonalize $V(r)$, as this may diagonalize S. To do this we suggest a new trial wave function $u=U(r)(u_1+u_2S)a$, where $U(r)$ is an orthogonal matrix, and a supplementary condition so that $du/dr=U(r)(du_1/dr+Sdu_2/dr)a$. The resulting equation for S is

$$\alpha\frac{dS}{dr}=(u_1+Su_2)[U^{-1}(V-q)U+q](u_1+u_2S)+pK, \qquad \ldots\ldots(24)$$

where $K=(u_1'+Su_2')(U^{-1}\,dU/dr)(u_1+u_2S)-(u_1+Su_2)(U^{-1}\,dU/dr)(u_1'+u_2'S)$.

The matrix q is already diagonal; so our aim of a diagonal S is completely achieved only if $U^{-1}(V-q)U$ and K are diagonal, and this is not possible. Moreover, to achieve any simplification we need, $K=0$ or $U=\text{constant}$. Now a constant matrix U other than unity does not commute with q unless q has a special form, so that U can at best be chosen to reduce the off-diagonal elements of V. This can be completely done if all the elements of V depend on r in the same way.

§ 6. SCATTERING WITH TENSOR FORCES

To show the relevance of § 5 to scattering problems we apply it first to the wave equation and then show that $\lim_{r\to\infty} S(r)$ is in fact needed to calculate the scattering. As these equations have been discussed many times in the literature we do not give all the details, but merely give the essential steps in a suitable form.

Non-central forces affect the triplet, but not the singlet, state of a two-nucleon problem. Triplet states of given total angular momentum J, M are derived from orbital angular momenta $L=J, J\pm 1$. With non-central forces the last two are coupled. For an attractive potential

$$V=v_1(r)-2(\mathbf{L}\,.\,\mathbf{S})v_2(r)+\{3(\sigma_1.r)(\sigma_2.r)/r_2-\sigma_1.\sigma_2\}v_3(r);$$

the wave functions are of the form

$$\psi_{JM}=\sum_{L=J-1}^{J+1}\frac{1}{kr}u^L_{JM}(kr)f^L_{JM} \qquad \ldots\ldots(25)$$

where $f^L_{JM}=\Sigma^{+1}_{m=-1}c^{Lm}_{JM}Y_{L,\,M-m}\chi_m$ are the appropriate spin–orbit functions (cf. Rosenfeld 1948). The radial wave functions u^L satisfy the equations

$$\frac{d^2u^{J-1}}{dr^2}+\left(k^2-\frac{J(J-1)}{r^2}\right)u^{J-1}$$
$$=-\left\{v_1-2(J-1)\left(v_2+\frac{v_3}{2J+1}\right)\right\}u^{J-1}+\frac{6\{J(J+1)\}^{1/2}}{2J+1}v_3u^{J+1}$$
$$\frac{d^2u^J}{dr^2}+\left(k^2-\frac{J(J+1)}{r^2}\right)u^J=-\{v_1+2(v_2+v_3)\}u^J$$
$$\frac{d^2u^{J+1}}{dr^2}+\left(k^2-\frac{(J+1)(J+2)}{r^2}\right)u^{J+1}$$
$$=-\left\{v_1+2(J+2)\left(v_2-\frac{v_3}{2J+1}\right)\right\}u^{J+1}+\frac{6\{J(J+1)\}^{1/2}}{2J+1}v_3u^{J+1}$$

In scattering problems we start with waves of given L and M, so that it is convenient to treat these three equations together. Comparing them with the equations in the previous section we see that $S^{(J)}_{LL'}$ is a 3×3 matrix with only off-diagonal elements connecting $L=J\pm 1$. The equations for $S^{(J)}$ are (22) with the appropriate potentials, which we do not write in full. There is a single equation for S_{JJ} and three simultaneous equations for $S_{J-1,\,J-1}$, $S_{J+1,\,J+1}$, $S_{J-1,\,J+1}$.

The scattering for given M is described by an incoming plane wave $e^{ikz}\chi_M$ and a scattered wave ψ_{sc}, which have both to be expanded in terms of the spin–orbit functions. If the scattered wave is $\psi_{sc}\sim kr^{-1}e^{ikr}\,\Sigma_{J,\,L}\,d^L_{JM}f^L_{JM}$, then the solutions for the radial wave functions have the asymptotic form

$$u^L_{JM}\sim(i)^L\{4\pi(2L+1)\}^{1/2}c^{LM}_{JM}\sin\left(kr-\tfrac{1}{2}L\pi\right)+d^L_{JM}e^{ikr}.$$

Now suppose we choose u_1 and u_2 in the equations (22) so that the assumed solution and its asymptotic form are*

$$u=(u_1+u_2T)a\sim\{(i)^L \sin(kr-\tfrac{1}{2}L\pi)a_L+e^{ikr}T_{LL'}a_{L'}\},$$

then clearly the matrices $a(\infty)$ and $T(\infty)$ are such that

$$d^L_{JM}=\sum_{L'=J-1}^{J+1} T_{LL'}a_{L'},\quad a_L=c^{LM}_{JM}\{4\pi(2L+1)\}^{1/2}=\alpha^L_{JM}.$$

Thus $a(\infty)$ is known and ψ_{sc} is determined by $T(\infty)$. The scattering cross sections are given by

$$k^2d\sigma_M=d\Omega\sum_{\text{spins}}\Big|\sum_{J,L} d^L_{JM}f^L_{JM}\Big|^2=d\Omega\sum_{|m|<1}\Big|\sum_{J,L,L'} Y_{L,M-m}c^{Lm}_{JM}T^{(J)}_{LL'}c^{L'M}_{JM}\{4\pi(2L'+1)\}^{1/2}\Big|^2$$

and

$$k^2\sigma_M=\sum_J|d^L_{JM}|^2=\sum_{J,L',L'',L}\alpha^{L'*}_{JM}T^{J*}_{LL'}T^J_{LL''}\alpha^{L''}_{JM}=\sum_{J,L',L''}-\tfrac{1}{2}i\alpha^{L'}_{JM}(T-T^*)^J_{L'L''}\alpha^{L''}_{JM}$$

since $S_0=1+2iT$ is unitary and symmetric. On averaging over M this can be reduced further to $k^2\bar{\sigma}=\frac{1}{3}k^2\Sigma\sigma_M=\Sigma_J\frac{4}{3}\pi(2J+1)\mathrm{Sp}\{-\frac{1}{2}i(T-T^*)\}$. For central forces all these results reduce to the usual forms.

The expression for the angular distribution can be reduced on averaging over M, using relationships between the Wigner coefficients c^{Lm}_{JM}; without tensor forces T is diagonal and the reduction has been made by Case and Pais (1950) using projection operators. Apart from this reduction it is clearly useful to be able to express T or S_0 as the transform of a diagonal matrix, especially as the total cross section depends only on Spur T, which is invariant under unitary transformations. Thus, if the unitary matrix S has eigenvalues $\exp 2i\delta^J_\lambda$ $(\lambda=0\pm1)$, then Spur $\{-\frac{1}{2}i(T-T^*)\}=\Sigma_\lambda \sin^2\delta_\lambda$.

In the previous section we discussed one method of achieving this during the calculation of the matrix $T(r)$. The potential was diagonalized so that a modified T was calculated whose off-diagonal elements were relatively small, the bulk of the effect of the non-central forces having been transferred to the diagonal elements and the transformation matrix $U(r)$.

Apart from the term K, the relevant factor in eqn. (24) for our equation is $[U^{-1}(V-q)U+q]$ with $q=L(L+1)/r^2$. When there is a tensor force this connects $L=J\pm1$. Let us first consider V alone. If the spin–orbit coupling factor $v_2(r)$ is a simple multiple of $v_3(r)$ (including zero) the matrix V is diagonalized by a *constant* orthogonal matrix

$$U=\begin{pmatrix}\cos\theta & \sin\theta\\ -\sin\theta & \cos\theta\end{pmatrix}\qquad\text{......(26)}$$

where θ depends on the potential constants and J. As U is constant, $K=0$. This is very satisfactory, but off-diagonal terms still arise from $U^{-1}qU$ of the form $(2J+1/r^2)\sin 2\theta$. The precise effect of this term is difficult to say and depends on θ, but it is known that centrifugal terms $L(L+1)/r^2$ lead to large phase shifts in central forces, and the same may be true here.

The alternative procedure of choosing U so that $U^{-1}(V-q)U$ is diagonal bears some resemblance to that adopted by Christian and Hart (1950). This time θ varies with r, but K simplifies in view of the relation

$$U^{-1}\frac{dU}{dr}=i\sigma_y\frac{d\theta}{dr}=\begin{pmatrix}\cdot & 1\\ -1 & \cdot\end{pmatrix}\frac{d\theta}{dr}.$$

---

* We have used T rather than S to avoid confusion later.

The remaining factor in K is rather complicated. The whole expression is similar to that which would arise from a potential $d\theta/dr$ and is, therefore, probably small. For example, if there is no spin–orbit potential and the tensor force $v_3=(b\kappa/r)\exp-\kappa r$, where b has a value less than 2 (the value to give binding for a central force of the type), we find $2\theta=\tan^{-1}\{2\sqrt{2b\kappa r}/(b\kappa r-6\exp\kappa r)\}$. Then θ is always negative, decreases from zero to about $-\tfrac{1}{6}\pi$ at $r=1$ and back to zero as r increases. Thus these considerations are not inconsistent with the calculations of Christian and Hart, who found that the error in the phases when these off-diagonal terms were neglected was about 10% for states other than the S state ($J=1$).

There is need for a brief discussion of two more points. The first is the relation between T (or S_0) and the phase matrices S_1, S_2, which would be calculated using a trial function of the form $u_L=(u_1S_1+u_2S_2)_{LL'}A^{L'}$. If in fact we have chosen the free wave functions so that

$$u_1^{LL}\sim\lambda_1\,\mathrm{e}^{-i(kr-L\pi)}-\mu_1\,\mathrm{e}^{ikr},\quad u_2^{LL}\sim\lambda_2\,\mathrm{e}^{-i(kr-L\pi)}-\mu_2\,\mathrm{e}^{ikr},$$

then, after a certain amount of algebra, it is found that

$$S_0=1+2iT=(\mu_1S_1+\mu_1S_2)(\lambda_1S_1+\lambda_2S_2)^{-1}.$$

Thus $S_2=S_0$ if $S_1=1$ and $\mu_1=\lambda_2=0$, $\mu_2=\lambda_1=1$.

In general, in calculations we choose $S_1=1$, but in order to make a correspondence between the quantities calculated and the phases δ which occur in central forces we have determined two representations where S involved three phases, corresponding to the three phases for $L=J, J\pm1$ when there are no tensor forces, and a mixing parameter λ. These are given in the Appendix with the requisite equations.

§7. THE HEISENBERG S MATRIX

The S matrix is a unitary matrix which determines the scattering. It can be simply defined as a matrix S such that the asymptotic form of any stationary state is of the form

$$r\psi=\mathrm{e}^{-ikr}f(\theta,\phi)-\mathrm{e}^{ikr}(Sf). \qquad \ldots\ldots(27)$$

In a representation where J and L are diagonal, as for central forces, the asymptotic form of the radial functions $u_L(r)\sim\sin(kr+\delta_L-\tfrac{1}{2}L\pi)$ shows that S is diagonal in L and has matrix elements $S_{LL}{}'=(-)^L\exp 2i\delta_L\,\delta_{LL}{}'$. When there are tensor or other non-central forces S may not be diagonal in L, although diagonal in J. In fact the last remarks of the previous section show that $S_{LL'}^{(J)}=(-)^{(L+L')/2}(S_0)_{LL'}$.

It therefore appears that our equations lead directly to a first-order differential equation for the S matrix, and that this equation is obtained by inserting for u_1 and u_2 those combinations of $j_L(kr)$ and $n_L(kr)$ which have the asymptotic forms e^{-ikr} and e^{ikr} respectively. If these are $h_-(kr)$ and $h_+(kr)$ then the equation for S is $2ik\,dS/dr=(h_--Sh_+)V(h_--h_+S)$, where $S=1$ at $r=0$. Thus for the singlet S state with potential $v(r)$ the equation becomes

$$2ik\,dS/dr=v(r)\,\{\exp(-ikr)-S\exp(ikr)\}^2. \qquad \ldots\ldots(28)$$

Since this equation is true for any potential it follows that $S(r)$ is unitary for all values of r.

This unitary matrix is in some ways more desirable than the real matrices considered in the previous section, and for this reason it is interesting to notice the following result. The matrix $S(r)$ can by analytic continuation be evaluated for the imaginary values $k=-ik_0$, and for this value of k the equation (28) becomes

$$2k_0 dS/dr = v(r)\{\exp(-ik_0 r) - S\exp(ik_0 r)\}^2 \qquad \ldots\ldots(29)$$

with $S=1$ when $r=0$, which is a real equation. If an analytic expression for S as a function of k_0 can be obtained then the S matrix for scattering at positive energies is found by replacing k_0 by ik.

§8. BOUND STATES AND THE S MATRIX

The discussion at the end of the previous section is clearly related to the existence and the energies of bound states. We can deduce these in two ways, and we illustrate these for the singlet S state.

The first method uses analytic continuation. As usually applied, the Heisenberg S matrix is calculated, i.e. $S(\infty)$, as a function of k. By analytical continuation this is extended to the imaginary values $k=-ik_0$. For these imaginary values the energies of the bound states $E=-\hbar^2k^2/M$ are obtained by finding those values of k_0 such that $S(\infty)=0$.

We see how this condition arises by considering the wave function which we assume to obtain eqn. (29). It is

$$u=\{\exp(-k_0 r) - S\exp(k_0 r)\}a, \qquad \ldots\ldots(30)$$

together with a subsidiary condition on the functions a and S, so that $du/dr=\{-k_0\exp(-k_0 r) - Sk_0\exp(k_0 r)\}a$. The condition $S(\infty)=0$ then eliminates the exponentially increasing terms in the brackets.

This condition is clearly not sufficient. A more stringent condition has to be applied: $\lim_{r\to\infty} S\exp 2k_0 r=0$. This can be seen from eqn. (30) or the ratio

$$\frac{1}{u}\frac{du}{dr} = -k_0\frac{1+S\exp 2k_0 r}{1-S\exp 2k_0 r},$$

which eliminates the unknown factor $a(r)$.

A second method, which eliminates the necessity of knowing S as a function of k, is simply to integrate eqn. (29) directly with the conditions $S=1$ when $r=0$ and $\lim_{r\to\infty} S\exp 2k_0 r=0$. The equation is a little difficult as the conditions on S and the fact that it continually increases with r show that $S(r)$ diverges for some value or values of r and, in fact, the number of divergences equals the number of nodes in the wave function, including that at $r=0$.

Attempts have been made to find a systematic method of solving the equation, not for S, but for $y=S\exp 2k_0 r$, which is $2k_0 dy/dr - 4k_0^2 y = v(1-y)^2$, but without success.

§9. CONCLUSION

It is concluded that this method, which consists in taking seriously a well-known method of obtaining a first approximation to a single wave equation and then generalizing it, not only solves the equation in a reasonable form but is capable of producing useful general results. Its main disadvantage is that it requires a representation in which the angular momenta are diagonalized, but this may be related to the fact that we are working in ordinary space. It is significant that, when the momentum is diagonalized, which is desirable when the incident waves are plane waves, and momentum space is used, the equation for the state function is very similar in form to that given by the integrals of our differential equations.

ACKNOWLEDGMENT

I should like to express my gratitude to Professor R. Peierls for the interest he has shown in this work, and for many interesting discussions.

REFERENCES

Bergmann, O., 1950, *Acta Phys. Austriaca*, **4** (no. 1), 62.
Case, K. M., and Pais, A., 1950, *Phys. Rev.*, **80**, 203.
Chew, G. F., and Goldberger, M. .L, 1949, *Phys. Rev.*, **75**, 1637.
Christian, R. S., and Hart, E. W., 1950, *Phys. Rev.*, **77**, 441.
Heisenberg, W., 1943, *Z. Phys*,, **120** (9–10), 513.
Kynch, G. J., 1952, *Proc. Phys. Soc.* A, **65**, 94.
Landau, L., and Smorodinski, J., 1944, *J. Phys. Acad. Sci., U.S.S.R.*, **8**. 154.
Rosenfeld, L., 1948, *Theory of Nuclear Forces* (Amsterdam : North Holland Publishing Co.).
Yost, F. L., Wheeler, J. A., and Breit, G., 1936, *Phys. Rev.*, **49**, 174.

APPENDIX

The following summarizes (i) the wave functions, (ii) the equations needed to give the matrices S, and (iii) the matrix S_0 needed for the scattering cross section, with tensor forces.

The free wave functions used are $u_1 = j_L(kr)$; $u_2 = n_L(kr)$.

The diagonal element corresponding to $L = J$ is omitted.

The δ and λ in A are *not* the same as those in B.

Method A. $u = (u_1 + u_2 S)a$: $S = \begin{pmatrix} S_{11} & S_{12} \\ S_{21} & S_{22} \end{pmatrix} = \begin{pmatrix} \tan\delta_1 & \lambda \\ \lambda & \tan\delta_2 \end{pmatrix}$

$$S_0 = \begin{pmatrix} e^{2i\delta 1} - \lambda\mu(1 + e^{2i\delta 1}) & 2i\mu \\ 2i\mu & e^{2i\delta 2} - \lambda\mu(1 + e^{2i\delta 2}) \end{pmatrix}$$

$$k\frac{dS}{dr} = (u_1 + Su_2)V(u_1 + u_2 S)$$

$$\frac{4\lambda\mu}{1 - \lambda\mu} = (1 + e^{2i\delta 1})(1 + e^{2i\delta 2}).$$

Method B. $u = (u_1 S_1 + u_2 S_2)A$:

$$S_1 = \begin{pmatrix} \cos\delta_1 & \lambda(\cos\delta_2 - \sin\delta_2) \\ \lambda(\cos\delta_1 - \sin\delta_1) & \cos\delta_2 \end{pmatrix}$$

$$S_2 = \begin{pmatrix} \sin\delta_1 & \lambda(\cos\delta_2 - \sin\delta_2) \\ \lambda(\cos\delta_1 - \sin\delta_1) & \sin\delta_2 \end{pmatrix}$$

$$S_0 = \begin{pmatrix} e^{2i\delta 1} - \lambda\mu(i - e^{2i\delta 2}) & \mu \\ \mu & e^{2i\delta 2} - \lambda\mu(i - e^{2i\delta 2}) \end{pmatrix}$$

$$k\left(S_1'\frac{dS_2}{dr} - S_2'\frac{dS_1}{dr}\right) = k\Omega = (S_1'u_1 + S_2'u_2)V(u_1 S_1 + u_2 S_2)$$

$$\Omega = \begin{pmatrix} \delta_1' & \lambda'(\cos\delta_2 - \sin\delta_2)(\cos\delta_1 - \sin\delta_1) \\ \lambda'(\cos\delta_2 - \sin\delta_2)(\cos\delta_1 - \sin\delta_1) & \delta_2' \end{pmatrix}$$

$$\frac{\mu\lambda}{1 + \mu\lambda} = \lambda^2(i - e^{2i\delta 1})(i - e^{2i\delta 2});\ \ \lambda' = d\lambda/dr,\ \delta_1' = d\delta_1/dr.$$

The Two-Body Scattering Problem with Non-Central Forces: II—Relativistic

By G. J. KYNCH
Department of Mathematical Physics, The University, Birmingham

MS. received 17*th July* 1951

ABSTRACT. It has been shown that both for one particle scattered by a centre of force and in the two-body problem, treated relativistically, equations for the S matrix of the Riccati type can be found exactly similar to and as simple in form as those of the non-relativistic approximation. The analytic continuation of this matrix, to determine bound states, has the same limitations as in the non-relativistic problem.

§ 1. INTRODUCTION

The perturbation method used in the previous paper (Kynch 1952, to be referred to as I) showed that the scattering problem could be reduced to the calculation of a phase-matrix $S(r)$ from a set of first-order simultaneous equations. This suggests that a similar technique could be applied to the relativistic equations of Dirac. Existing calculations for one particle using these equations (e.g. Mott and Massey 1949) have usually reduced the four equations for a single particle to a single Schrödinger equation, by the elimination of all the components of the wave function except one. This equation is then solved by any of the usual methods.

We have found that the assumption of a wave function similar to those used in I results in a great simplification in the solution. An equation for a phase function $S(r)$ is obtained which is not essentially different from that obtained for the non-relativistic calculation. The potential appears in the same way, and so do the free-particle wave functions. The alteration is due to an extra term arising from the relativistic coupling of the states $L=J\pm\frac{1}{2}$. The potentials are only assumed to be invariant under rotations and inversion, in order to conserve the total angular momentum and parity. Apart from the form of the equation, which makes it easy to discuss relativistic corrections, one feature of the method is that the phase function $S=\tan\delta(r)$ is the same for all components of the Dirac equation.

In the two-particle problem of given angular momentum J, M, in the absence of a potential there are four states which in the non-relativistic limit reduce to the singlet $L=J$, the triplet $L=J$ and the two triplet states $L=J\pm 1$. When there is a potential satisfying the conditions mentioned in the previous paragraph, the last two states are mixed. Since the particles are free before and after scattering, we aim at the calculation of an S-matrix for these states at most yielding matrix elements between the last two, entirely analogous to that obtained in I. This aim has been achieved, and the required equation appears as a matrix product. There is some difficulty here because of the occurrence of non-differential relations between the components, but this can be overcome.

One difference between the solution of the Schrödinger and the Dirac equations is that the former required the introduction of auxiliary conditions before the solution was completed, but the latter does not. The general conclusion seems to be that the present method has advantages over former methods for the relativistic equations, both at low energies where corrections to the Schrödinger equation are required and at high energies where a rigorous calculation is necessary.

§ 2. DIRAC PARTICLE IN STATIC FIELD

The Dirac equation of an electron in a static potential can be written as

$$\{-i\rho_1(\sigma\,.\,\nabla)+\kappa\rho_3+E+v\}\psi=0, \qquad \ldots\ldots(1)$$

using units $\hbar=c=1$. In any other units the potential is $V=v\hbar c$. The momentum $-i\nabla=p$ has eigenvalues such that $E^2=\kappa^2+p^2$.

The solution of this equation in polar coordinates has already been discussed by Darwin (1927) and Dirac (1932). To derive the solution we use the relation $r^2(\sigma.p)=(\sigma.r)(p.r)-(\sigma.r\times L)$, so that

$$\left[-i\rho_1\left\{\frac{1}{r}(\sigma\,.\,r)\frac{\partial}{\partial r}-\frac{i}{r^2}(\sigma\,.\,r\times L)\right\}+\kappa\rho_3+E\right]\psi=-v\psi. \qquad \ldots\ldots(2)$$

We now introduce a representation in which $J=L+\frac{1}{2}\sigma$ and $M=J_z$ are diagonal. Their eigenfunctions f^{L-J}_{JM} are constructed in the usual way from the spherical harmonics $Y_{L,\,M}$ and the eigenfunctions α, β of σ^2 and σ_z. For each J, M there are two eigenfunctions f^+ and f^- obtained from $L-J=+\frac{1}{2}$ or $-\frac{1}{2}$ respectively. With the usual choice of phases in these functions the matrix elements of $(\sigma\,.\,r)$ are given by $(\sigma\,.\,r)f^+=rf^-$, $(\sigma\,.\,r)f^-=rf^+$.

The matrix elements of $(\sigma\,.\,r\times L)$ follow easily from the equation

$$[L^2,\sigma\,.\,r]=2(\sigma\,.\,r)+i(\sigma\,.\,r\times L). \qquad \ldots\ldots(3)$$

They are

$$-i(\sigma\,.\,r\times L)_{L\to L+1}=-L(\sigma\,.\,r)_{L\to L+1},\quad -i(\sigma\,.\,r\times L)_{L\to L-1}=(L+1)(\sigma\,.\,r)_{L\to L-1},$$

so that

$$\frac{1}{r}\left[(\sigma\,.\,r)\frac{\partial}{\partial r}-\frac{i}{r}(\sigma\,.\,r\times L)\right]_{L\to L+1}=\frac{1}{r}(\sigma\,.\,r)_{L\to L+1}\left(\frac{\partial}{\partial r}-\frac{L}{r}\right)$$

$$\frac{1}{r}\left[(\sigma\,.\,r)\frac{\partial}{\partial r}-\frac{i}{r}(\sigma\,.\,r\times L)\right]_{L\to L-1}=\frac{1}{r}(\sigma\,.\,r)_{L\to L-1}\left(\frac{\partial}{\partial r}+\frac{L+1}{r}\right).$$

Finally we choose ρ^2 and ρ_3 diagonal, $(\rho=\rho_1,\ \rho_2,\ \rho_3)$ with eigenfunctions $\chi_\beta\,(\beta=\pm 1$ as $\rho_3=\pm 1)$. Then for given J, M we write $r\psi=\Sigma_{\alpha,\beta=\pm 1}u^\beta_\alpha f^\alpha\chi_\beta$. The representatives u^β_α being written as a column matrix u, eqn. (2) is a matrix equation for $\psi\to u$ if v is replaced by a suitable matrix.

The potential V is assumed to commute not only with J and M but with the parity. The equation then breaks up into two representations of different parity. The two pairs of equations are (cf. Darwin 1927)

$$\left.\begin{aligned}-ikD_+u^-_+ +(E-\kappa)\,u^+_- &= -(vu)^+_-\\ -ikD_-u^+_- +(E+\kappa)\,u^-_+ &= -(vu)^-_+\end{aligned}\right\} \qquad \ldots\ldots(4a)$$

$$\left.\begin{aligned}-ikD_+u^-_- +(E+\kappa)\,u^+_+ &= -(vu)^+_+\\ -ikD_-u^+_+ +(E-\kappa)\,u^-_- &= -(vu)^-_-\end{aligned}\right\} \qquad \ldots\ldots(4b)$$

(The upper suffix is the value of $2(L-J)$ and the lower the value of ρ_3.) The abbreviations $D_+=k^{-1}\{\partial/\partial r-(L+1)/r\}$, $D_-=k^{-1}\{\partial/dr+L/r\}$ are used, operating on u^{L-J}.

In the absence of a potential these equations can be solved in terms of Bessel functions. As in I, we use

$$j_L(x)=\sqrt{}(\tfrac{1}{2}\pi x)^{1/2}J_{L+\frac{1}{2}}(x)\sim\sin(x-\tfrac{1}{2}L\pi)$$

$$n_L(x)=\sqrt{}(\tfrac{1}{2}\pi x)^{1/2}J_{-(L+\frac{1}{2})}(x)\sim\cos(x-\tfrac{1}{2}L\pi)$$

with the properties, if $x=kr$, that $D_+j_L=-j_{L+1}$, $D_-j_L=j_{L-1}$. Clearly we assume for a regular solution $u^-\propto j_{J-\frac{1}{2}}(kr)$, $u^+\propto j_{J+\frac{1}{2}}(kr)$. The equations are consistent if $E^2 = \kappa^2 + k^2$ and we find

$$u_{-}^{+} = j_{J+\frac{1}{2}}(kr)\,,\quad u_{+}^{-} = i\lambda j_{J-\frac{1}{2}}(kr), \qquad \ldots\ldots(5a)$$

$$u_{-}^{-} = j_{J-\frac{1}{2}}(kr)\,,\quad u_{+}^{+} = -i\lambda j_{J+\frac{1}{2}}(kr). \qquad \ldots\ldots(5b)$$

There are other solutions involving the irregular functions n_L instead of j_L. The factor $\lambda^2 = (E-\kappa)/(E+\kappa)$ serves to distinguish small terms in the non-relativistic approximation.

For eqns. ($4a$) we now put, as in our previous procedure,

$$u_{-}^{+} = (j_{J+\frac{1}{2}} + Sn_{J+\frac{1}{2}})a = U_{-}^{+}a, \qquad u_{+}^{-} = i\lambda(j_{J-\frac{1}{2}} + Sn_{J-\frac{1}{2}})a = U_{+}^{-}a.$$

This assumption is consistent with the equations, and eliminating da/dr and using the relation $j_L n_{L+1} - n_L j_{L+1} = 1$, we derive the following equation for S, without any further assumptions :

$$\lambda\frac{dS}{dr} = U_{-}^{+}{}^{*}(vU)_{-}^{+} + U_{+}^{-}{}^{*}(vU)_{+}^{-}. \qquad \ldots\ldots(6)$$

A similar assumption for eqns. ($4b$) leads to a similar equation for S.

To appreciate the simplicity of this equation it is best to assume central forces, with no ρ or σ dependent factors in the original expression. On insertion of the expressions for U, eqn. (6) is

$$k\frac{dS}{dr} = (e+\kappa)\,v(j_{J-\frac{1}{2}} + Sn_{J-\frac{1}{2}})^2 + (e-\kappa)\,v(j_{J+\frac{1}{2}} + Sn_{J+\frac{1}{2}})^2. \qquad \ldots\ldots(7)$$

The non-relativistic approximation is obtained for $e \to \kappa$ and $(e+\kappa)v \to 2\kappa v = 2mV/\hbar^2$, and is identical with the equations of I. The corrections to this due to the use of Dirac's equation are, therefore, the inclusion of the second term and the replacement of 2κ by $(e+\kappa)$. Both these corrections are of order λ^2, and both increase the magnitude of the phase compared with its non-relativistic limit.

The appearance of the second term is, of course, related to the derived spin-dependent potentials which appear when the transition from the Dirac equation to the Schrödinger equation is carried through.

Born approximation is obtained by neglecting terms in S on the right-hand side of the equation. The exact equation shows that S is then underestimated, but that, in so far as Born approximation gives $S(\infty)$ finite in the limit $k \to \infty$, so also does the exact solution.

§ 3. RELATIVISTIC TWO-BODY PROBLEM

The two-body problem where both particles satisfy Dirac's equation has been examined in considerable detail by Kemmer (1937). After eliminating the mass-centre coordinates and momenta the wave equation is

$$\{(\rho_1^{\mathrm{N}}\sigma_1^{\mathrm{N}} - \rho_1^{\mathrm{P}}\sigma^{\mathrm{P}}) \,.\, p + \kappa(\rho_3^{\mathrm{N}} + \rho_3^{\mathrm{P}}) + 2e + v\}\psi = 0$$

where $2e$ is used for the energy to eliminate factors of 2 subsequently, $p = \frac{1}{2}(p^{\mathrm{N}} - p^{\mathrm{P}})$ and $r = r^{\mathrm{N}} - r^{\mathrm{P}}$ (the neutron and proton mass are assumed equal). Using the substitution mentioned in the previous section for $r^2(\sigma \,.\, p)$ we obtain

$$\Big[-\tfrac{1}{2}i\bar{\rho}_1\Big\{(\sigma \,.\, r)\frac{\partial}{\partial r} - \frac{i}{r^2}(\sigma \,.\, r \times L)\Big\} - \tfrac{1}{2}i\rho_1\Big\{\frac{1}{r}(\bar{\sigma} \,.\, r)\frac{\partial}{\partial r} - \frac{i}{r^2}(\bar{\sigma} \,.\, r \times L)\Big\}$$

$$+\kappa\rho_3 + v + 2e\Big]\psi = 0 \qquad \ldots\ldots(8)$$

where $\sigma = \sigma^{\mathrm{N}} + \sigma^{\mathrm{P}}$, $\bar{\sigma} = \sigma^{\mathrm{N}} - \sigma^{\mathrm{P}}$, and similarly for ρ and $\bar{\rho}$. Owing to the relation (3) the same relation exists between the matrix elements of $(\sigma \,.\, r)$ and $(\sigma \,.\, r \times L)$, or $(\bar{\sigma} \,.\, r)$ and $(\bar{\sigma} \,.\, r \times L)$ as held in the previous section.

We now choose a suitable representation so that the total angular momentum J is diagonal. The 16 elements in ψ separate into four groups ($\rho_3^{\mathrm{N}} = \pm 1, \rho_3^{\mathrm{P}} = \pm 1$, say, if these are diagonalized), each containing four rows which can be chosen so that J is diagonal.

Let α, β be eigenfunctions of σ_z and a, b eigenfunctions of ρ_3. Then any ψ is expressible as a sum of multiples of such products as $a^{\mathrm{N}} b^{\mathrm{P}} \alpha^{\mathrm{N}} \alpha^{\mathrm{P}}$. The states of neutron and proton can be combined to give eigenfunctions of the total spin : $\chi_m (m=0, \pm 1)$ for the triplet, and χ_S for the singlet. Combining these with suitable angular functions, we obtain, as in I, normalized eigenfunctions of the total angular momentum J, M:

$$\begin{array}{ll} \text{Triplet}: & f_{JM}^{L-J} = \Sigma c_{JM}^{Lm} Y_{L, M-m} \chi_m \quad (L-J=0, \pm 1) \\ \text{Singlet}: & f_{JM}^{S} = Y_{L, M} \chi_S. \end{array}$$

(Except for normalization, f^-, f^0, f^+ are $\mathfrak{X}$, $\mathfrak{Y}$, $\mathfrak{Z}$ in Kemmer's notation.)

In order to diagonalize his potentials Kemmer now uses a representation for the ρ_1, so that $\rho_3^{\mathrm{N}} \rho_3^{\mathrm{P}}$ and $\rho_1^{\mathrm{N}} \rho_1^{\mathrm{P}}$ are diagonalized. We prefer to use that in which ρ_3 and ρ^2 are diagonal, as the large and small components are conveniently separated, i.e. we use eigenfunctions $\zeta_{0, \pm 1}$, ζ_S defined in terms of a, b in the same way as χ_m, χ_S are defined in terms of α, β. The operator $\rho_1^{\mathrm{N}} \rho_1^{\mathrm{P}}$ then mixes the states $\zeta_{\pm 1}$.

The wave function for given J, M is expanded as*

$$r\psi = \Sigma u_\alpha^\beta f^\alpha \zeta_\beta \quad (\alpha, \beta = 0, \pm 1, S)$$

where some suffixes J, M have been dropped.

As found by Kemmer, there are three non-zero representations, one of parity $(-)^{J+1}$ containing six of the u_β^α, two of parity $(-)^J$ containing four each. The functions u_S^S, u_0^0 are identically zero.

The wave equations are easily written down using the abbreviations D_+ and D_- as before and $\alpha = \{2(J+1)/(2J+1)\}^{1/2} k$, $\beta = \{2J/(2J+1)\}^{1/2} k$.

$$\begin{array}{ll} & i\beta D_+(u_-^+ + u_-^-) - i\alpha D_-(u_+^- + u_+^+) + 2eu_S^0 = -(vu)_S^0 \\ & i\alpha D_+(u_-^- - u_-^+) + i\beta D_-(u_+^- - u_+^+) + 2eu_0^S = -(vu)_S^0 \\ \text{I}(a) & i\alpha D_- u_0^S + i\beta D_- u_S^0 + 2(e-\kappa) u_-^- = -(vu)_-^- \\ & i\beta D_+ u_0^S - i\alpha D_+ u_S^0 + 2(e-\kappa) u_+^- = -(vu)_+^- \\ & -i\alpha D_- u_0^S + i\beta D_- u_S^0 + 2(e+\kappa) u_-^+ = -(vu)_-^+ \\ & -i\beta D_+ u_0^S - i\alpha D_+ u_S^0 + 2(e+\kappa) u_+^+ = -(vu)_+^+ \end{array}$$

$$\begin{array}{ll} & i\beta D_+ u_0^- - i\beta D_+ u_0^+ + 2eu_+^S = -(vu)_+^S \\ & i\alpha D_- u_0^- - i\alpha D_- u_0^+ + 2eu_-^S = -(vu)_-^S \\ \text{I}(b) & i\alpha D_+ u_-^S + i\beta D_- u_+^S + 2(e-\kappa) u_0^- = -(vu)_0^- \\ & -i\alpha D_+ u_-^S - i\beta D_- u_+^S + 2(e+\kappa) u_0^+ = -(vu)_0^+ \end{array}$$

$$\begin{array}{ll} & -i\alpha D_+(u_S^+ + u_S^-) + 2eu_+^0 = -(vu)_+^0 \\ & i\beta D_-(u_S^+ + u_S^-) + 2eu_-^0 = -(vu)_-^0 \\ \text{II}(b) & i\beta D_+ u_-^0 - i\alpha D_- u_+^0 + 2(e+\kappa) u_S^+ = -(vu)_S^+ \\ & i\beta D_+ u_-^0 - i\alpha D_- u_+^0 + 2(e-\kappa) u_S^- = -(vu^0{}_S^- \end{array}$$

In these equations we have expanded $v\psi = \Sigma_{\alpha, \beta} (vu)_\alpha^\beta f^\alpha \zeta_\beta$.

---

* The following matrix elements are used :

$$\begin{array}{lll} (\sigma . r) f^+ = -2\beta r f^0 \; ; & (\sigma . r) f^- = -2\alpha r f^0 \; ; & (\sigma . r) f^0 = -2r(\alpha f^- + \beta f^+) \\ (\bar{\sigma} . r) f^+ = 2\alpha r f S \; ; & (\bar{\sigma} . r) f^- = -2\beta r f S \; ; & (\sigma . r) f S = -2r(\beta f^- - \alpha f^+) \\ \alpha^2 = (J+1)/(2J+1) \; ; & \beta^2 = J/(2J+1). & \end{array}$$

Potentials of the type assumed by Kemmer at most connect states u^+ and u^-, so that it is clear that certain components are then multiples of others, the ratios depending on the potentials, e.g. in II (*b*) the two components u_S^+ and u_S^-.

The solution for free particles in terms of the modified Bessel functions are:

$$\begin{array}{lllll}
\mathrm{I}(a) & \text{(i)} & u_-^- = j_-, & u_-^+ = -\tfrac{1}{2}\lambda^2(\alpha^2-\beta^2)j_-, & u_0^S = i\alpha\lambda j_0, \\
 & & u_+^- = 0, & u_+^+ = \alpha\beta\lambda^2 j_+, & u_S^0 = i\beta\lambda j_0. \\
 & \text{(ii)} & u_-^- = 0, & u_-^+ = \alpha\beta\lambda^2 j_-, & u_0^S = -i\beta\lambda j_0, \\
 & & u_+^- = j_+, & u_+^+ = \tfrac{1}{2}(\alpha^2-\beta^2)\lambda^2 j_+, & u_S^0 = i\alpha\lambda j_0. \\
\mathrm{I}(b). & & u_0^- = j_0, & u_0^+ = -\lambda^2 j_0, & \\
 & & u_-^S = -i\alpha\lambda j_-, & u_+^S = i\beta\lambda j_+. & \\
\mathrm{II}(b) & & u_S^- = j_0, & u_S^+ = \lambda^2 j_0, & \\
 & & u_+^0 = -i\alpha\lambda j_+, & u_-^0 = -i\beta\lambda j_-. &
\end{array}$$

§4. SOLUTION WITH POTENTIALS

The aim of our method of solution is to obtain an equation for a single function $S(r)$, or a matrix, which only contains S, the free wave functions and the potentials. There is some difficulty if we try simple substitution of the form $u=(j_L+Sn_L)a$ because of the components of the wave function which are direct multiples of others. The procedure adopted here has the merit of simplicity and is easy to carry through, but it is not at all elegant. We shall carry it through for the solution II (*b*) and state the results in other cases.

In the set of equations II (*b*) there are four wave functions which we separate into two parts; one gives the asymptotic form of the type previously assumed and contains the function $S(r)$; the other is to be proportional to the potentials

$$u_\alpha^\beta = U_\alpha^\beta a + W_\alpha^\beta, \qquad U_S^- = j_0 + Sn_0, \qquad U_+^0 = -i\alpha\lambda(j_+ + Sn_+),$$
$$U_S^+ = \lambda^2(j_0 + Sn_0), \qquad U_-^0 = -i\beta\lambda(j_- + Sn_-).$$

The arguments of j_L and n_L are always (kr), where $k^2=e^2-\kappa^2$. These reduce when $S=0$ to the correct regular solutions with no potential.

There are six unknown functions, and four equations. Two of the equations give relations between the W, the others are equations for S and a. Two further conditions can be imposed on the W, which are used to eliminate their derivatives.

To obtain an equation so that $a(r)$ and its derivatives are eliminated we write the functions $u(r)$ as a column matrix, u^+ as its adjoint (conjugate) row matrix, and the potential as a square matrix.

The derivatives of the W are eliminated if $W_S^- + W_S^+ = 0$; $W_-^0 = \alpha K$, $W_+^0 = \beta K$, where K is still to be determined. The remaining terms in K can almost be eliminated. Multiplying the equations by U_α^β and adding, the W only remain with the potentials

$$\frac{4ek}{(e+\kappa)^2}\frac{dS}{dr}a = U^+Vu. \qquad \ldots\ldots(9)$$

From the relations satisfied by the W we find

$$4eW_S^+ = -4eW_S^- = (vu)_S^+ - (vu)_S^-, \qquad 2eK = \beta(vu)_+^0 + \alpha(vu)_-^0$$

from which it follows that $2eW^+W = W^+Vu$. These equations show that in fact the W are proportional to $a(r)$ and that eqn. (9) can be divided by $a(r)$, thus leaving an equation for S alone.

This procedure, though cumbersome, is straightforward and easy to carry through. The result would be more elegant if the W could be eliminated from the equations completely before inserting their values. They influence the scattering although they disappear from the asymptotic form of the wave function.

§ 5. GENERAL SOLUTION OF TWO-BODY EQUATIONS

The procedure used in the previous section for the representation II (b) can be used for the others, or, indeed, on the wave equation as a whole. It follows the following common pattern. Using obvious abbreviations, eqn. (8) has the form

$$\{(F\partial/\partial r+G)+\kappa\rho_3+2e+v\}u=0, \qquad \ldots\ldots(10)$$

where F and G are operators, and u is a column matrix of the representatives u^{α}_{β} in eqn. (8).

When there is no potential there are four regular solutions each of the form $u_{\alpha}=J_{\alpha}$, where the J_{α} are proportional to the functions $j_L(kr)$ with an appropriate value of L. There are four more irregular solutions with $n_L(kr)$ instead of $j_L(kr)$. These solutions are arranged in four columns to form matrices J, N.

We now assume $u=(J+NS)a+W$, where S and a are (4×4) and (4×1) matrices, respectively, which are functions of r, and the W have still to be chosen. The W are chosen so that their derivatives do not appear in the wave equation, i.e. $FW=0$. Now this equation has eight constant solutions, normalized and orthogonal :

$(2k\omega_1)$: $u^{+}_{+}={}^{-}\alpha$, $u^{-}_{+}=\alpha$, $u^{+}_{-}=-\beta$, $u^{-}_{-}=\beta$.
$(2k\omega_2)$: $u^{+}_{+}=\beta$, $u^{-}_{+}=\beta$, $u^{+}_{-}=\alpha$, $u^{-}_{-}=\alpha$.
$(\sqrt{2}\omega_3)$: $u^{+}_{0}=u^{-}_{0}=1$.
$(\sqrt{2}k\omega_4)$: $u^{S}_{+}=\alpha$, $u^{S}_{-}=-\beta$.
$(\sqrt{2}\omega_5)$: $u^{+}_{S}=-u^{-}_{S}=1$
$(\sqrt{2}k\omega_6)$: $u^{0}_{+}=\beta$ $u^{0}_{-}=\alpha$.
(ω_7) : $u^{S}_{S}=1$.
(ω_8) : $u^{0}_{0}=1$.

The last two involve u^{S}_{S} and u^{0}_{0}, which are known to be zero components and can therefore be ignored. The most general form for W is, therefore, a sum of the remainder multiplied by six arbitrary functions $\lambda(r)$ of r :

$$W=\omega\lambda. \qquad \ldots\ldots(11)$$

Substitute these expressions in eqn. (10): it becomes

$$F\left\{J\frac{\partial a}{\partial r}+N\frac{\partial}{\partial r}(Sa)\right\}+(G+\kappa\rho_3+2e)W=-vu. \qquad \ldots\ldots\ldots(12)$$

The equations are multiplied by the adjoint matrix $(J+NS)^{+}$. The following terms in W are zero :

$$(J+NS)^{+}(G+\kappa\rho_3+2e)W=-\left(\frac{\partial J^{+}}{\partial r}+S^{+}\frac{\partial N^{+}}{dr}\right)F^{+}W$$

since $F^{+}W=FW=0$. The term in $\partial a/\partial r$ is $(J+NS)^{+}\ F(J+NS)\ \partial a/\partial r=0$, as the multiplier is effectively the expectation value of F in a free state, which is zero. Also $(J+NS)^{+}FN=J^{+}FN=-2\lambda(1+\lambda^{2})$, where $\lambda^{2}=(e-\kappa)/(e+\kappa)$, so that, finally, if $k^{2}=e^{2}-\kappa^{2}$,

$$k\frac{dS}{dr}a=+\frac{(e+\kappa)^{2}}{4e}(J+NS)^{+}v\{(J+NS)a+W\}. \qquad \ldots\ldots(13)$$

We now show that a matrix $a(r)$ can be dropped from this equation because the W are proportional to a. The evaluation of the W starts from eqns. (11) and (12). It may easily be shown that GW and $\rho_3 W$ are orthogonal to all ω_α. Consequently, since the ω are normalized and orthogonal $\omega^+\omega = 1$, if eqn. (12) is multiplied by ω^+, then $2e\lambda = \omega^+ v(J+NS)a + \omega^+ v\omega\lambda$. This equation can be solved for the λ, giving, for example, $\lambda = \Lambda(J+NS)a$. Thus from eqn. (13) we obtain the following equation for the matrix S consistent with the wave equations:

$$k\frac{dS}{dr} = \frac{(e+\kappa)^2}{4e}(J+NS)^+ v(1+\omega\Lambda)(J+NS).$$

In view of the discussion of § 3, the phase matrix S and the whole of the equation reduce to a single equation each for the S matrix element for the representations I (b) and II (b) and a 2×2 matrix for S for the representation I (a).

§ 6. SUMMARY

The form of the solutions which have been assumed for the wave functions shows that the asymptotic values of S at infinity are related to the phases required to calculate the scattering. For example, if $S(\infty) = \tan\delta$, then $j_L + Sn_L \sim \sin(kr - \frac{1}{2}L\pi + \delta)/\cos\delta$. Moreover, if we substitute $S(r) - \tan\delta(r)$, then our equations show that $\delta(r)$ increases monotonically with r to its maximum value. In I we gave the necessary modifications if S is a matrix.

It has been established that the relativistic scattering of particles can be determined in exactly the same way as for non-relativistic scattering. This means that many statements of a qualitative nature apply at both low and very high energies. Thus it is unnecessary to discuss in detail many statements made in I, although there are some points which deserve explicit mention.

The comparison between n–p and p–p scattering is now of little importance. At very high energies the Coulomb term is a small perturbation. If it is necessary, however, a comparison by the method used in I can be made for the one-particle problem; for the two-body problem it can also be done formally, but the coulomb term enters into the calculation of the W, which is undesirable in view of its behaviour at infinity.

It was also pointed out that our equations needed only slight modification to become differential equations for a unitary matrix $S(r)$ which was asymptotically the Heisenberg S matrix in the representation. This is still true in relativistic calculations, the modification being simply to replace $(j+Sn)$ everywhere by $(h_1 - Sh_2)$, where h_1 and h_2 are asymptotically e^{-ikr} and e^{ikr}, respectively.

The S matrix form naturally raises the question of calculating the energies of bound states, assuming the Dirac equation, by analytical continuation of this matrix in k-space. It was shown in I that a necessary condition for a bound state at $k = -ik_0$ of energy $-k_0^2$ was $\lim_{r\to\infty} S(r)\exp 2k_0 r = 0$. This agreed, in particular, with the proof given by Jost (1947) that the condition $S(\infty) = 0$ is sufficient for any potential which is cut off at a certain distance, since $dS/dr = 0$ for such a potential outside this range. It is now clear than the same condition applies using the Dirac equations at all energies, and it is also probable that the conditions recently given by Pais and Yost (unpublished) also apply to all states.

The appearance of the functions $W(r)$ in the two-body problem may be due to a wrong treatment of the equation. Apart from this it would be satisfactory if in fact they were zero when the correct potentials were inserted, but, of course, this cannot be shown until the potentials are known.

REFERENCES

Darwin, C. G., 1928, *Proc. Roy. Soc.* A, **118**, 654.
Dirac, P. A. M., 1932, *Quantum Mechanics* (Oxford : University Press).
Jost, R., 1947, *Helv. Phys. Acta*, **20**, 256.
Jost, R., and Pais, A., 1951, *Phys. Rev.*, **82**, 840.
Kemmer, N., 1937, *Helv. Phys. Acta*, **10**, 47.
Kynch, G. J., 1952, *Proc. Phys. Soc.*, A, **65**, 83.
Mott, N. F., and Massey, H. S. W., 1949, *The Theory of Atomic Collisions*, 2nd edn. (Oxford : University Press).

Analysis of High-Energy Neutron Production

By F. MANDL and T. H. R. SKYRME

Atomic Energy Research Establishment, Harwell, Didcot, Berks.

Communicated by R. E. Peierls ; MS. received 13th August 1951

ABSTRACT. The energy spectra of neutrons scattered in the forward direction when different target nuclei are bombarded with high energy protons are calculated and compared with recent measurements. The calculation is subdivided into three stages : (i) as a crude analogue to the nuclear scattering, the scattering of a single neutron in a square well is calculated using Born approximation; (ii) single scattering processes are estimated classically using the results of (i) to allow for the momentum distribution of the target neutron, and allowing for the attenuation of incident and scattered beams; (iii) multiple scattering is estimated similarly. Several simplifying assumptions have to be made and double collisions only are estimated.

The calculated differential cross sections are in fairly good agreement with experiment, but the calculated energy spectrum falls off too quickly. The effect of neglecting certain processes, such as triple collisions, is discussed, as well as the applicability of the nuclear model used.

.A
5
2

§ 1. INTRODUCTION

The object of this paper is the calculation of the energy spectrum of neutrons scattered in the forward direction when different target nuclei are bombarded with 171 Mev protons. Such spectra have recently been measured for beryllium, carbon and aluminium (Cassels, Randle, Pickavance and Taylor 1951 a). A comparison of these results will indicate to what extent the nuclear model used is adequate at high energies. In particular, the experimental results show two characteristic features which should be explained. Firstly, the differential cross section is much smaller than N times the free particle cross section. Secondly, the energy spectrum has a maximum at about 150 Mev; for smaller energies it decreases only slowly. For example, the intensity of 100 Mev neutrons is still 67% of the maximum intensity.

The general features of high energy nuclear reactions are well known (Serber 1947, Fernbach, Serber and Taylor 1949), but in detailed calculations considerable difficulties are encountered. There are no satisfactory nuclear models. There are indications that nuclear forces are many-body forces, but even if one avoids these, there are no satisfactory two-nucleon potentials to account for the known free particle scattering data (see Christian and Noyes 1950, Christian and Hart 1950, where references to experimental papers are given). This difficulty can be overcome by expressing all processes approximately in terms of single-particle collisions and then using the experimental data. Finally one is here dealing with a many-body problem, and only quite crude approximate calculations are practicable.

Apart from these general considerations, to see the points of importance involved let us consider qualitatively the scattering of protons by nuclei.

When an incident proton hits a nuclear particle many processes may occur, but on the Serber picture the most frequent result will be for two nucleons to be ejected from the nucleus. There is a much smaller chance at these high energies of only one nucleon being ejected and the nucleus remaining in an excited state; in any case such transitions will only affect the intensity of neutrons of almost the maximum energy (at most a few Mev below). As the target nucleon is bound in the nucleus it is no longer possible to assume conservation of energy and momentum for the two nucleons colliding. We assume conservation of energy, but any spare momentum can always be taken up by the nucleus.

At 170 Mev the mean free path of protons in nuclear matter is of the same order as the nuclear radius ($\lambda = 2{\cdot}8 \times 10^{-13}$ cm), hence multiple collisions will matter. Their effect is to cause an attenuation of incident and scattered waves and to produce a broadening of the energy spectrum. These two effects should be responsible for the characteristics of the experiments mentioned above. The Coulomb scattering, being due to long-range forces, can be estimated for the nucleus as a whole and turns out to be negligible at these energies.

The calculation is subdivided into three sections:

(i) As a crude analogue to the nuclear scattering process that we want to consider, we calculate the scattering of a 170 Mev proton by a single neutron in a square well, of such depth that its binding energy is 8 Mev, using Born approximation, which should be quite good at these energies. One can avoid using a specific (p, n) interaction potential and can express the results in terms of the known differential cross section for free (p, n) scattering. This calculation corresponds to the scattering from a 'typical' nuclear neutron (§ 2).

(ii) Single scattering processes are estimated classically, using the results of (i) to allow for the momentum distribution of the target neutron and allowing for the attenuation of incident and scattered beams. The nucleus is considered as consisting of individual non-interacting particles distributed uniformly throughout the nucleus. The Pauli principle, however, is taken into account by forbidding transitions to 'occupied states' in the calculation of the mean free paths (Goldberger 1948) (§ 3).

(iii) Multiple scattering can be estimated similarly but leads to very heavy computation, and some simplifying assumptions must be made. We have only calculated double collision processes, allowing for the various possible processes of direct and exchange scattering (§ 4). The effects of neglecting triple and higher order processes should not be serious. It will be discussed together with the results of these calculations and the applicability to high-energy scattering problems of the nuclear model used (§ 5).

§ 2. PROTON SCATTERING BY A SINGLE NEUTRON IN A POTENTIAL WELL

Let $\phi(\mathbf{r}_2)$ be the wave function of a neutron in the 1s state of a spherical square well potential of radius R and depth U_0, where for R we take the nuclear radius and U_0 is so chosen that the binding energy ϵ of the 1s level is 8 Mev. Then

$\phi(r_2) = Ar_2^{-1} \sin \alpha r_2$, $r_2 \leqslant R$; $\phi(r_2) = Br_2^{-1} \exp - \beta r_2$, $r_2 \geqslant R$; A and B are determined from the normalization of ϕ and the continuity of its logarithmic derivative at $r_2 = R$. Describe the incident proton, energy E_1, momentum $\hbar \mathbf{k}_1$ by a plane wave $\exp(i\mathbf{k}_1 . \mathbf{r}_1)$. In the final state both neutron and proton are ejected from the well, with momenta $\hbar \mathbf{k}_1'$, $\hbar \mathbf{k}_2'$, into elements of solid angle $d\Omega_1'$, $d\Omega_2'$, with energy E_1', E_2' respectively. The differential cross section for the incident proton of energy E_1 to be ejected into the solid angle $d\Omega_1'$ with energy in the range $(E_1', E_1' + dE_1')$ is then given by

$$\sigma(E_1, E_1')\, d\Omega_1'\, dE_1' = \frac{M}{\hbar k_1} \frac{2\pi}{\hbar} \int |H_{if}|^2 \, \delta(E_1' + E_2' - E_1 + \epsilon)$$

$$\times \frac{1}{(2\pi)^6} k_1'^2 \frac{dk_1'}{dE_1'} dE_1' k_2'^2 \, dk_2' \, d\Omega_1' \, d\Omega_2' \qquad \ldots\ldots(1)$$

the integration being over $\mathbf{k}_2'$. The δ-function ensures conservation of energy. H_{if} is the matrix element for the transition. If the (p, n) interaction is described by a Serber potential $\frac{1}{2}(1+P)V(r)$, $(\mathbf{r} = \mathbf{r}_1 - \mathbf{r}_2)$, then

$$H_{if} = \int \phi(\mathbf{r}_2) \exp(i\mathbf{k}_1 . \mathbf{r}_1) \{\tfrac{1}{2} V(r) \exp(-i\mathbf{k}_1' . \mathbf{r}_1 - i\mathbf{k}_2' . \mathbf{r}_2)$$

$$+ \tfrac{1}{2} V(r) \exp(-i\mathbf{k}_1' . \mathbf{r}_2 - i\mathbf{k}_2' . \mathbf{r}_1)\} \, d\mathbf{r}_1 . d\mathbf{r}_2$$

and

$$|H_{if}|^2 = |\int \phi(\mathbf{r}_2) \exp\{-i(\mathbf{k}_1' + \mathbf{k}_2' - \mathbf{k}_1)\mathbf{r}_2\} \, d\mathbf{r}_2|^2$$

$$\times |\tfrac{1}{2} \int V(r) \exp\{i(\mathbf{k}_1 - \mathbf{k}_1')\mathbf{r}\} \, d\mathbf{r} + \tfrac{1}{2} \int V(r) \exp\{i(\mathbf{k}_1 - \mathbf{k}_2')\mathbf{r}\} \, d\mathbf{r}|^2 . \qquad \ldots\ldots(2)$$

The first term on the right-hand side gives the momentum distribution of the neutron in the square well. If we were dealing with a free neutron, $\phi(\mathbf{r}_2)$ would also be a plane wave and this first integral would reduce to the δ-function expressing conservation of momentum. Of the two Fourier transforms of the potential $V(r)$, the first corresponds to exchange, the second to direct scattering.

The differential cross section $\Sigma(E_1, 2\delta)$ in the centre-of-mass system, for a proton of energy E_1 to suffer an exchange scattering through an angle 2δ when striking a free neutron, is given in Born approximation by

$$\Sigma(E_1, 2\delta) \left(\frac{4\pi\hbar^2}{M}\right)^2 = |\tfrac{1}{2} \int V(r) \exp\{i(\mathbf{K} - \mathbf{K}')\mathbf{r}\} \, d\mathbf{r} + \tfrac{1}{2} \int V(r) \exp\{i(\mathbf{K} + \mathbf{K}')\mathbf{r}\} \, d\mathbf{r}|^2, \qquad \ldots\ldots(3)$$

where $\hbar \mathbf{K}$, $-\hbar \mathbf{K}'$ are the momenta of the proton before and after collision respectively (in the centre-of-mass system). In eqns. (2) and (3) the last terms can be neglected as we shall only consider final states in which a neutron is scattered in the forward direction. We can then identify these two equations if we make $|\mathbf{k}_1 - \mathbf{k}_1'| = |\mathbf{K} - \mathbf{K}'|$, i.e. define δ by

$$\sin \delta = |\mathbf{k}_1 - \mathbf{k}_1'| / k_1 = 1 - (E_1'/E_1)^{1/2} \qquad (0 \leqslant \delta \leqslant \tfrac{1}{2}\pi).$$

Using the Berkeley data for $\Sigma(E_1, 2\delta)$, the calculation of $\sigma(E_1, E_1')$, eqn. (1), is quite straightforward, though lengthy. If calculation is limited to the energy spectrum of neutrons in the forward direction, all the integrations can be carried out analytically except the radial integration in the Fourier transforms of $\phi(\mathbf{r}_2)$. $\sigma(E_1, E_1')$ is, however, not quite the quantity required to compare our results with the measurements of Cassels *et al.* for the proton beam in the cyclotron is not monoenergetic but, due to multiple traversal of the target, has an energy spectrum given approximately by $I(E_1) = I_0 \exp[(171 - E_1)/15]$. $\sigma(E_1, E_1')$ must be integrated over this energy spectrum to obtain the differential cross section $\sigma_s(E_1')$ in the forward direction per unit solid angle per unit energy for the exchange scattering process considered. $\sigma_s(E_1')$ is plotted against E_1' in fig. 1, the radius of the well R having been taken equal to the radius of the Be nucleus.

We shall, however, also use the same function $\sigma_s(E_1')$ for scattering by ^{12}C and ^{27}Al targets. The error thereby introduced should not be serious, as all we require is a typical 'smearing function'. Furthermore, the nuclear radius R (i.e. the well radius) varies only as the cube root of the atomic number A.

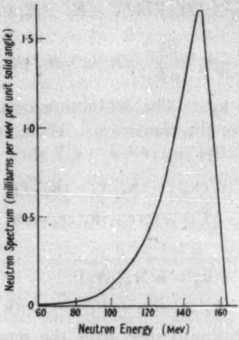

Fig. 1. Energy spectrum $\sigma_s(E)$ of neutrons ejected in forward direction from a square well as a function of the neutron energy E.

We have also calculated the quantity analogous to $\sigma_s(E_1')$ for (p, p) scattering. Though the absolute magnitude differs, the energy dependence is very nearly the same in the two cases. We shall need to make use of this result when considering double collisions.

§ 3. SINGLE SCATTERING PROCESSES

We next consider those processes where the incident proton collides with a nuclear neutron so that the neutron is scattered in the forward direction and emitted from the nucleus without further collisions, allowing for the attenuation of incident and scattered beams.

Consider a nucleus with N neutrons and Z protons and assume that these are uniformly distributed with density n throughout the nucleus, pictured as spherical of radius R.

If the incident proton, energy E_0, moves in the direction of the positive z axis of a coordinate system whose origin is at the centre of the nucleus, and it enters the nucleus at the point with polar coordinates (R, θ, ϕ), then the differential cross section $\sigma_1(E_1)\,dE_1\,d\Omega_1$ for a neutron with energy in the range (E_1, E_1+dE_1) to be emitted into $d\Omega_1$ in the forward direction, due to a single collision, is given by

$$\sigma_1(E_1) = \int_{\theta=\pi}^{\pi/2}\int_{\zeta=0}^{-2R\cos\theta} \exp(-\zeta/l_0) \times \left[\left(\frac{nN}{A}\right)2\pi R^2 \sin\theta\cos\theta\,d\theta\,d\zeta\,\sigma_s(E_1)\right]\exp\{(2R\cos\theta+\zeta)/l_1\}. \quad \ldots\ldots(4)$$

Here the square bracket gives the probability of a collision of the desired kind occurring in the volume element $2\pi R^2 \sin\theta \cos\theta \, d\theta \, d\zeta$. The two exponentials give the attenuation of the incident and scattered beams. The mean free path $l_i = l(E_i)$ of a proton of energy E_i in the nucleus is calculated from σ_{pn}, σ_{pp}, the free proton–neutron and proton–proton cross sections:

$$l(E) = \frac{4\pi R^3}{3}[\alpha_{\mathrm{np}} N \sigma_{\mathrm{np}} + \alpha_{\mathrm{pp}} Z \sigma_{\mathrm{pp}}]^{-1} \qquad \ldots\ldots(5)$$

where α_{np} and α_{pp} are numbers smaller than unity allowing for the fact that on account of the Pauli principle some transitions are forbidden (Goldberger 1948, Cassels, Randle, Pickavance and Taylor 1951 b). All energies occurring in (4) are measured relative to a potential well of the same depth ($U_0 = 21$ MeV) as the one used in § 2. l_0 is calculated at the mean energy E_0 of the incident proton beam, but $l(E)$ is a slowly varying function of E over energy ranges of 10 to 20 MeV when E is of the order of 100 to 200 MeV. Apart from this simplification, we have, however, allowed properly for the energy spectrum of the proton beam, by using $\sigma_s(E_1)$. Eqn. (4) simplifies to

$$\sigma_1(E_1) = \frac{3N}{4}\frac{l_0}{R} f_1(E_0, E_1)\sigma_s(E_1), \qquad \ldots\ldots(6)$$

where
$$f_1(E_0, E_1) = \frac{2}{l_0}\int_0^1 \mu \, d\mu \int_0^{2R\mu} d\zeta \exp\left\{-\frac{2R}{l_1}\mu - \left(\frac{1}{l_0} - \frac{1}{l_1}\right)\zeta\right\} \qquad \ldots\ldots(7)$$

is the probability of making exactly one collision with the scattered neutron moving in the forward direction with energy E_1.

§ 4. MULTIPLE SCATTERING PROCESSES

Apart from the scattering processes considered in the last section there are two other types of processes to be considered.

Firstly, there are processes in which only one nucleon is ejected from the nucleus which remains in an excited state. On a shell model where the A lowest levels are all filled up and the spacing of levels corresponds to a mean binding energy of 8 MeV, such processes lead to ejected nucleons with energy within a few MeV of the incident proton energy. These processes are thus not of importance at more than 8 MeV below the proton energy. Furthermore it seems likely that their contribution to the cross section will not be large.

Secondly, there are multiple collision processes. As a result of a collision a high-energy particle will in general be deflected through only a small angle into a cone of not more than 40° half-angle, retaining most of its original energy. (In an exchange collision it will of course change from proton to neutron or vice versa.) The target particle will gain only a small fraction of this energy. As we are only interested in neutrons which are ultimately ejected in the forward direction with more than 60 MeV, this being the lowest observed energy, we shall throughout assume that only the high-energy component of a collision, scattered through not more than 40°, will lead to observable neutrons.

The calculation of multiple processes, i.e. processes in which the high-energy component makes several collisions before being ejected in the forward direction as neutron, is much more complicated than for single collision processes. For we must now also consider cases where the high-energy particle is deflected. We shall treat only double collisions, as adequate calculations for triple and higher order processes are very heavy and do not seem worth while in view of the rather crude model used. The effect of neglecting these processes will be discussed in § 5.

Double collisions in which a high-energy neutron is ejected can be subdivided into four groups according to the nature of the particles involved: (i) (p, p) collision followed by exchange (p, n) collision, (ii) direct (p, n) collision followed by exchange (p, n) collision, (iii) exchange (p, n) collision followed by (n, n) collision, (iv) exchange (p, n) collision followed by direct (p, n) collision. For definiteness we shall consider a process of the first class and then generalize our result to allow for all four possibilities.

Using the same coordinate system and notation as in § 3, suppose the first collision of the incident proton with a nuclear proton occurs at the same point P_1 as the single collision in § 3. Suppose $\sigma_{\mathrm{pp}}(E_0, \alpha; E_1)\, d\Omega_1\, dE_1$ to be the cross section for a proton with energy E_0 to be scattered through an angle α into a solid angle $d\Omega_1$, with energy in the range $(E_1, E_1 + dE_1)$, the velocity vector $\mathbf{v}_1$ of the scattered high-energy proton having polar angles α, β. Suppose the scattered proton, after travelling a distance s, makes a collision with a neutron in the volume element $s^2\, ds \sin\alpha\, d\alpha\, d\beta$ such that the neutron is scattered into a solid angle $d\Omega_2$ in the forward direction, with energy in the range $(E_2, E_2 + dE_2)$, the cross section for such a process being $\sigma_{\mathrm{pn}}{}^{\mathrm{x}}(E_1, \alpha; E_2)\, d\Omega_2\, dE_2$, and let ζ' be the distance this neutron has to go before leaving the nucleus. Then the cross section for processes of this group is given, analogously to (4), by

$$\begin{aligned}\sigma_2(E_2)\, dE_2\, d\Omega_2 = \int_{\theta=\pi}^{\pi/2} \int_{\zeta=0}^{-2R\cos\theta} \int_{\alpha=0}^{\pi/2} \int_{\beta=0}^{2\pi} \int_{s=0}^{s_0} \int_{E_1=0}^{\infty} \exp(-\zeta/l_0) \\ \times \left\{ 2\pi R^2 \sin\theta\, d\theta\, d\zeta \left[\frac{nZ}{A} \sigma_{\mathrm{pp}}(E_0, \alpha; E_1) \right] d\Omega_1\, dE_1 \right\} \frac{\exp(-s/l_1)}{s^2 d\Omega_1} \\ \times \left\{ s^2\, ds \sin\alpha\, d\alpha\, d\beta \left[\frac{nN}{A} \sigma_{\mathrm{pn}}{}^{\mathrm{x}}(E_1, \alpha; E_2) \right] d\Omega_2\, dE_2 \right\} \exp(-\zeta'/l_2).\end{aligned} \qquad \ldots\ldots(8)$$

The term $s^2\, d\Omega_1$ in the denominator allows for the divergence of the proton beam between the two collisions. The integration over s goes from $s = 0$ to $s = s_0$, corresponding to the point where the velocity vector $\mathbf{v}_1$ intersects the nuclear surface. In practice the ranges of integration of E_1 and α are restricted by conservation of energy considerations.

We obtain equations similar to (8) for processes of groups (ii), (iii) and (iv) with the appropriate factors replacing $[(nZ/A)\sigma_{\mathrm{pp}}(E_0, \alpha; E_1)]$ and $[(nN/A)\sigma_{\mathrm{pn}}{}^{\mathrm{x}}(E_1, \alpha; E_2)]$.

The quantities $\sigma_{\mathrm{pp}}(E_0, \alpha; E_1)$ etc. allow for the dependence on the energy E_0 of the incident particle and the resulting energy spread for the various processes. In § 2 we calculated this quantity for exchange (p, n) scattering for the case where the emitted neutron is ejected in the forward direction. In principle we should repeat this calculation for all the processes considered obtaining the angular distributions. Such a calculation is clearly not worth doing, and we have hence made several approximations and simplifying assumptions.

Firstly, we take for $\sigma_{\mathrm{pp}}(E_0, \alpha; E_1)$ (and similarly for the other cross sections)

$$\left.\begin{aligned}\sigma_{\mathrm{pp}}(E_0, \alpha; E_1) &= 4\cos\alpha\, \Sigma_{\mathrm{pp}}(E_0, 2\alpha)\, y(E_0\cos^2\alpha - E_1) \qquad && E_1 < E_0\cos^2\alpha \\ &= 0 && E_1 > E_0\cos^2\alpha\end{aligned}\right\} \qquad \ldots\ldots(9)$$

where $\Sigma_{pp}(E_0, 2\alpha)$ is the differential cross section in the centre-of-mass system for free (p, p) scattering through an angle 2α, and $y(x) = N^{-1}\sigma_s(E_0 - x)$ where σ_s is the function defined in §2, and N is a normalizing factor so chosen that $\int_{x=0}^{E_0} y(x)\,dx = 1$. The function $y(x)$ can be represented analytically to a very good approximation by an expression of the form $y = Ax^2 \exp(-\nu x)$, A and ν being constants.

We thus assume that a proton with initial energy E_0, scattered through an angle α, will have a maximum energy $E_0 \cos^2 \alpha$, corresponding to the free particle case. This is accurately true for $\alpha = 0$, and at high energies it is approximately true for deflected particles. Furthermore we assume the energy spread to be a function of $E_0 \cos^2 \alpha - E_1$ only, but otherwise independent of the angle α. Without carrying out the complete calculation this seems the best and simplest assumption. In practice one expects a larger energy spread for larger angles of deflection, but the error made by our assumption should not be too serious.

Secondly, it is desirable to introduce approximations in (8) so that all the integrations except that over α can be carried out analytically (for each value of E_2). For this purpose we take $E_1 = (E_0 - 25)\cos^2 \alpha$ in $\Sigma_{pn}{}^x(E_1, 2\alpha)$, which for $\alpha = 0$ reduces to $E_1 = E_0 - 25$, the mean energy of the scattered proton for the energy distribution (9), and in $l_1 = l(E_1)$ we take $E_1 = (E_0 E_2)^{1/2}$, corresponding to the case of free particle scattering. In (8) we put $\alpha = 0$ in s_0 and ζ'. This corresponds to assuming, for the purpose of calculating the fraction of particles making exactly two collisions, that they are not deflected. Again, this assumption will not introduce a large error as we are dealing with scattering directed strongly forward, and furthermore, the effects of inward and outward scattering from different regions of the nucleus roughly cancel out.

Finally, using the symmetry of Σ_{pn}, and the fact that Σ_{pp} (taken equal to Σ_{nn}) can be taken as constant over the energy range concerned, all cross sections can be replaced by either Σ_{pn} or Σ_{pp}. In this we have assumed, as in §2, that the experimental cross section corresponds entirely to ordinary or exchange scattering for small or large deflections respectively.

§ 5. RESULTS AND DISCUSSION

We have calculated the differential cross sections in the forward direction for neutrons with energy E of more than 60 Mev for single collision processes ($\sigma_1(E \geqslant 60)$) and for double collision processes ($\sigma_2(E \geqslant 60)$) for beryllium, carbon and aluminium. These values, as well as $\sigma(E \geqslant 60) = \sigma_1(E \geqslant 60) + \sigma_2(E \geqslant 60)$, are given in the table.

	Theoretical cross sections (millibarns per unit solid angle)			Experimental cross sections (millibarns per unit solid angle)	
Target element	$\sigma_1(E \geqslant 60)$	$\sigma_2(E \geqslant 60)$	$\sigma(E \geqslant 60)$	$2\frac{1}{2}°$	5°
Beryllium	55	11	66	91^{+45}_{-30}	99 ± 19
Carbon	56	12	68	47^{+23}_{-16}	72 ± 15
Aluminium	84	21	105	122^{+61}_{-41}	—

The last two columns give the experimentally measured differential cross sections (Cassels *et al.* 1951 a); the two columns refer to different methods of measurement and angles of observation of 2½° and 5° respectively. The calculated values correspond to 0°. The measurements at 5° are much more accurate than those at 2½°. In the latter there was some uncertainty as regards the absolute cyclotron current due to multiple traversal effects. In particular, the cross section for carbon should be multiplied by a factor 1·5 approximately, giving a differential cross section of 70 millibarns per unit solid angle.

The energy spectra $\sigma_1(E)$, $\sigma_2(E)$ for single and double scattering in the forward direction have also been calculated for Be, C, Al. These energy spectra, together with $\sigma(E)=\sigma_1(E)+\sigma_2(E)$, are plotted against E for beryllium in fig. 2. Curve *d* of fig. 2 gives the experimental curve, with ordinates adjusted so that the maxima of the two curves agree. Very similar curves were obtained for the other two elements, and we shall therefore only discuss this case.

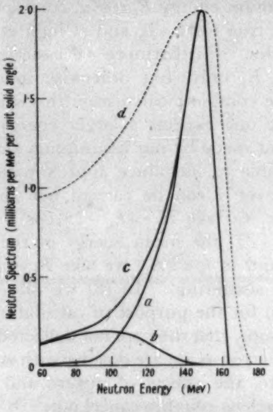

Fig. 2. Energy spectra of neutrons ejected in forward direction from beryllium as a function of the neutron energy E: *a*, single collision spectrum $\sigma_1(E)$; *b*, double collision spectrum $\sigma_2(E)$; *c*, $\sigma(E)=\sigma_1(E)+\sigma_2(E)$; *d*, experimental curve of Cassels *et al.*

As is seen from the table, the calculated differential cross sections are in fairly good agreement with experiment. The cross section for triple collisions one would expect to be of the same order as σ_2 though somewhat smaller. Cross sections for fourth order and higher collisions should become less and less important. We have also neglected transitions leading to excited nuclei, which should only matter for the high-energy end of the spectrum but hardly for the cross section. Thus, allowing for these processes will increase the cross section $\sigma(E\geqslant 60)$ by not more than 20%, so that the agreement persists.

As regards the energy spectrum, the intensity falls off too rapidly with decreasing energy, compared with experiment. At 100 Mev, where double collisions are most effective, the theoretical result is too small by a factor 4. This will be somewhat improved, but clearly not enough, by allowing for triple and higher collisions which lead to neutrons of lower energy.

The energy spectrum depends much more delicately on the nuclear model used than does the differential cross section. For the latter it suffices to take account of the screening effects etc. in an approximate way, otherwise using the free particle cross sections. The energy spectrum, however, depends very sensitively on the way the incident particle and the nucleus can exchange energy. Thus on our crude model better agreement is hardly to be expected.

But one can see how the model has to be changed. We considered a nucleus consisting of individual non-interacting particles. To obtain a broader energy-spectrum one requires strong interactions between the nucleons, as in a liquid drop, for example. During a collision energy can then be exchanged in a large number of ways, so that the nucleus can remain in a much more highly excited state than our assumptions would allow. That an independent nucleon model, for instance the model we have used, or a shell model, is inadequate for treating nuclear reactions, and that for these one must assume strong interactions between nucleons, has recently been pointed out by Weisskopf (1950).

ACKNOWLEDGMENTS

We should like to express our thanks to Drs. J. M. Cassels and T. G. Pickavance for discussions of their experiments, and to Dr. J. Howlett for kindly carrying out the computations. This work is published by kind permission of the Director, Atomic Energy Research Establishment, Harwell.

REFERENCES

Cassels, J. M., Randle, T. C., Pickavance, T. G., and Taylor, A. E., 1951 a, *Phil. Mag.*, **42**, 215; 1951 b, *Phil. Mag.*, **42**, 751.
Christian, R. S., and Hart, E. W., 1950, *Phys. Rev.*, **77**, 441.
Christian, R. S., and Noyes, H. P., 1950, *Phys. Rev.*, **79**, 85.
Fernbach, S., Serber, R., and Taylor, T. B., 1949, *Phys. Rev.*, **75**, 1352.
Goldberger, M. L., 1948, *Phys. Rev.*, **74**, 1269.
Serber, R., 1947, *Phys. Rev.*, **72**, 1114.
Weisskopf, V. F., 1950, *Helv. Phys. Acta*, **23**, 187.

The Frequency Spectrum of a Two-Dimensional Ionic Lattice*

By M. SMOLLETT
Physics Department, Imperial College, London

Communicated by M. Blackman; *MS. received* 19*th September* 1951

ABSTRACT. The frequency spectrum of a two-dimensional ionic lattice has been evaluated. A method is given for calculating the exact density of the spectrum at special points in phase space. Two logarithmic infinities, first found by Montroll using a quasi-elastic forces model, are confirmed for an ionic lattice. The bearing of these infinities on the interpretation of the second-order Raman spectra is discussed.

§ 1. INTRODUCTION

A KNOWLEDGE of the frequency spectrum is necessary for the calculation of those properties of a crystal which depend on the vibration of its constituent particles. A review of the investigations into the form of the spectrum has been given by Blackman (1941).

Montroll (1947) deduced an exact expression for the frequency spectrum of a two-dimensional square lattice; quasi-elastic forces were used, adjusted to give elastic isotropy. The exact analytic form of the spectrum had previously been unknown except for a one-dimensional lattice. Montroll found two infinities in the frequency spectrum which had appeared as finite peaks in earlier work because of the use of numerical methods. These infinities were further shown to arise generally with any type of quasi-elastic binding.

---

* This paper forms part of the thesis submitted to the University of London for the degree of Ph.D.

In this paper Montroll's work has been extended to a two-dimensional ionic lattice, similar in structure to the (100) face of a rock-salt crystal. The ions introduce long-range Coulomb forces. No analytic expression for the whole spectrum has been found, but a method for deducing the exact density of vibrations at special points is given. This method is valid in general for any type of force as well as Coulomb-law forces. The two infinite densities found by Montroll are confirmed for the spectrum of a square ionic lattice. Some new features arising in the phase-space contour maps and the frequency spectrum have also been described.

§ 2. THE CALCULATION OF THE PHASE-SPACE MAPS AND THE FREQUENCY SPECTRUM

The methods given by Blackman (1935 a, b) and Kellermann (1940) are used in this paper. The secular determinant is set up and a suitable set of frequencies is evaluated. These frequencies are then used to construct phase-space maps from which the frequency spectrum can be deduced.

These calculations have been performed for an ionic lattice of the type described in the introduction. The masses of the particles in the lattice are taken to be equal. This model would appear to require two particles per cell, i.e. the negative and positive ions; but if we assume the repulsive forces between any pair of particles to be independent of the type of particle, then the equations of motion are the same for each ion and only one particle per cell need be used.

We can write the vibrational equations of motion in a form similar to that given by Born (1923):

$$\left.\begin{aligned}(\omega^2 M + A_{xx})u_x + A_{xy}u_y &= 0,\\ A_{xy}u_x + (\omega^2 M + A_{yy})u_y &= 0.\end{aligned}\right\} \qquad \ldots\ldots(1)$$

In the above equation

$$A_{\alpha\beta} = \sum_{m_1 m_2} \Phi_{\alpha\beta}^{m_1 m_2} \exp\{-i\tau(\mathbf{r}_{m_1 m_2}\cdot\mathbf{s})\}. \qquad \ldots\ldots(2)$$

The unit vector $\mathbf{s}$ specifies the direction of propagation of a plane wave in the lattice; $\tau = 2\pi/\lambda$, where λ is the wavelength; $\omega = 2\pi\nu$, where ν is the frequency; u_x, u_y are the components of the amplitude of an ion in the reference cell; $|\mathbf{r}_{m_1 m_2}|$ is the distance of a particle from the reference cell. For a square lattice $\mathbf{r}_{m_1 m_2}{}^2 = x_{m_1}{}^2 + y_{m_2}{}^2$, where $x_{m_1} = m_1 r_0$ and $y_{m_2} = m_2 r_0$; r_0 is the distance between adjacent positive and negative ions and is taken to be 3 Å in the following calculations. The m_1, m_2 values are integral and range from $-\infty$ to $+\infty$. The potential energy between a particle at the point $\mathbf{r}_{m_1 m_2}$ and the particle in the reference cell is $\Phi^{m_1 m_2}$; $\Phi_{\alpha\beta}^{m_1 m_2}$ is the appropriate derivate of the potential energy, which is assumed to be of the usual form for alkali halides: $\Phi(r) = \pm e^2/r + \beta/r^9$, where the first term is the Coulomb potential between two ions (the sign of the term varies according to the charges). The second term is the repulsive potential energy; β is a constant. Full details of the method for calculating the value of A_{xx} and similar terms by means of Epstein zeta-functions have been given in a paper by Smollett and Blackman (1951).

The secular determinant for the frequencies follows immediately from equation (1) and is

$$\begin{vmatrix} 4\pi M\nu^2 + A_{xx} & A_{xy} \\ A_{xy} & 4\pi M\nu^2 + A_{yy} \end{vmatrix} = 0.$$

If we write $4\pi^2 M\nu^2 = f^2$ we have at once the quadratic equation

$$f^2 = \tfrac{1}{2}[-(A_{xx}+A_{yy}) \pm \{(A_{xx}-A_{yy})^2 + 4A_{xy}{}^2\}^{1/2}]. \qquad \ldots\ldots(3)$$

Now the boundary conditions of a cyclic lattice restrict the components of the phase vector to a discrete set ranging from 0 to π (see Born 1923). The phase components for the wave are $\tau r_0 s_x$ and $\tau r_0 s_y$, and the conditions become $\phi_1 = \tau r_0 s_x = a_x \pi / N$ and $\phi_2 = \tau r_0 s_y = a_y \pi / N$, where a_x, a_y are integers ranging from $-N$ to $+N$ and N is the total number of particles along the positive axis. This discrete variation of the phase components gives the correct number of normal modes, i.e. $8N^2$ in the secular determinant.

The $A_{\alpha\beta}$ now become functions of ϕ_1 and ϕ_2. Also, as we may regard f as a frequency measured in units of $1/2\pi M^{1/2}$, then by eqn. (3) the frequency is also a function of ϕ_1, ϕ_2. The variation of the frequency with the phases is plotted in figs. 1 (*a*) and 1 (*b*) in the form of a contour map. The two diagrams correspond to the upper and lower frequency branches given by the two roots in eqn. (3). The phase has been divided into units of $\pi/10$ and the frequency is given in units of $10^{11}e/2\pi M^{1/2}$.

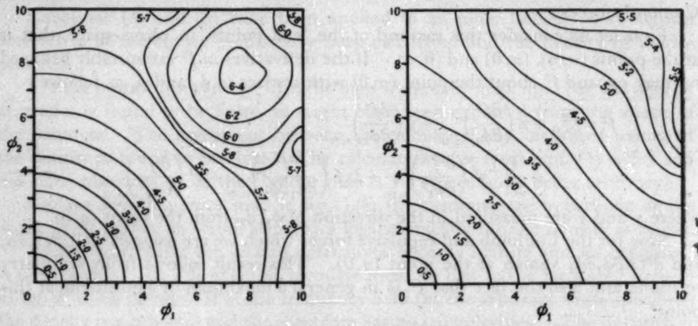

Fig. 1 (*a*). The upper-frequency contour map. Fig. 1 (*b*). The lower-frequency contour map.
The frequency values are marked on the contours in units of $10^{11}e/2\pi M^{1/2}$; ϕ_1 is in units of $\pi/10$.

The frequency spectrum has been constructed from the contour maps. The spectra of the low- and high-frequency branches are shown in fig. 2 together with the complete spectrum. The units of density are arbitrary; the units of frequency have been given. The position of the infinities is indicated by lines. A description of the features of these diagrams is given later.

§ 3. THE DENSITY OF THE SPECTRUM AT SPECIAL POINTS AND MONTROLL'S WORK

Montroll (1947) has discussed the nature of the frequency spectrum of a two-dimensional square lattice with the masses of the particle equal and quasi-elastic forces between them. Montroll obtained an explicit formula for the frequency spectrum in the special example where the binding constants gave elastic isotropy. This formula involved the integration of the expression for the density of normal modes. If $g(f)$ is the density of modes for a frequency f then

$$g(f)=\frac{1}{4\pi^2}\frac{\partial}{\partial f}\iint d\phi_1\,d\phi_2,$$

where the double integral is taken over all portions of the phase-space map in which the frequency is less than f. The result of the integration was expressed in terms involving complete elliptic integrals.

The density function confirmed the general appearance of the spectrum found by Blackman (1935 b); but it also showed the important feature that the peaks in the spectrum were actually logarithmic-type infinities. Montroll proved as well that for quasi-elastic forces in a square lattice two logarithmic infinities would arise generally in the spectrum, one infinity belonging to the low-frequency spectrum and the other to the high-frequency spectrum. Montroll deduced this last result by a method of approximation that would appear to be useful for quasi-elastic forces only.

The main purpose of this paper is to extend Montroll's work to Coulomb forces. The density of the spectrum has been found at a number of special points depending on the features of the contour lines in phase-space. The method which is developed here can be used for any type of force provided that the first three derivatives of f^2 with respect to ϕ_1 and ϕ_2 are continuous and finite. The two logarithmic infinities found by Montroll have also been found for Coulomb forces.

First let us consider this method at the 'end points' in phase-space, that is at the points (π,π), $(\pi,0)$ and $(0,\pi)$. If the derivatives of f^2 are suitably behaved we may expand f^2 about the point $(\pi,0)$ with respect to ϕ_1 and ϕ_2 as follows:

$$\begin{aligned}f^2=f^2_{\pi,0}&+x\left(\frac{\partial f^2}{\partial\phi_1}\right)_{\pi,0}+y\left(\frac{\partial f^2}{\partial\phi_2}\right)_{\pi,0}\\&+\frac{1}{2!}\left\{x^2\left(\frac{\partial^2 f^2}{\partial\phi_1^2}\right)_{\pi,0}+2xy\left(\frac{\partial^2 f^2}{\partial\phi_1\partial\phi_2}\right)_{\pi,0}+y^2\left(\frac{\partial^2 f^2}{\partial\phi_2^2}\right)_{\pi,0}\right\},\end{aligned}$$

where x and y are measured in the direction of ϕ_1, ϕ_2 from the point $(\pi,0)$.

Now for the Coulomb and repulsive forces which we are using $\partial f^2/\partial\phi_1$, $\partial f^2/\partial\phi_2$ and $\partial^2 f^2/\partial\phi_1\partial\phi_2$ vanish at the point $(\pi,0)$. This result follows from symmetry relations and also the fact that f^2 is in general a maximum or a minimum at this point.

If we put $f^2_{\pi,0}=A$, $\tfrac{1}{2}(\partial^2 f^2/\partial\phi_1^2)_{\pi,0}=B$, $\tfrac{1}{2}(\partial^2 f^2/\partial\phi_2^2)_{\pi,0}=C$, where B and C are assumed to be positive, then, neglecting higher order terms, we find for a contour of frequency f close to $(\pi,0)$ that $f^2=A+Bx^2+Cy^2$, giving $x=B^{-1/2}[(f^2-A)-Cy^2]^{1/2}$. Now in the equation for the density,

$$g(f)=\frac{1}{4\pi^2}\frac{\partial}{\partial f}\iint d\phi_1\,d\phi_2,$$

we may replace $\iint d\phi_1\,d\phi_2$ by $\iint dx\,dy=\int_0^{y_1}x\,dy$,

where y_1 is small and is the value of ϕ_2 where the chosen contourc uts this axis. Using the approximation for x given above we have

$$\begin{aligned}g(f)&=\frac{1}{4\pi^2}\frac{\partial}{\partial f}\int_0^{y_1}\frac{1}{B^{1/2}}[(f^2-A)-Cy^2]^{1/2}\,dy\\&=\frac{1}{4\pi^2}\frac{f}{(BC)^{1/2}}\int_0^{y_1}\left[\frac{f^2-A}{C}-y^2\right]^{-1/2}dy=\frac{1}{4\pi^2}\frac{f}{(BC)^{1/2}}\sin^{-1}\frac{y_1C^{1/2}}{(f^2-A)^{1/2}}.\end{aligned}$$

Then with this result we may find the exact value of $g(f)$ at the point $(\pi, 0)$ by letting x and y tend to zero.

If $x=0$ and $y_1 \to 0$ then $y_1 C^{1/2}/(f^2-A)^{1/2} \to 1$ and we have

$$g(f)=f/8\pi(BC)^{1/2}. \qquad \ldots\ldots(4)$$

This result is true for a contour that tends to an elliptical shape like that shown in the $(\pi, 0)$ corner in fig. 1 (*a*). If the contour is hyperbolic as in fig. 1 (*b*), at the $(\pi, 0)$ corner, then the equation for f^2 becomes $f^2=A-Bx^2+Cy^2$. Proceeding as before, we have

$$g(f)=\frac{1}{4\pi^2}\frac{f}{(BC)^{1/2}}\int_0^{y_1}\left[\frac{A-f^2}{C}+y^2\right]^{1/2} dy.$$

Integrating, we find

$$g(f)=-\frac{f}{4\pi^2(BC)^{1/2}}\ln\left(\frac{A-f^2}{C}\right)^{1/2}+\text{a constant term.} \qquad \ldots\ldots(5)$$

If $f^2 \to A$ then $g(f) \to \infty$.

The density in this example rises to a logarithmic infinity. This method is justified because the large contribution to the density near $(\pi, 0)$ allows us to approximate to the rest of the contour.

The results in eqns. (4) and (5) are the same as those obtained by Montroll. The equations deduced here, however, can be applied to any type of force at a point in phase-space where the contours have the necessary elliptical or hyperbolic form.

Equations (4) and (5) have been applied to an ionic lattice. The second derivatives at the corner points have been calculated and the density of modes deduced.

For the points $(0, \pi)$ and $(\pi, 0)$ in the high-frequency map, fig. 1 (*a*), the density of modes is found to be finite, as might have been expected from the shape of the contours. The agreement between the calculated and measured values of the density is found to be close. The calculated value from eqn. (4) is 5·9 and the value measured from the contour map is 5·8 (these units being arbitrary).

For the low-frequency map in fig. 1 (*b*) the contours are hyperbolic at the $(0, \pi)$, $(\pi, 0)$ points, and from eqn. (5) a logarithmically infinite density is found.

At the (π, π) point the second derivatives become infinite and an expansion is not possible. In this example recourse must be had to the measured density in fig. 2 which shows that at the frequency 5·45 (in the arbitrary units specified) the density is a constant and the spectrum has no irregularities. The derivatives were investigated at the (π, π) point for a general potential law $1/r^n$. It was found that the second derivatives approach infinity as n tends to 2. For all values of n less than 2 the derivatives are infinite and no expansion can be made. The density can be shown, by means of eqn. (5), to approach $y \ln y + D$ as $n \to 2$ where $y \to 0$ as the (π, π) point is approached; D is a constant. The density thus becomes a constant and not an infinity when $n \to 2$.

The density was also investigated in the region of the high-frequency contour map, fig. 1 (*a*), where the contour lines form closed curves. The density where the curves converge to apoint is found to be a constant of value 9·6, in agreement with the measured value of the density, which is 9·7. No unusual features arise here.

The one other region where the density can be gauged is the region lying between the contour lines 5·7 and 5·8 in the high-frequency spectrum. In this region the contours can be seen to be approaching a saddle-point whose exact position cannot easily be found directly. However, at a saddle-point we know that contour lines become hyperbolic. In accordance with our analysis in eqn. (5), we know that hyperbolic contours will give rise to a logarithmic infinity in the frequency spectrum as long as the second derivatives are finite. Examination of the second derivatives shows that these can only become infinite at the point (π, π), but not at any other point. So we may conclude that between the frequencies 5·7 and 5·8 the spectrum has a logarithmic infinity. This conclusion is substantiated by the pronounced maximum shown in the measured value of the density.

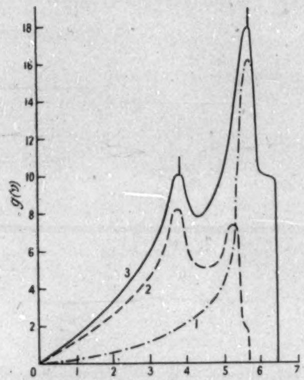

Fig. 2. The vibrational spectrum of a two-dimensional ionic lattice.

1—Upper-frequency branch. 2—Lower-frequency branch. 3—Resultant curve giving the complete spectrum. ν is in units of $10^{11}e/2\pi M^{1/2}$; $g(\nu)$ is in arbitrary units.

§ 4. DETAILS OF THE PHASE-SPACE MAPS AND THE FREQUENCY SPECTRUM

The contour maps for a lattice with Coulomb forces differ in appearance from those found by Montroll using quasi-elastic forces. The main difference in the high-frequency map, fig. 1 (*a*), is the existence of a peak-like prominence in the three-dimensional space of ϕ_1, ϕ_2 and f, rising to a maximum frequency of 6·45 and lying on the diagonal. This frequency is the highest in the upper-frequency branch and is also the highest frequency of the lattice. In quasi-elastic force models the highest and lowest frequencies lie on a corner point in phase space. This peak is a general feature of the contour map, and it has been calculated that the position of the peak varies very little with the variation of the repulsive power law. The peak is not found for quasi-elastic forces.

The low-frequency contours also have their highest frequency at a point other than the phase-space corners. It occurs at the points $(\pi, 0{\cdot}6\,\pi)$ and $(0{\cdot}6\,\pi, \pi)$. In the region of the (π, π) point the contours split to form saddle-back surfaces in the three-dimensional space described. This phenomenon does not occur for quasi-elastic forces.

The complete spectrum in plotted in fig. 2. The positions of the two logarithmically infinite peaks are indicated by vertical lines. The chief difference from Montroll's work is a subsidiary peak at the frequency 5·25 in the low-frequency spectrum. This peak is not infinite as there are no 'saddle-back' contours in the region of the contour map giving rise to this maximum.

§ 5. CONCLUSION

The infinite peaks found in the frequency spectrum are important in the Raman effect in crystals. We may conclude from Blackman's work on lattices (1935 b, 1937) that the frequency spectrum of three-dimensional crystals will be similar to the spectrum of two-dimensional crystals: in fact the spectra of ionic crystals calculated by Kellermann (1940) and Iona (1941) show a strong resemblance to the spectrum of the two-dimensional ionic lattice shown in fig. 2. In the spectrum of a three-dimensional ionic crystal two steep peaks are found which we may expect by analogy to correspond to infinite densities, though this has not been proved. These peaks will give rise to steep narrow maxima associated with a continuous background in the second-order Raman spectrum. This spectrum was first observed by Fermi and Rasetti (1931). Born and Bradburn (1947) gave a detailed theoretical account of these maxima using Kellermann's data (1940) to construct the theoretical spectrum.

ACKNOWLEDGMENTS

The author wishes to express his thanks to Dr. Blackman for suggesting this problem and for his constant interest and advice during the course of the work. The author wishes also to thank the Department of Scientific and Industrial Research for a maintenance grant.

REFERENCES

Blackman, M., 1935 a, *Proc. Roy. Soc.* A, **148**, 365, 384; 1935 b, *Ibid.*, **149**, 117, 126; 1937, *Ibid.*, **159**, 416; 1941, *Rep. Prog. Phys.*, **8**, 11 (London : Physical Society).
Born, M., 1923, *Atomtheorie des festen Zustandes*, 2nd Ed. (Leipzig and Berlin : Teubner).
Born, M., and Bradburn, M., 1947, *Proc. Roy. Soc.* A, **188**, 161.
Fermi, E., and Rasetti, F., 1931, *Z. Phys.*, **71**, 689.
Iona, M., 1941, *Phys. Rev.*, **60**, 822.
Kellermann, E., 1940, *Phil. Trans. Roy. Soc.* A, **238**, 513.
Montroll, E., 1947, *J. Chem. Phys.*, **15**, 575.
Smollett, M., and Blackman, M., 1951, *Proc. Phys. Soc.* A, **64**, 683.

The Rotational Analysis of the (0,0) and (0,1) Bands of the $^7\Pi \rightarrow {}^7\Sigma$ System of Manganese Deuteride

By T. E. NEVIN, M. CONWAY* and M. CRANLEY
Physics Department, University College, Dublin

MS. received 11*th May* 1951; *read at Science Meeting at Belfast* 6*th July* 1951

ABSTRACT. The band spectrum of manganese deuteride has been photographed at a dispersion of 1·25 Å/mm. The heads of the (0,0) and (0,1) bands of the $^7\Pi \rightarrow {}^7\Sigma$ system are at λ5703·7 Å and λ6073·3 Å. respectively. It has been possible to make a rotational analysis of the two bands. The constants of the final state have been derived from the analysis and the fine structure resulting from the interaction of spin and rotation has been studied. The $^7\Pi$ state is perturbed and the terms have been evaluated from the term expressions for the final state and the wave numbers of the P, Q and R branches. The results throughout are in good agreement with the results for the corresponding bands in the spectrum of manganese hydride.

---

* Miss Conway's part of the work was completed at Dunsink Observatory.

§ 1. INTRODUCTION

The band spectrum of manganese hydride, first investigated by Heimer (1936) and Gaydon and Pearse (1937), consists of a number of very complex bands distributed through the visible spectrum. Three of these bands degraded to shorter wavelengths, with 'heads' at 5683 Å, 6209 Å and 5206 Å, are respectively the (0,0) and (0,1) and (1,0) bands of a single system the rotational structure of which has been studied by Nevin (1942, 1945) and Nevin and Doyle (1948), to be referred to as I, II and III respectively, who have shown that the bands involve a transition from a $^7\Pi$ to a $^7\Sigma$ state*. A diagram showing the principal branches for this type of transition is given in I. Each band contains seven P, seven Q and seven R branches, six ^{O}P branches and six ^{S}R branches, which with other satellite branches bring the total of branches observed in the (0,0) band to fifty.

The spin fine structure of the $^7\Sigma$ state is well resolved and is determined mainly by the interaction of the resultant spin S with the rotation of the molecule. The $^7\Pi$ state as shown by the lines missing at the origin of certain branches is normal, and the appearance at low values of K, of N, O and S branches, shows that at low quantum numbers the state tends to case *a*. At high quantum numbers it tends to case *b*. In both the vibrational levels $v'=0$ and $v'=1$ the lower rotational levels are perturbed in a regular manner from their expected positions. The effect of this perturbation on the appearance of the P_1 branch of the (0,0) band can be seen very clearly in the reproduction of this band in I. The lines of the branch appear to be converging to a head at 5683 Å, but instead of turning back again to shorter wavelengths in the usual way, diverge again to longer wavelengths.

Because of the very small number of bands of multiplicity higher than three recorded in the literature it appeared worth while to photograph the spectrum of manganese deuteride, especially as a rotational analysis of the $^7\Pi \rightarrow {^7\Sigma}$ transition should be possible.

§ 2. EXPERIMENTAL

The discharge tube used to produce the spectrum is a modification of the design of tube used by Pearse and Gaydon (1938) in their work on manganese hydride. It consists of a Pyrex tube 50 cm long, 3·5 cm internal diameter, with three side tubes (see figure). A brass cap A waxed over one end carries two water-cooled terminals sheathed along their lengths with close-fitting Pyrex tubes. A spiral B of 12–16 turns of tungsten wire of diameter 1 mm is wound round an alumina capillary 7·5 cm long, 4 mm internal diameter, with a wall thickness 1·5 mm. The ends of the spiral fit into holes drilled in the water-cooled terminals and are held in

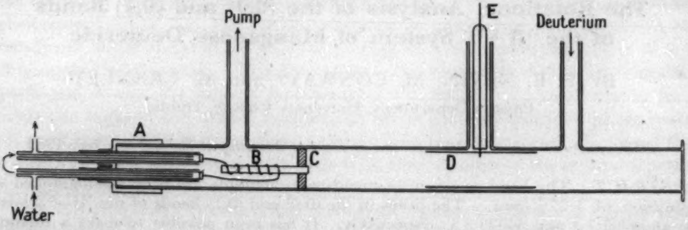

---

* In *The Identification of Molecular Spectra* (Pearse and Gaydon 1941 and 1950) the transition is recognized as $^7\Pi \rightarrow {^7\Sigma}$.

place by set screws. One end of the capillary fits snugly into a hole in the centre of a steel disc C 6 mm thick which fits fairly closely inside the Pyrex tube.

The tungsten spiral forms one electrode of the discharge tube. The second electrode D is formed by a sheet of nickel 10 cm long bent into a cylinder sprung into the Pyrex tube. Connection to the cylinder is made by a tungsten wire E sealed into a capillary tube which sheaths it along its length. This capillary is waxed into the middle side tube of the discharge tube. The other side tubes serve as inlets for the deuterium and outlet to the Hyvac pump used to evacuate the discharge tube. The discharge tube is placed in a wooden box through which water flows, the open end projecting through a hole in the side of the box with the joint made watertight. This open end of the tube is closed by a window fastened on with sealing wax. Before sealing on the window, five or six small pieces of pure manganese metal of total mass 0·2 – 0·3 gramme are introduced into the capillary tube and uniformly spaced along the part of the tube surrounded by the tungsten spiral.

When a discharge is passed, the steel disc, as in Pearse and Gaydon's tube, constrains the discharge to pass through the capillary, which becomes very hot. Additional heat is supplied by passing a current up to 50 amp through the tungsten spiral by means of a 15 v transformer joined to the water-cooled terminals. This heating current can be varied by a resistance in the primary. The use of auxiliary heating for the capillary is advantageous as it enables the temperature of the capillary to be varied within limits independently of the discharge current. The discharge current used in the experiments was usually about 1·5 amp, obtained from the secondary of a 3 000 v transformer.

At the beginning the tube was cleared by a discharge current gradually raised to 1·5 amp with the tube connected to the pump. After about twenty minutes' running the pressure became too low for the transformer to maintain the discharge. Deuterium gas stored in a two-litre flask was allowed to enter the tube through a needle valve. By proper adjustment of the pressure the nickel electrode could be made red hot, and this helped further to outgas the tube. By raising the pressure with a current of 30–40 amp through the spiral and a discharge current of 1·2–1·4 amp the manganese deuteride spectrum could be made to appear strongly. Under the best conditions the discharge converged from the nickel electrode to the mouth of the capillary in the form of a cone. At too high a pressure the discharge tended to pass from the nickel electrode to the tungsten spiral between the edge of the steel disc and the wall of the Pyrex tube. During a run deuterium gas was allowed to flow slowly through the tube, the rate of outflow to the pump being reduced to conserve gas and the rate of inflow adjusted to maintain the proper conditions for the appearance of the spectrum.

Although a considerable number of photographs were obtained, the tube cannot be regarded as entirely satisfactory. Owing to the necessity of allowing for expansion due to heating, the steel disc cannot be made too close a fit in the Pyrex tube. The small gap between the wall and the disc was increased by deviations of the Pyrex tube from cylindrical form, and occasionally, while adjustments were being made to obtain the best conditions, the discharge would strike through this gap, leading to fracture of the tube in a few seconds. The average life of a number of tubes was thirty-five minutes, the individual lives ranging from two minutes to two and a half hours. In each case the life was terminated by fracture at the steel disc. Another source of trouble was failure of the alumina capillaries by cracking or puncture. Quartz discharge tubes did not prove satisfactory. They were not sufficiently cylindrical, and two specimens we had constructed tapered outwards from the ends to the centre, so that a steel disc which would enter fitted too loosely in the central part.

In the course of the experiments the region 3800 Å to 6200 Å was photographed in the second order of the 21-ft. grating in this laboratory at a dispersion of 1·25 Å/mm. Ilford Special Rapid panchromatic plates were used for the range 6200–4600 Å and Ilford Special Rapid plates for 4600–3800 Å. The panchromatic plates were hypersensitized by bathing for two minutes in a 0·5% solution of triethanolamine and drying rapidly with a fan. This procedure increased the red sensitivity by a factor of two and the green sensitivity by a factor of one half. The 75 cm long plate holder enabled a range of 900 Å to be photographed in one exposure at a particular setting of the grating. The exposures varied between fourteen and forty-five minutes.

Each of the two bands with which the present paper is concerned was measured on two plates, one of moderate intensity to give good resolution of close strong lines and one of high intensity to show weak lines. The plates were measured with respect to second and third order I.A.U. standard iron lines and additional iron lines, the wavelengths of which were taken from the M.I.T. tables.

The intensities of the lines are eye estimates checked against a microphotometer trace and large-scale prints of the bands. The microphotometer trace has also been used to check visual estimates of the resolution of very close groups of lines. Both bands are very well resolved in the second order. In the (0,1) band three greatly over-exposed Mn lines, λ6013·5, λ6016·5, λ 6021·8, fall on the early part of the Q branches and on the middle part of the P branches but, beyond masking a single P and single Q line in some components, do not interfere with the analysis. The deuterium oxide used to prepare the deuterium gas was of 99% purity, but the intensity of the MnH bands is about 10% that of the MnD bands, presumably due to occluded hydrogen. In the circumstances the intensity of the MnH bands is satisfactorily low and, though increasing the labour of measuring the plates, did not add to the difficulty of the analysis.

§ 3. ANALYSIS OF THE BANDS

Inspection of a twenty-fold enlargement of the plates of the (0,0) band shows a head at 5703·7 Å (17 527·5 cm^{-1}), heads at 5699·7 Å (17 540 cm^{-1}) and 5696·1 Å (17 551 cm^{-1}) and a complex group of lines at 5693·1 Å (17 560 cm^{-1}), all of which were considered to be ^{O}P heads. In the region 17 570 cm^{-1} to 17 610 cm^{-1} the P_1 branch and its satellite $^{P}Q_{12}$ can be picked out on the prints. From 17 600 cm^{-1} to 18 500 cm^{-1} the band is very complex and without any apparent regularities. Because of the closer rotational structure which corresponds to the higher moment of inertia, the occurrence of groups of seven to fourteen lines which had been observed in MnH at a distance of some hundreds of wave numbers from the heads is not evident in MnD.

Rough calculations based on the isotope effect showed that at high rotational quantum numbers the separation of the lines of the Q and R branches should be about two-thirds of the corresponding separation in MnH and that the second wave number differences of successive lines in a branch should be about 0·4 cm^{-1}.

Corresponding R and P branches are related by the combination difference

$$\Delta_2 F_i''(K) = F_i''(K+1) - F_i''(K-1) = R_i(K-1) - P_i(K+1). \quad \ldots\ldots(1)$$

The spin fine structure of the $^7\Sigma$ state causes $\Delta_2 F_i''(K)$ to decrease slightly with increasing i from component to component, but the effect is small, so that one can write

$$\Delta_2 F''(K) = (4B_v + 6D_v)(K+\tfrac{1}{2}) + (8D_v - 34H_v)(K+\tfrac{1}{2})^3 + 12H_v(K+\tfrac{1}{2})^5. \quad \ldots\ldots (2)$$

The known values of the constants B, D and H for MnH and the well-known relations connecting the values of corresponding constants for isotopic molecules enabled the values of $\Delta_2 F''(K)$ to be calculated for MnD.

Starting about 18 400 cm^{-1} a search was made by trial and error for series of strong lines of the expected separation, decreasing to lower wave number in arithmetical progression, and eventually twelve such series or branches were found. These twelve branches could be divided into two sets, one containing seven and the other five branches, tentatively assumed to be Q and R branches, because at a few hundred wave numbers from their beginning the separation of the lines of each of the branches in each set was practically identical, while the separation in the R set was two wave numbers greater than in the Q set. The two remaining R branches were found subsequently.

The R branches were tentatively numbered R_1, R_2, R_3 etc. in order of increasing frequency at high quantum numbers. Successive values of K starting with $K=0$ were given to the R_1 branch, and eqn. (1) was used in conjunction with the calculated values of $\Delta_2 F''(K)$ to calculate the P_1 branch. The correct numbering was obtained when the wave numbers of the calculated branch agreed closely with the P_1 branch already picked out on the enlargements. Once the correct numbering of the R_1 branch had been found, the numbering of the other R branches was evident, and the corresponding P branches were readily calculated and the lines picked out on the enlargements and in the wave number tables.

The $^P Q_{i,i+1}$ branches are the high-frequency satellites to the P_i branches with the numbering of each line the same as that of the adjacent P_i line. The $^P Q_{12}$ branch is particularly clear. It is first resolved from the P_1 branch for $K=6$, the separation being 0·18 cm^{-1}, and can be traced to about $K=25$, where the separation is 0·44 cm^{-1}. For convenience the separation of adjacent lines in a P_i and $^P Q_{i,i+1}$ branch is denoted by $\Delta f''_{i,i+1}(K) = F_i''(K) - F''_{i+1}(K)$. To number the Q branches and obtain the $^O P$ branches the relation

$$\Delta_2 F''_{i+1}(K) = Q_i(K-1) - {}^O P_{i,i+1}(K+1) + \Delta f''_{i,i+1}(K-1) \qquad \ldots\ldots (3)$$

was used with an approximate allowance for $\Delta f''_{i,i+1}(K-1)$. The procedure was similar to that used to correlate the R and P branches. The $^O P_{12}$ branch forming a head at 17 526·5 cm^{-1} represents the start of the band and is very clear. The $^S R$ branches were found by the relation

$$\Delta_2 F_i''(K) = {}^S R_{i+1,i}(K-1) - Q_{i+1}(K+1) + \Delta f''_{i,i+1}(K+1). \qquad \ldots\ldots (4)$$

Substantial $^N P_{13}$ and $^N P_{24}$ branches have been identified. All of the $^N P_{13}$ and a considerable part of the $^N P_{24}$ branch lies beyond the $^O P_{13}$ head in a region free from overlapping lines of other branches. The lines of the branches can be calculated from the expressions $^N P_{i,i+2}(K) = {}^P Q_{i,i+1}(K-2) - \Delta_2 F''_{i+2}(K-1) + \Delta f''_{i+1,i+2}(K-2)$, the identification of the lines in the calculated positions giving a valuable check on the correctness of the analysis of the components $^7\Pi_{-2} \rightarrow {}^7\Sigma$ and $^7\Pi_{-1} \rightarrow {}^7\Sigma$ at low values of K.

The study of the (0,1) band was undertaken when the analysis of the (0,0) band was fairly complete, and the details do not require comment. The $^O P_{12}$ branch has a head at 16 461 cm^{-1} (6073·3 Å). From about 16 500 cm^{-1} the lines are closely spaced, and this dense region continues for some hundreds of wave numbers. The Q and R branches can be traced right back to the start of the (0,0) band.

When the analysis of the two bands had been carried as far as possible, the combination differences were tabulated in the form used for MnH in I. To save printing, the tables of the wave numbers of the branches and combination differences have not been reproduced in this paper* as they can be reconstructed from the wave-number tables. In the final checking of the analysis and in tracing the branches to the lowest values of K the relations in eqns. (3) and (4) are very useful. Because of the nature of the fine structure, $\Delta f''_{i,i+1}(K)$ is nearly independent of i, and it is correct to write ${}^{S}R_{i+1,i}(K-1)-Q_{i+1}(K+1)=Q_i(K-1)-{}^{O}P_{i,i+1}(K+1)$.

These expressions furnish twelve sets of differences very nearly equal to one another in each band and slightly smaller than the true $\Delta_2 F''_i(K)$ values. Since

$$\begin{aligned}\Delta_2 F'_{ia}(K)=F'_{ia}(K+1)-F'_{ia}(K-1)&={}^{S}R_{i,i-1}(K-1)-Q_i(K-1)+\Delta f''_{i-1,i}(K-1)\\&=Q_i(K+1)-{}^{O}P_{i,i+1}(K+1)+\Delta f''_{i,i+1}(K+1),\end{aligned}$$

the values of ${}^{S}R_{i,i-1}(K-1)-Q_i(K-1)$ and $Q_i(K+1)-{}^{O}P_{i,i+1}(K+1)$ should be closely the same for a particular component in both bands as they have a common initial state.

The various tables were systematically examined for disagreements and discrepancies. Any discrepancy exceeding 0·15 cm^{-1} was specially studied. In some cases one of the lines involved was a blend or was diffuse because of imperfect resolution. In some cases the wrong line had been chosen. The structure of the bands is much closer than in MnH and the branches go to higher rotational quantum numbers. Moreover, though the MnH bands appear weakly on the plates, a number of lines, because of their great intensity in MnH, are moderately strong. These factors mean that there is more blending and overlapping of lines, and although the inherent accuracy of measurement is the same as on the MnH plates, the actual wave numbers are not quite so accurate in parts of the bands, especially where the density of the lines is very great. The large number of lines on the plates makes it difficult in some cases to determine the exact end-point of the branches, a line of low intensity being followed by a strong line which by chance coincides with the next line of the branch in question. For the same reason it is difficult to be certain of the ${}^{R}Q$ branches which lie in a crowded region of the band. A number of intensity irregularities may be attributed to the same cause.

The analyses of both bands are internally consistent and consistent with each other and with the MnH bands. It has not been found possible to trace the branches of the inner components to the values of K at which for a normal $^7\Pi$ state they should begin. At low values of K the lines of the branches become weak and it is difficult, if not impossible, to be sure of the correct assignments. In addition, it is possible that because of systematic perturbations the lines deviate more and more from their expected positions. It is possible to make assignments of lines but not possible to exclude the possibility that agreements in the combination differences are due to chance. It does seem, however, that a number of fairly strong ${}^{O}P$ lines belonging to the inner components are present on the plates of lower K values than are given in the tables, but in the absence of combination differences correct identifications cannot be made.

---

* A limited number of copies of the wave-number tables are available upon application to the authors or to the offices of the Physical Society.

§4. DISCUSSION OF THE INITIAL AND FINAL STATES

The spin fine structure of $^7\Sigma$ states is discussed in II. In MnH effects due to spin–spin interactions are negligible and the observed structure is determined almost completely by the interaction of the resultant spin S with K in accordance with the quantum-mechanical cosine rule

$$f_i(K, J-K) = \tfrac{1}{2}\gamma[J(J+1) - K(K+1) - S(S+1)],$$

where $J = K+3$ for $f_1 \ldots J = K-3$ for f_7. The separation of adjacent components of a rotational level is given by

$$\Delta f_{i,i+1}(K) = (4-i)\gamma + \gamma K, \qquad \ldots\ldots(5)$$

and increases linearly with K. Consideration of the experimental data for MnD suggests that, because of blending, the most accurate data on the fine structure should be obtained from $\Delta f_{i,i+1}(K) = {}^P\mathrm{Q}_{i,i+1}(K) - \mathrm{P}_i(K)$, ignoring the results given by the other possible expressions.

The observations in the (0,0) band are fairly complete and, within the limits of observational error, the slopes of the straight lines obtained by plotting $\Delta f_{i,i+1}$ against K are identical and yield a value 0·0141 cm^{-1} for γ. As in MnH, the expression for the constant term in equation (5) is not completely confirmed by experiment. The disagreement is undoubtedly due to the spin–spin interaction. The data for the (0,1) band are much less accurate and extensive but yield a value 0·0145 cm^{-1} for γ.

It was shown in II that $\Delta_2 F_4''(K+\frac{1}{2})$ is given accurately by eqn. (2), and this relation has been used to calculate B_v'', D_v'' and H_v'' by the method already used for MnH. The final values of B_v'' and D_v'' were calculated by the method of least squares.

The agreement of the term values derived from

$$F_i''(K) = B_v''K(K+1) + D_v''K^2(K+1)^2 + H_v''K^3(K+1)^3 + \tfrac{1}{2}\gamma[2K(4-i) + (i-8)(i-1)]$$

has been compared with the experimental values derived from $\Delta_2 F_i''(K)$ for $F_1''(K)$, $F_4''(K)$ and $F_7''(K)$. While in MnH very good agreement was obtained for $F_4''(K)$, the difference between the experimental and the calculated values for $F_1''(K)$ and $F_7''(K)$ increased in proportion to K^2 to about 0·5 cm^{-1} at $K = 35$, the difference being positive for F_1 and negative for F_7. This discrepancy was attributed to a dependence of the fine-structure constant γ on K and could be removed by assuming $\gamma = \gamma_0(1+\mu K)$. In MnD satisfactory agreement between experimental and calculated term values is obtained throughout for a constant value of γ, and if any dependence of γ on K exists it is too small to be detected.

Using the calculated term values of the $^7\Sigma$ state, the terms of the $^7\Pi$ state can be calculated from the expressions

$$F_{ib}(K) = \mathrm{R}_i(K-1) + F_i''(K-1) = \mathrm{P}_i(K+1) + F_i''(K+1)$$

and

$$F_{ia}(K) = \mathrm{Q}_i(K) - F_i''(K).$$

These terms are given in table 1. The Λ doubling for the seven components defined by $\Delta\nu_{iba} = F_{ib}(K) - F_{ia}(K)$ can be obtained at once from the term values.

For multiple states intermediate between case *a* and case *b*

$$\tfrac{1}{7}\sum_{i=1}^{i=7} \Delta_2 F_i(J) = (4B_v + 6D_v)(J+\tfrac{1}{2}) + 8D_v(J+\tfrac{1}{2})^3 + 12H_v(J+\tfrac{1}{2})^5. \qquad \ldots\ldots(6)$$

To reduce the effect of the Λ doubling $\Delta_2 F_i(J)$ is taken as the mean of $\Delta_2 F_{ib}(J)$ and $\Delta_2 F_{ia}(J)$. In spite of the perturbation of the $^7\Pi$ state, the mean of the seven values

Table 1. Term Values for $^7\Pi$ State $v' = 0$

K	$^7\Pi_{-2}$		$^7\Pi_{-1}$		$^7\Pi_0$		$^7\Pi_1$		$^7\Pi_2$		$^7\Pi_3$		$^7\Pi_4$	
	$F_{1b}(K)$	$F_{1a}(K)$	$F_{2b}(K)$	$F_{2a}(K)$	$F_{3b}(K)$	$F_{3a}(K)$	$F_{4b}(K)$	$F_{4a}(K)$	$F_{5b}(K)$	$F_{5a}(K)$	$F_{6b}(K)$	$F_{6a}(K)$	$F_{7b}(K)$	$F_{7a}(K)$
	17543·41													
0	556·69	17556·87												
1	575·10	574·90												
2	597·62	597·88	17637·80	17635·94										
3	625·45	625·81	660·61	659·71										
4	658·50	658·89	690·05	689·02										
5	696·50	697·37	724·90	724·53										
6	740·31	741·32	765·55	765·58										
7	789·70	790·87	812·68	812·57										
8	844·85	846·19	865·23	865·79										
9	905·92	907·41	924·27	924·97		17939·16								
10	972·90	974·53	989·56	990·51		18003·47								
11	18045·92	18047·66	18061·29	18062·28		074·05				18088·36	18089·14			
12	124·90	126·88	139·06	140·38	18149·87	151·09	18157·31	18158·93		163·66	165·32		18163·15	18163·70
13	210·08	211·97	223·12	224·51	233·35	234·40	240·59	241·43		246·05	248·11	18247·18	246·90	247·03
14	301·23	303·28	313·42	314·91	322·93	324·14	329·95	330·88	18334·35	335·44	337·05	336·47	336·88	336·85
15	398·54	400·64	409·92	411·50	418·87	420·15	425·50	426·44	430·02	430·39	432·49	432·01	432·93	432·46
16	501·90	503·99	512·61	514·32	521·11	522·50	527·37	528·29	531·75	532·08	534·20	533·84	535·01	534·22
17	611·35	613·54	621·50	623·20	629·50	630·82	635·51	636·43	639·69	640·04	642·31	641·84	642·96	642·28
18	726·84	729·00	736·45	738·16	744·08	745·40	749·85	750·73	753·90	754·19	756·40	755·97	757·23	756·48
19	848·37	850·56	857·51	859·23	864·78	866·10	870·31	871·15	874·38	874·55	876·69	876·29	877·76	876·79
20	975·82	978·09	984·61	986·35	991·52	992·89	996·90	997·73	19000·76	19000·96	19003·20	19002·66	19004·21	19003·22
21	19109·27	19111·53	19117·64	19119·48	19124·32	19125·66	19129·54	19130·35	133·29	133·46	135·69	135·10	136·75	135·68

22	248·60	250·93	256·68	258·48	263·14	264·47	268·15	268·93	271·83	271·94	274·24	273·57	275·31	274·18
23	393·88	396·13	401·59	403·41	407·86	409·21	412·77	413·50	416·33	416·32	418·75	417·99	419·78	418·54
24	544·90	547·26	552·41	554·24	558·44	559·80	563·25	563·93	566·77	566·73	569·09	568·29	570·21	568·85
25	701·70	704·08	708·96	710·81	714·90	716·19	719·50	720·20	722·94	722·88	725·33	724·39	726·43	724·94
26	864·55	866·55	871·29	873·13	877·06	878·31	881·59	882·14	884·84	884·79	887·30	886·26	888·46	886·86
27	20032·55	20034·79	20039·40	20041·11	20044·96	20046·15	20049·37	20049·92	20052·72	20052·48	20054·90	20053·91	20056·16	20054·44
28	206·38	208·66	213·06	214·78	218·55	219·63	222·82	223·35	226·39	225·78	228·56	227·15	229·18	227·71
29	385·80	388·10	392·33	394·03	397·62	398·76	401·93	402·32	405·14	404·72	406·33	405·08	408·56	406·62
30	570·73	572·95	576·96	578·79	582·20	583·43	586·48	586·87	589·41	589·20	591·87	590·49	593·04	590·99
31	761·12	763·28	767·45	768·99	772·39	773·46	776·48	776·90	779·58	779·05	781·78	780·43	783·06	780·88
32	956·86	959·07	963·02	964·55	967·99	968·95	972·01	972·22	975·05	974·44	977·30	975·72	978·49	976·15
33	21157·88	21160·14	21163·83	21165·53	21168·79	21169·80	21172·76	21173·03	21175·78	21175·18	21177·93	21176·40	21179·15	21176·88
34	364·30	366·27	370·09	371·57	374·94	375·77	378·80	378·91	381·48	381·03	383·95	382·23	385·20	382·63
35	575·71	577·71	581·42	582·86	586·15	587·00	589·99	590·10	593·01	592·18	595·07	593·29	596·27	593·69
36	792·26	794·23	797·87	799·31	802·53	803·21	806·34	—	809·21	808·38	811·42	809·51	812·59	809·86
37	22013·75	22015·81	22019·21	22020·80	22023·98	22024·68	22027·64	22027·68	22030·55	22029·64	22032·68	22030·80	22033·88	22031·10
38	240·34	242·29	245·81	247·14	250·36	251·06	254·06	253·92	256·89	255·84	258·98	256·97	260·21	257·24
39	471·73	473·65	477·12	478·41	481·62	482·26	—	485·10	488·07	487·03	490·08	488·08	491·38	488·35
40	707·95	709·84	713·28	714·62	717·71	718·30	721·32	721·08	724·10	722·92	726·15	723·97	727·40	724·26
41	948·87	950·64	954·14	955·37	958·51	959·04	962·07	961·76	—	963·61	966·86	964·57	968·12	964·88
42	23194·47	23196·32	23199·66	23200·88	23203·95	23204·47	23207·45	23207·22	23210·22	23208·84	23212·19	23209·94	23213·48	23210·19
43	444·61	446·43	449·69	450·87	453·97	454·40	457·44	457·05	460·18	458·80	—	459·75	463·42	460·01
44	699·18	700·93	704·21	705·35	708·44	708·84	711·86	711·41	714·56	713·18	716·53	714·09	717·75	714·31
45	958·15	959·82	963·15	964·21	967·31	967·66	970·68	970·19	973·35	971·90	975·35	972·82	976·60	973·02
46	24221·46	24223·12	24226·38	24227·40	24230·48	24230·78	24233·82	24233·31	24236·45	24234·95	24238·42	24235·87	24239·62	24236·04
47	488·92	490·58	493·77	494·78	497·81	498·10	501·18	500·58	503·78	502·24	505·69	503·10	506·92	503·27
48	760·51	762·14	765·33	766·27	769·33	769·56	772·63	—	775·24	773·63			778·35	774·63
49	25036·12	25037·74	25040·87	—	—	25045·06	25048·46	25047·49	25050·69	25049·07			25053·83	25050·06
50	315·70	317·25	320·45	25321·30	25324·39	324·56	328·27	326·86	330·14	328·44			333·24	329·39

of $\Delta_2 F_i(J)$ from $J=14$, the lowest value observed for all components, to $J=45$, the highest value observed, agrees remarkably well with eqn. (5). However, in view of the perturbations, it is not certain that the constants have their usual meaning, and their values have been determined graphically.

In the absence of theoretical expressions with which to compare the terms it is difficult to discuss adequately the overall distortion of the $^7\Pi$ state especially as it has not been found possible to trace the branches to such low values of K as in MnH. A comparison of table 1 with the corresponding table 2 for MnH in II indicates that the general character of the perturbations is similar in the two cases. In particular a distortion of the P_1 branch occurs similar to that in MnH, but not of so marked a character. The lines are closest together about $K=7$ but, instead of forming a head, diverge again to longer wavelengths.

Table 2. Molecular Constants derived from the (0,0) and (0,1) Bands of the $^7\Pi \rightarrow {}^7\Sigma$ Transition in MnD

	$v''=0$	$v''=1$
B''_v (cm^{-1})	2·86959	2·81427
D''_v (cm^{-1})	$-7{\cdot}9514 \times 10^{-5}$	$-8{\cdot}2212 \times 10^{-5}$
H''_v (cm^{-1})	$1{\cdot}41 \times 10^{-9}$	$2{\cdot}17 \times 10^{-9}$
2γ (cm^{-1})	0·0141	0·0145

$B''_e = 2{\cdot}89725$ cm^{-1}, $D''_e = -7{\cdot}8165 \times 10^{-4}$ cm^{-1}, $\alpha''_e = 0{\cdot}05532$ cm^{-1},
$\beta''_e = 0{\cdot}2698 \times 10^{-4}$ cm^{-1}, $H''_e = 1{\cdot}03 \times 10^{-9}$ cm^{-1}, $\gamma''_e = 0{\cdot}76 \times 10^{-9}$ cm^{-1},
$I''_e = 9{\cdot}6598 \times 10^{-40}$ g.cm^2, $r''_e = 1{\cdot}7234 \times 10^{-8}$ cm.

Initial state $v'=0$:

$$B_0' = 3{\cdot}244 \text{ cm}^{-1},\ D_0' = -9{\cdot}51 \times 10^{-5} \text{ cm}^{-1},\ H_0' = 1{\cdot}2 \times 10^{-9} \text{ cm}^{-1}.$$

The constants of the initial and final states derived from the rotational analysis are collected in table 2. It is well known (Herzberg 1950) that for deuterides and hydrides the spectroscopically determined value of ρ^2, the ratio of the reduced mass of XH to XD, is greater than the value determined from the atomic masses.

For MnH and MnD, $\rho^2 = B_e(\text{MnD})/B_e(\text{MnH}) = 0{\cdot}50959$, while the value determined from the atomic masses is 0·50932.

REFERENCES

Gaydon, A. G., and Pearse, R. W. B., 1937, *Nature, Lond.*, **139,** 590.

Heimer, T., 1936, *Naturwiss.*, **24,** 521.

Herzberg, G., 1950, *Molecular Spectra and Molecular Structure*, Vol. I—*Band Spectra of Diatomic Molecules*, 2nd Edn., p. 164.

Nevin, T. E., 1942, *Proc. Roy. Irish Acad.*, **48,** 1; 1945, *Ibid.*, **50,** 123.

Nevin, T. E., and Doyle, P. G., 1948, *Proc. Roy. Irish Acad.*, **52,** 35.

Pearse, R. W. B., and Gaydon, A. G., 1938, *Proc. Phys. Soc.*, **50,** 201.

The Excitation and Intensity Distribution of CH Bands in Flames

By R. A. DURIE
Department of Chemical Engineering, Imperial College, London

Communicated by A. G. Gaydon; *MS. received* 10*th July* 1951

ABSTRACT. An apparent selective excitation to the $v'=1$ level of the CH 3900 Å ($^2\Sigma^- \rightarrow {}^2\Pi$) system occurs in hydrogen flames containing small amounts of organic compounds since the (1, 0) and (1, 1) bands are abnormally strong. This is accompanied by a suppression of the usual predissociation in this system. An additional band of this system, the (1, 2) at 4494·5 Å has been observed for the first time.

The suppression of the CH predissociation is interpreted as showing that conditions in hydrogen flames approach thermal equilibrium. The appearance of the CH predissociation in normal flames indicates that the excitation is not thermal.

§ 1. INTRODUCTION

ALTHOUGH CH, together with C_2 and OH, bands form the strongest feature of the spectra of all hydrocarbon–oxygen (and air) flames the mechanism of the formation and excitation of the CH and C_2 radicals is unknown (Gaydon 1950).

Under normal flame conditions where CH is excited, only the (0, 0) bands of two different systems appear. The 4315 Å (0, 0) CH band is always the strongest and arises from a $^2\Delta \rightarrow {}^2\Pi$ transition. The 3872 Å (0, 0) CH, due to a $^2\Sigma^- \rightarrow {}^2\Pi$ transition, is also reasonably strong. In very hot flames (i.e. oxyacetylene) the 3628 Å (1, 0) and the 4025 Å (1, 1) bands of the CH 3900 Å ($^2\Sigma^- \rightarrow {}^2\Pi$) system (which has (0, 0) head at 3872 Å) also appear; under these conditions the 3143 Å CH ($^2\Sigma^+ \rightarrow {}^2\Pi$) band may also appear weakly (Gaydon 1948, p. 44).

During an investigation of the spectra of hydrogen–air flames containing small amounts of the fluorocarbons, the C_2 and CH (and other) bands were observed but there appeared to be an apparent selective excitation to the $v'=1$ level of the 3900 Å CH system since the (1, 0) and (1, 1) bands were unusually strong (Plate, (*a*)). The same effect was also observed when small amounts of carbon tetrachloride, methyl iodide or ethylene were added to a hydrogen–air flame. The phenomenon thus appeared to be a characteristic of the hydrogen flame rather than of the organic additives.

This effect has been subjected to a detailed investigation and the results together with a possible explanation are given in this paper.

§ 2. EXPERIMENTAL

The change in the spectra of flames of both ethylene and acetylene with both air and oxygen has been studied as the hydrocarbon is gradually replaced by hydrogen. During this replacement the total mixture strength, defined by λ, was kept constant. λ is the ratio of the amount of oxygen actually used to that required for complete combustion of the total fuel (i.e. hydrocarbon + hydrogen); $\lambda = 1$ for a stoichiometric mixture, $\lambda < 1$ for a fuel-rich mixture and $\lambda > 1$ for a weak mixture. These experiments were carried out for a wide range of λ.

The spectra of hydrogen–oxygen flames containing small amounts of methane, hexane, benzene, methyl alcohol, acetone and acetic acid have also been studied.

All flows were measured using capillary type flowmeters. A quartz Smithell's flame separator was used for the air flames and an oxyacetylene welding burner for the oxygen flames.

The spectra were photographed on a Hilger E518 Raman spectrograph (aperture f/4) using both the quartz and glass trains. Large dispersion plates were obtained with a quartz Littrow spectrograph.

To obtain an estimate of the relative intensity of the (0, 0) and (1, 1) bands the plates were calibrated using a tungsten strip lamp and rotating stepped sector.

§ 3. RESULTS AND DISCUSSION

Vibrational Intensity Distribution in the CH 3900 Å *System*

For the hydrogen–ethylene–air flame the high excitation of the (1, 0) and (1, 1) CH bands only occurs for low ethylene concentrations in rich mixtures (i.e. λ low). The effect does not set in suddenly, but gradually appears as λ and the ethylene concentration are reduced, becoming noticeable with 3% ethylene (expressed as a percentage of the total fuel, i.e. hydrocarbon plus hydrogen) and $\lambda = 0{\cdot}4$; it is strongest at approximately 1·5% ethylene at $\lambda = 0{\cdot}4$. It is observed for all ethylene concentrations less than 3% when λ is less than 0·4 until eventually the ethylene concentration is too small to give an inner cone and therefore no C_2 or CH appear at all.

In the hydrogen–ethylene–oxygen flame the effect is apparent when λ is less than 0·4 and ethylene concentration not greater than 2%. Similar results have been obtained in the hydrogen–oxygen flames when acetylene, methane, benzene, acetone or acetic acid are used.

Under conditions where the (1, 1) and (1, 0) CH bands are strongest an additional red-degraded band appears with head at 4495·5 Å (see Plate, (*b*)). This band appears to be the R head of the previously unknown (1, 2) band of the 3900 Å CH system since it gives a value of $x_e''\omega_e'' = 62{\cdot}5$ and $\omega_e'' = 2844$ in good agreement with the values already known for the CH ground state (Herzberg 1950, p. 518). The appearance of this band provides further evidence of the high excitation to the $v' = 1$ level.

An estimate of the relative intensity of the (0, 0) and (1, 1) band in a hydrogen–ethylene–air flame (2% C_2H_4, $\lambda = 0{\cdot}4$) gives the intensity of the (1, 1) band as being approximately one quarter the intensity of the (0, 0) band.

Suppression of the CH Predissociation

When flames showing the above effect are studied under higher dispersion (i.e. with Raman glass spectrograph) the high excitation to the $v' = 1$ level is found to be accompanied by an unusual appearance of the rotational structure of the CH 3872 Å (0, 0) band (see Plate, (*b*)).

In the usual discharge and arc sources and in normal flames the 3900 Å CH system exhibits a well-marked predissociation (Gaydon 1948) in the (0, 0), (1, 0) and (1, 1) bands. Each branch in the rotational structure remains normal in intensity until a certain K' value beyond which the next line becomes diffuse and faint and the branch suddenly stops. Under these conditions the last observed line is usually $K' = 17$ for (0, 0) and $K' = 7$ for the (1, 0) and (1, 1) bands (Shidei

1936). However, in the hydrogen flames studied the predissociation does not set in and the branches extend to higher K' values. Lines up to $K' = 20$ in the (0, 0) band and $K' = 13$ in the (1, 0) and (1, 1) bands appear (Plate, (*c*)).

Interpretation

Predissociation may be observed in emission when the excited state of a molecule is being depopulated by radiationless transitions, either to an unstable state whose potential energy curve intersects the potential energy curve of the stable excited state, or, as appears to be the case for the $^2\Sigma^-$ state of CH, by a quantum-mechanical passage through a potential barrier (i.e. tunnel effect). All lines in a band arising from levels above the point where these radiationless transitions begin will therefore tend to be considerably weaker or even entirely absent (for full treatment of the theory of predissociation see Herzberg 1950, p. 405).

When thermal equilibrium exists the number of molecules predissociating in the upper state will be balanced by the formation of new molecules in this state by the inverse process and the intensity of the spectral lines in emission will be unaffected although the levels affected by predissociation will be broadened by the lack of rigid quantization. Therefore the weakening of lines arising from the predissociated levels immediately shows that the excitation of the spectrum is not of a thermal nature.

We are therefore led to conclude that conditions in very rich hydrogen flames (where CH predissociation is suppressed) more nearly approach thermal equilibrium and the CH is excited thermally when small amounts of organic compounds are introduced. The unusually high intensity of the (1, 0), (1, 1) bands and the appearance of the (1, 2) band occur because the $v' = 1$ level is now populated according to the Boltzmann distribution law. However, since the vibrational transition probabilities for CH are not known, it is not possible to determine the relative intensity of the CH bands to be expected at the flame temperatures (assuming thermal equilibrium) for comparison with the observed relative intensities.

This conclusion is in complete agreement with the observation that the radiation in the (0, 0) OH band is probably thermal in origin in the oxy-hydrogen flame (Gaydon 1948, p. 30). Further, the rotational temperature of the OH (0, 0) band in low pressure oxy-hydrogen flames is around 2300° K compared with a theoretical flame temperature of 2500° K (Gaydon and Wolfhard 1948).

The Excitation of CH in other Flames

The observation of the CH predissociation in normal hydrocarbon–air and hydrocarbon–oxygen flames shows that the CH is not excited thermally. This supports the observations of Gaydon and Wolfhard (1949) that in low pressure flames the CH has an abnormally high translational temperature; this has led these authors to favour excitation by collision with some active species in the flame (rather than a true chemiluminescence since the rotational temperature is approximately normal).

The gradual setting in of the suppression of the results of predissociation when the hydrocarbon is replaced by hydrogen suggests that at some stage the CH excitation is occurring by at least two competing processes, i.e. thermal and the usual hydrocarbon mechanism. The thermal excitation gradually becomes predominant at low hydrocarbon concentrations and for low values.

Gaydon and Wolfhard (1951) have shown that the reaction zones of most organic flames exhibit abnormally high electronic excitation temperatures since when iron carbonyl is introduced lines in the Fe spectrum requiring at least 173 kcal/mole for their excitation appear. This abnormal excitation does not extend into the interconal gases, or the mantle that is often present around the inner cone in rich flames. This caused them to suggest that these mantles are probably in thermal equilibrium. However, a study of the CH bands emitted by the mantles in oxyacetylene and oxyethylene flames shows that the predissociation is observed as in the reaction zone. This shows that thermal equilibrium has not been fully established. Further evidence for this is provided by Lewis and von Elbe (1943) who have observed that temperatures measured by the sodium-line reversal method exceed the theoretical temperatures for this region of the flame for rich mixtures of fuel with oxygen.

§4. CONCLUSION

On the basis of this work it seems that observations on the predissociation in CH when organic substances are introduced into flames may provide a simple method of determining if thermal equilibrium has been established.

ACKNOWLEDGMENTS

The author would like to express his thanks to Dr. A. G. Gaydon for many helpful discussions during this work. He is also indebted to the Australian Department of Supply for a scholarship.

REFERENCES

Gaydon, A. G., 1948, *Spectroscopy and Combustion Theory*, 2nd Edition (London : Chapman & Hall); 1950, *Quart. Rev. Chem. Soc.*, **4**, 6.

Gaydon, A. G., and Wolfhard, H. G., 1948, *Colloq. Internat. du Centre Nat. Rech. Scient., Paris*, **16**, 129; 1949, *Proc. Roy. Soc.* A, **199**, 89; 1951, *Ibid.*, **205**, 118.

Herzberg, G., 1950, *Spectra of Diatomic Molecules*, 2nd Edition (New York: Van Nostrand).

Lewis, B., and von Elbe, G., 1943, *J. Chem. Phys.*, **11**, 75.

Shidei, T., 1936, *Jap. J. Phys.*, **11**, 23.

The Domain Structure of a Silicon–Iron Crystal

By L. F. BATES and C. D. MEE*
University of Nottingham

MS. received 9th August 1951

ABSTRACT. Powder patterns have been obtained on the (100) and (011) surfaces of a carefully shaped single crystal of 3% silicon–iron, of dimensions 13 mm × 6 mm × 6 mm, and these have permitted a more thorough quantitative test of proposed ferromagnetic domain structures than has been made hitherto. The patterns on the (011) surface are very beautiful and complicated. Although the measurements of domain spacings on both planes under Mode III magnetization conditions, as well as measurements of the angles between the domain vectors and main domain boundaries, confirm the essential features of the main structure proposed by Néel, there are found considerable numerical discrepancies which are attributed to the complicated nature of the closure domains on the (011) surface.

§1. INTRODUCTION

In this communication we give an account of a careful examination of the domain structure of a single crystal of silicon–iron by the powder pattern technique. In essentials, this technique is a kind of field plotting in which the coarse iron filings of one's student days are replaced by the fine particles in a colloidal solution of magnetite. When a drop of this solution is placed upon the carefully polished surface of a single crystal of a ferromagnetic metal, in general the colloidal particles settle upon the surface to form patterns which are sometimes called Bitter figures (Bitter 1931) and which are easily photographed using a metallurgical microscope with bright field illumination. In the papers by Williams, Bozorth and Shockley (1949) and by Bates and Neale (1950) full accounts of the method of preparation of the solution and necessary photographic procedure are given. Consequently, we deal here only with certain improvements which have been effected in the course of the present work.

The technique has provided much new information concerning the domain structure of ferromagnetic crystals. Very beautiful figures and convincing interpretations of certain characteristic patterns, such as 'fir-tree' patterns, have been given by Bozorth and his colleagues, while attempts at quantitative measurements have been made by Williams and Shockley (1949) and by Bates and Neale. In particular, the latter workers studied the powder patterns on the surface of a silicon–iron single crystal strip which was (approximately) a (100) plane, in which the [110] axis was (approximately) parallel to the long axis of the strip. This closely approaches the case which was studied theoretically by Néel (1944), and for which he suggested the domain structure shown in fig. 1 (*a*) when no field, or only a very weak one, is applied along the [0$\bar{1}$1] direction.

In fig. 1 (*a*) the main domains are leaf-shaped sections with their planes perpendicular to the [0$\bar{1}$1] axis and their magnetization vectors alternately directed along the [001] and [0$\bar{1}$0] directions. In addition, there are postulated certain closure, or antiparallel, q domains, in order to reduce the very high magnetostatic energy which would otherwise arise from the presence of free poles distributed along the sides of the specimen.

---

* Now with The Steel Company of Wales Ltd., Lysaght Works, Newport.

When a small (effective) field acts upon the crystal parallel to the $[0\bar{1}1]$ direction, we have the onset of what Néel terms Mode III magnetization (see Bates 1950, 1951 b) and the domain structure suggested is that of fig. 1 (*b*). The magnetization vectors of the main domains now turn inwards to make an angle θ which is a function of the effective field H with the $[0\bar{1}1]$ axis. At the same time there appears a new set of closure domains, the so-called parallel, p domains, which are magnetized as shown in fig. 1 (*b*).

It is the latter case which gives the possibility of a quantitative check of the domain theory, since Néel proved that for a single crystal of pure iron the domain period represented by the distance D, which is the thickness of a pair of successive domains, is given by $D=[\gamma L(W_{\mathrm{p}}+W_{\mathrm{q}})/W_{\mathrm{p}}W_{\mathrm{q}}]^{1/2}$, where γ is the energy per cm^2 of a domain wall or boundary between successive domains, L is the width of the strip specimen, and W_{p} and W_{q} are respectively proportional to the energies in erg/cm^3 required to change the directions of magnetization of the main domains to those of the p and q domains. W_{p} and W_{q} are therefore functions of θ, which in turn is a function of H. It is therefore possible to plot a graph of the theoretical values of D against H.

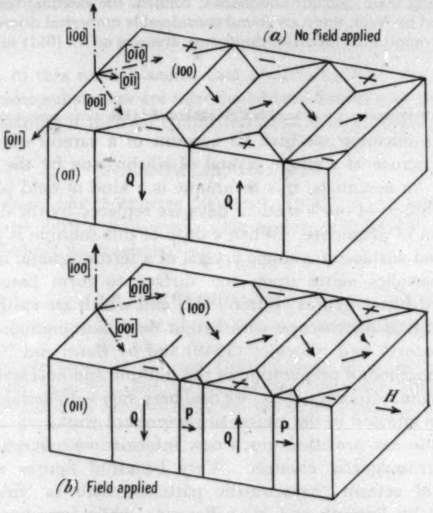

Fig. 1. Domain structures proposed by Néel.

Bates and Neale (1949, 1950) made a large number of measurements of D and H, and their work undoubtedly provided much evidence for the essential correctness of Néel's views, but it was incomplete in certain respects. For example, they had to use thin strips of single crystal specimens of silicon–iron made from transformer sheet material, whereas the Néel theory was given for the case of a thick crystal of pure iron. Consequently, when it was found that a predicted minimum in Néel's (D, H) curve was not found in the experiments, it was natural to conclude that the excessive thinness of the specimens was the cause of the lack of agreement. The magnetic anisotropy coefficients of pure iron and of silicon–iron are not sufficiently different to be regarded as a main cause of the lack of agreement, particularly as the anisotropy constant enters into the expression for D as $K^{-1/4}$. But, of course, the excessive thinness of the material meant that it was impossible to shape the specimen so that the surface was exactly a (100) plane. Moreover, there was no appreciable [110] face on the specimens, whose edges were rounded by mechanical and electrolytic polishing, thus making the closure domain surfaces semicircular instead of plane, so that additional magnetostatic energy could arise from free poles on them. In any case, at low fields the width of a q domain is of the same order as its depth, hence for free poles to be maintained on its ends much energy would be required. Indeed, it almost looks *a priori* as if the periodicity of the whole primary domain structure might be profoundly affected by accidental blemishes on the edges of the specimen. It was therefore clear that to obtain more reliable quantitative results thick crystals had to be used and their surfaces more ideally shaped than heretofore.

§ 2. EXPERIMENTAL TECHNIQUES

An excellent ingot of 3% silicon–iron some 7 cm long and about 1 cm in diameter was kindly presented to us by Dr. D. Shoenberg. It contained about six large single crystals and the largest of them was cut from the ingot by means of a rock cutting machine, a rapidly rotating diamond-impregnated disc which could be pressed very gently against the metal to give minimum strain, the metal being water cooled during cutting.

After etching to reveal [100] planes, the approximate orientation of the crystal with respect to the specimen faces was measured with a two-circle goniometer as in the work of Bates and Neale. The surfaces were then ground parallel to the desired crystal planes to within some 3°. This was done by mounting the crystal in a brass face-plate with sealing wax. The orientation of the crystal with respect to the mount was calculated from the goniometer readings and the required crystal plane was then set parallel to the face-plate, by placing the face to be ground on another face-plate whose setting with respect to the first face-plate could be adjusted with a micrometer. The crystal was then ground parallel to the first face-plate. When four sides had been ground in this way, the specimen had as its longest direction the $[0\bar{1}1]$ direction, and as sides the (100) and (011) planes, and the following treatment permitted us to cut the crystal surfaces parallel to crystal planes to within some half a degree.

A surface grinder was modified to grind off layers of 0·0005 in. maximum thickness per cut, in order to minimize strains in the specimen. The same replaceable crystal mount was used in the grinder and in an X-ray goniometer. After a flat surface had been ground on the crystal, the deformed surface layer was removed by a rapid electropolish, and the two X-ray photographs, necessary for computing the angles between the surface and the crystal plane measured about two axes of rotation on the surface grinder, were taken. The specimen was then replaced in the surface grinder and rotated through the known angles to bring the crystal plane parallel to the grinding surface. The new surface was then ground parallel to the desired crystal plane, and its orientation checked by another X-ray examination. This procedure was also carried out for the

.A
5
2

(100) face and the (011) face; the other two sides of the crystal were then ground parallel to these planes, and the ends of the crystal perpendicular thereto. The final dimensions were 13 mm × 6 mm × 6 mm, approximately.

Following the final grinding, the cold-worked surface metal was removed by electrolytic polishing in which great care was taken to avoid rounding the crystal edges by mounting the specimen in a polystyrene mould. It was found necessary to use a special type of polishing cell with a rotating anode and an electrolyte with a slower polishing action than that used by Bates and Neale. (In later forms of the apparatus used at Nottingham both anode and cathode are rotated.) A special bridge (Bates and Mee 1950) was devised for the automatic measurement of the resistance of the cell during polishing. This was particularly important as we obtained best surfaces with the non-explosive chromic acid–acetic acid bath (800 cm^3 glacial acetic acid, 38 cm^3 distilled water and 150 g chromium trioxide), for which the conditions for maximum anode film thickness are rather critical. The usual polishing time was about 20 minutes. After polishing, the specimen was washed in commercially pure alcohol and dried in a hot air blast. The specimen was then annealed for one hour at 1 100° C *in vacuo*.

§ 3. RESULTS

Bozorth and his colleagues found that the patterns observed on a surface of a demagnetized silicon–iron crystal give conclusive information concerning the inclination of the surface to a true (100) crystal plane. We obtained many excellent 'tree' pattern photographs during the initial grinding of the specimen and from them we were able to make valuable deductions about the inclination of the surface and to satisfy ourselves of the correctness of Bozorth's interpretation of such patterns. Considerations of space prevent their reproduction here, and although some of the patterns allowed us to deduce, for example, that in some cases of large inclination the mechanism of the change from Mode I to Mode III magnetization consisted of elongated 'tree' branches growing deep into the crystal by 90° boundary displacements and by the elimination of 180° domains by 180° boundary displacements, attention will be confined to a few of the patterns on the more perfectly ground surfaces only.

In fig. 2 (*a*) (Plate I) are reproduced the patterns found near the edge of the (100) plane when an effective field of 8 Oe, sufficient to produce the two-phase structure of fig. 1 (*b*), is applied in the $[0\bar{1}1]$ direction. A marked decrease in domain width occurred with an increase in field of only 2 Oe; incidentally, the effective field was always measured directly with a small magnetic potentiometer. The reason for the heavy deposits of colloid was that the crystal surface was inclined at an angle of about 2° to one easy direction of magnetization, the $[0\bar{1}0]$ direction, and so free poles were formed. However, the [001] direction was in the surface and therefore closure domains magnetized along the latter direction are colloid-free and show up sharply against the black background. Alternate domains magnetized in the [001] direction have upon them streaks of colloid perpendicular to the direction of magnetization. The patterns are similar to the 'tree' patterns of the second type observed by Bozorth for small inclinations of the surface to the (100) plane. However, nearer the edge the surface inclination is greater and branches are formed at angles of 45° to the main domain boundaries. These branches, in turn, have small secondary branches, and it is possible to give a relatively simple diagram of this structure.

Similar patterns with 71° walls have been observed (Yamamoto and Iwata 1951, see also Bates and Wilson 1951) near the edge of a (110) plane of nickel where the main domain structure has 71° walls corresponding to the 90° walls of iron.

When the surface approached still more closely, within 0·5°, to a (100) plane, the two-phase structure of fig. 2 (*a*) had no closure domains. Fig. 2 (*b*) shows the pattern on a specially chosen part of the final surface where the striations of colloid—perpendicular to the directions of magnetization—show up well, but no colloid has settled on the domain boundaries. We think that this is due to the effective field having a vertical component in opposition to the local field of the domain boundaries in this region, so preventing the attraction of colloid particles to them.

In figs. 2 (*c*) and 2 (*d*) are reproduced low magnification photographs of the line patterns observed on the (100) and (011) planes with moderate fields. We made many quantitative measurements with such photographs and the results are described below. Attention is now directed to the complicated structure of the individual lines of fig. 2 (*d*). The spacing between successive lines on the (011) plane was identified with the period of the main structure; quantitative measurements are described later. In higher fields the lines under low magnification have the appearance of doublets, but under high magnification the doublets are seen to be a complicated secondary structure which grows in size as the magnetization is increased. Incidentally, 'doublets' were previously observed by Kaya (1934) on a (110) surface of iron magnetized along a $[1\bar{1}0]$ direction, and probably represented a similar structure.

In fig. 3 (Plate II) is reproduced a set of high magnification pictures of the complicated structures for effective fields ranging from 13 to 110 Oe along the $[0\bar{1}1]$ direction. It was found that as the field was increased the complicated domains at first increased in width, and then multiplication of the pattern occurred by a new set of these domains suddenly shooting across the surface. To make room for this new set, the existing structures were reduced in width so that the new distribution was uniform. In fig. 3 (*d*) is shown a wide pattern about to divide.

We shall, provisionally, identify the black, heavily-coated deposits in fig. 3 (*a*) with the theoretical p closure domains. In fig. 3 (*a*), Mode III magnetization is beginning, the ratio of the width of a p domain to the width of a q domain is very small, and the heavy deposits on the p domains manifest the presence of free poles. In fig. 3 (*b*) we see that an increase in field from 13 to 17 Oe has caused a complete alteration in the appearance of the p domains, for a central, heavy deposit of colloid now separates two colloid-free portions within the p domain. The horizontal striations of colloid in the q domains show that the latter are magnetized along the [100] direction, which is parallel to the long edge of the paper.

In several parts of these pictures one can see no visible boundaries between the q domains and the colloid-free portions of the p domains, e.g. in the region of fig. 3 (*c*) slightly to the right and slightly below the centre of the picture, an observation which indicates that in such places the p and q structures are magnetized approximately in the same direction.

In fig. 3 (*d*) an increase in field has again caused the p structures to increase and again their appearance is greatly changed, for they are now further complicated by a fine lace-like structure; no significant change occurred on reversing the field, and up to a field of 100 Oe the p structures multiplied and lost clarity, without further significant change in pattern. With higher fields the q domain boundaries are no longer parallel to the [100] direction but assume zigzag forms as in fig. 3 (*f*), which are somewhat like the colloid-free areas of the p domains of fig. 3 (*d*). Above 250 Oe the patterns became less clear and rather 'woolly', because the colloid particles were very strongly directed parallel to the applied field and were less affected by the localized domain fields.

Figs. 3 (*e*) and (*f*) were taken when the thickness of the crystal had been deliberately reduced to 0·13 cm by systematic cutting in the course of experiments described below. Fig. 3 (*e*) is interesting because it shows a local disturbance which was probably due to a sub-surface inhomogeneity, and here again the disturbed q domain has the zigzag form similar to the colloid-free areas of the p domains in fig. 3 (*f*).

It was frequently noted that the colloid deposits were much heavier on one side of the p domain structure than on the other. This was attributed to a small component of field perpendicular to the surface. This explanation was tested by deliberately applying a small field, perpendicular to the surface and insufficient in magnitude to alter the main domain structure. The results are shown in fig. 4 (Plate III), and are consistent with the suggested explanation. They are most helpful in determining the underlying structure of the p domains since the sign of the surface free poles can be inferred and any predicted domain structure must produce surface poles of the same sign. It must also explain the beautiful complementary detail of the patterns when either the horizontal or the vertical field is reversed.

§ 4. DISCUSSION AND INTERPRETATION OF OBSERVED PATTERNS

As found by Bates and Neale, and often confirmed in the present work, colloid deposits occur only on alternate boundaries on the (100) plane. Mee (1950) has given an explanation of this fact based on his observations of the patterns observed on a single crystal of cobalt. In his view, the direction of polarization of the colloid dipoles by the external field, as well as the direction of the surface fields attracting them, must be taken into account. Thus, in zero applied field, the particles are attracted to the highly localized stray fields at the boundary walls and near the surface they will be oriented almost perpendicular to it. On applying a field parallel to the surface, the particles are aligned parallel thereto and no longer attracted to the boundaries themselves. They are only attracted by the less highly localized surface fields due to free poles of opposite sign appearing at the intersection of adjacent domains with the surface. But for the (100) plane under investigation these surface fields are in opposition to the applied field at alternate boundaries and are therefore ineffective, particularly as the colloid particles are so polarized that these opposition fields repel them. In this instance it is not possible to make the favoured and unfavoured boundaries exchange places by reversing the field, since the whole domain structure is altered by so doing, whereas the cobalt structure studied by Mee (1950) is unaffected by reversal of a small applied field.

The complex but regular patterns found on the (011) plane prove that the simple domain structures proposed by Néel, fig. 1, are not entirely correct. The fact that the domain spacing on the (011) plane is D and not $\frac{1}{2}D$ proves also that the domain scheme suggested by Lawton (1950) is unlikely. However, the observed patterns have much in common with the Néel scheme. Firstly, the q domains have colloid striations running in the $[0\bar{1}1]$ direction (fig. 3 (*b*)), and are therefore magnetized in the [100] and $[\bar{1}00]$ directions—a point which we proved by some compression experiments in which it was found that a compression in the $[0\bar{1}1]$ direction caused these domains to increase in size, because the magnetostriction coefficient of this silicon–iron is positive. Secondly, in the very weak fields required for the onset of Mode III magnetization, the q domains are very wide and cover the whole surface. Thirdly, with increase in field p domains appear between the q domains, although the observed p structure is quite different from the simple form postulated by Néel.

One naturally enquires whether further information on the closure structures can be obtained from observations of patterns on the (100) plane near the edge of the crystal. Unfortunately, the inevitable slight rounding of the edge caused by electrolytic polishing permits the formation of 'tree' patterns which mask the closure structure.

In fig. 3 (*a*) the new domains formed at 180° boundaries as the field is increased are heavily coated with colloid except for certain lozenge-shaped, colloid-free patches. These patches appear to represent a basic unit from which many of the more complicated structures are built (for example, they are found in the fine structure of figs. 3 (*d*) and 3 (*e*)). As magnetization proceeds, the long colloid-free lozenges divide into two sets with a heavy colloid deposit between them, as in figs. 3 (*b*) and 3 (*c*), and this new shape of colloid-free areas persists with only minor changes until magnetic saturation obtains.

We think that these areas, while remaining magnetized parallel to the surface, have their magnetic vectors turned away somewhat from those of the adjacent q domains. For, if the regular pattern is disturbed by a crystal imperfection, the q domains are sometimes directly joined to the p structure, as in fig. 3 (*e*), which means an approximate alignment of their magnetic vectors. Again, with increase in magnetization the q domains themselves assume the same zigzag shape as the p structures, as in fig. 3 (*f*), a most convincing point. Thus, the approximate magnetizations of the p structures are fairly well established, though their detailed sub-surface shape is not known.

We therefore see that in devising a closure domain scheme for the (011) surface the structure must satisfy the conclusions reached above with regard to the p structures and the vertical field patterns of fig. 4, and must roughly agree with Néel's predictions particularly in regard to the q domains. We tried several theoretical schemes of which the following two appear to us to be the most satisfactory.

The first, shown in the simplified diagram, fig. 5, contains the q domains predicted by Néel without the intervening p domains. The flux emerging from the q domains is therefore carried partly antiparallel to the applied field by a regular but complicated arrangement of domains magnetized approximately in the [100] and $[\bar{1}00]$ directions, and partly parallel to the field outside the crystal between adjacent free poles of opposite sign. We may thus explain the wide black deposits of colloid between colloid-free areas, and the asymmetric distribution of colloid found when the colloid particles are polarized perpendicular to the surface, as in fig. 4, a close study of which shows that asymmetric colloid distribution takes place on the boundaries themselves. In fig. 5 it is seen that the q domain boundaries have the same sign for the surface free poles as their adjacent main domains, so that there is a tendency for the colloid to deposit on alternate boundaries with a spacing *D*. Experimentally, the p structures also have an asymmetric distribution on their boundaries, but we cannot at present interpret it.

Of course, this simplified structure of fig. 5 does not account for the beautiful lace patterns, but an even more serious objection to it is that large magnetostatic energy is associated with the free poles in comparison with that associated with Néel's p domains, unless the extent of the surface occupied by free poles is restricted. An elementary calculation (Mee 1951) shows that 15% of the surface should not be exceeded in this case.

A second suggested structure is shown in fig. 6, in which the triangular closure domains are added to reduce the magnetostatic energy, although some magnetostatic energy is required for their formation, and the difference in energy between the two systems of figs. 5 and 6 may not be great. In addition to giving the same powder patterns, the second theoretical structure suggests why the q domains at high magnetizations assume the same zigzag form as the colloid-free p structure at small magnetizations. At high magnetizations the angle between the main domain vectors and the (011) plane is similar to that between the triangular closure domain vectors and this surface at low fields. It is therefore possible that closure domains magnetized parallel to the surface—q domains and colloid-free p structures respectively—will have the same general shape, since they occur on domains whose orientations are similar.

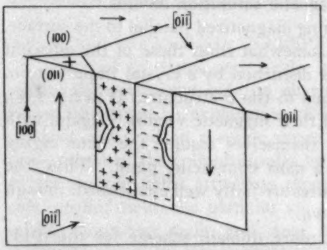

Fig. 5. Closure structure on (011) plane.

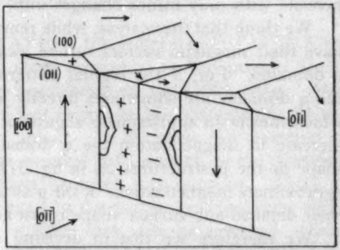

Fig. 6. Closure structure on (011) plane.

To sum up, we see that Néel's p domains are replaced in our scheme by a fine structure of domains magnetized approximately in the same direction as the adjacent q domains. If we denote the angle between the direction of the q magnetization vector and the $[0\bar{1}1]$ direction by ϕ, calculations (Mee 1951) on the same lines as those of Néel show that ϕ may vary between large limits for a comparatively small change in the energy of the q domain. It is therefore reasonable to consider that the zigzag shape of the q domains at high magnetizations is due to rotation of the q vectors from the [100] direction.

§ 5. QUANTITATIVE MEASUREMENTS

Measurements were made of the domain spacing *D* as a function of *H* on both the (100) and (011) surfaces, both with the original crystal and with the crystal when systematically reduced in width. The specimen was exposed to a uniform magnetic field by means of an electromagnet with specially shaped pole-pieces. The effective field acting on the specimen was measured by a calibrated magnetic potentiometer whose feet rested on the side of the specimen opposite the (011) plane surface investigated. The potentiometer had feet 6 mm wide and 2 mm thick and the distance between its feet centres was 7 mm. It consisted of a semi-circular ebonite former uniformly wound with four layers of double silk covered No. 46 s.w.g. copper wire. Using a sensitive galvanometer, fields of about 4 Oe were measured with a possible error of 3%, while with fields above 20 Oe the error was about 1%.

The average spacing of the powder lines was found by counting about 20 lines in the microscope image projected on a ground-glass screen and measuring their total width with a steel ruler. The magnification was later determined by replacing the specimen by a graticule. The specimen was not removed from the pole-pieces for washing between readings under different field conditions, but the surface was cleaned *in situ* with a water jet; this procedure had many obvious advantages.

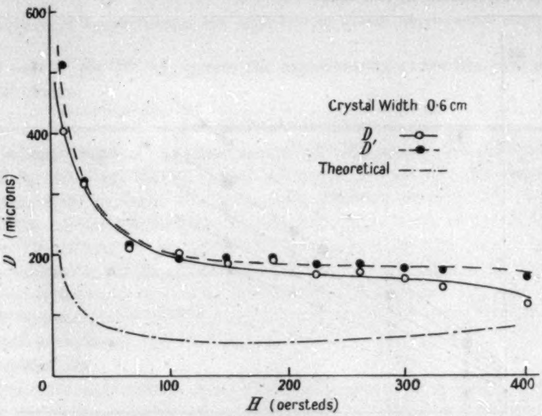

Fig. 7. Variation of domain spacings on (100) and (110) planes with field.

Prior to each determination the specimen was first demagnetized. A field of say 10 Oe was then applied and reversed many times to obtain cyclic conditions. A drop of colloid was now placed on the (100) surface and the line spacing *D* measured. The colloid was then washed away with the water jet. Magnetic field measurements were then made by noting the deflection of the galvanometer in the potentiometer circuit when the field current was reversed. The whole magnet assembly was next turned through 90° to bring the (011) plane horizontal and under the microscope. A drop of colloid was placed on the (011) plane and the spacing width *D′* on this plane was also measured as described above. Later it was found possible or preferable to take all readings up to saturation on one plane before taking any readings on the other.

In fig. 7 the encircled points and the filled circles represent the values of the domain spacing as a function of H obtained from measurements on the 0·6 cm thick crystal for the (100) plane and (011) planes respectively, while the broken curve is that calculated from Néel's theory based on fig. 1 (*b*). The crystal was then systematically reduced in width by careful grinding, and further sets of measurements on the two planes were taken for crystal widths of 0·43, 0·37, 0·24 and 0·13 cm, and curves similar to those of fig. 7 were obtained. In all cases there was very good agreement between the two sets of measurements for the domain spacings D and D'.

The values of the spacings D on the (100) plane for chosen fields are plotted as a function of $\sqrt{L}$, where L is the specimen width, in fig. 8, together with a theoretical curve from Néel's theory. The two points in the top right-hand corner of the figure are approximate only, as they were obtained by applying the field in the [011] direction, i.e. at 90° to the field direction in the preceding graphs, thus giving an effective value of $L = 1{\cdot}21$ cm, but the values of H could not be as accurately determined in this case.

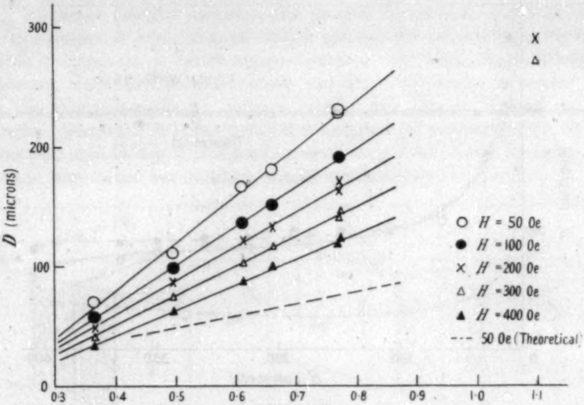

Fig. 8. Variation of domain spacing with width of specimen.

A close examination of the photographs of lines on the (100) plane shows that the colloid striations found on the sides of these lines changed direction as the applied field was increased, and it was possible to measure their directions on the original photographs. Now, it follows from the work of Williams, Bozorth and Shockley (1949) that colloid striations always form perpendicular to the main domain magnetization vector. Consequently, the angle θ between a striation and a colloid line should be equal to the angle between the domain vector and the resultant magnetization which is along the $[0\bar{1}1]$ direction. We can therefore measure θ directly.

The angles between striations and lines were measured by projecting a magnified image of a photographic negative on to a screen and tracing the colloid lines and striations. The mean of about 50 values of θ were taken for each of a series of negatives for a crystal in different fields. D was plotted against cos θ and compared with the theoretical curve based on Néel's calculations; the two curves are reproduced in fig. 9. The general agreement in outline of the two curves provides rather striking, fundamental support for Néel's theory, although as in the case of the (D, H) curves the experimental curve lies well above the theoretical curve.

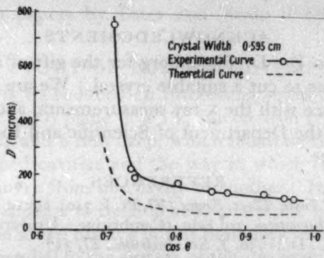

Fig. 9. Variation of domain spacings with angle between domain magnetization vector and field.

§ 6. CONCLUSIONS

The general shape of the experimental (D, H) curves agrees well with that predicted by the Néel theory, when allowance is made for the anisotropy of silicon–iron, and we have the supporting evidence of the (D', H) curves. Although the agreement between the (D, H) and (D', H) curves is reasonably good, the (D', H) curves always lie above the (D, H) curves at high fields, but here the sensitivity of the powder pattern method is lower. Moreover, line splitting occurred more frequently on the (100) plane than on the (011) plane and this tends to depress the D values with respect to the D' ones. The shape of the (D', H) curve conforms better the Néel's theoretical curve although no minimum was ever observed.

But the most outstanding feature is the fact that the experimental values of D are often as much as three times as great as the theoretical values. We had expected that the relatively small discrepancy observed by Bates and Neale would be removed when a bigger and better crystal and improved technique were available. In the measurements of Bates and Neale the discrepancy varied with the crystal width and they did not find a linear relation between D and $\sqrt{L}$, but in the present work we have very good proportionality between D and $\sqrt{L}$.

We think that all these discrepancies must be due, at least in part, to the complicated p structure observed, for which the energy must be smaller than W_p in the Néel expression $D=[\gamma L(W_p+W_q)/W_pW_q]^{1/2}$. A suitable reduction in W_p would, of course, give higher theoretical values for D and a greater slope to the theoretical $(D, \sqrt{L})$ graph. It is equally possible that a modified closure structure on the very narrow (011) faces of the specimens used by Bates and Neale would account for their results. We hope in a later communication to give a mathematical treatment of some of these cases.

It would be interesting to extend the above measurements to single crystals of very pure iron or, indeed, to any similar ferromagnetic crystals with suitable anisotropy constants, and to a specimen of iron or silicon–iron with a circular instead of a rectangular cross section, since, according to Néel, a two-phase structure exists when such a specimen is magnetized along the axis of the cylinder. The closure structure on the circumference of the cylinder might be very interesting, since Néel predicts that a continuous change from p to q structures will exist.

ACKNOWLEDGMENTS

We are grateful to Dr. D. Shoenberg for the gift of a valuable silicon–iron ingot which allowed us to cut a suitable crystal. We are indebted to Mr. S. C. Wallwork for assistance with the x-ray measurements, and one of us (C. D. M.) records his thanks to the Department of Scientific and Industrial Research for a maintenance allowance.

REFERENCES

Bates, L. F., 1950, *Proc. Instn. Elect. Engrs.*, **97**, Pt. I, 340; 1951a, *J. Phys. Radium*, **12**, 322; 1951b, *Modern Magnetism*, 3rd Edn. (Cambridge : University Press), p. 453.
Bates, L. F., and Mee, C. D. ,1950, *J. Sci. Instrum.*, **27**, 317.
Bates, L. F., and Neale, F. E., 1949, *Physica*, **15**, 220 ; 1950, *Proc. Phys. Soc.* A, **63**, 374.
Bates L. F., and Wilson, G. W., 1951, *Proc. Phys. Soc.* A, **64**, 691.
Bitter, F., 1931, *Phys. Rev.*, **38**, 1903.
Kaya, S., 1934, *Z. Phys.*, **90**, 551.
Lawton, H., 1950, *E.R.A. Report* N/T 58.
Mee, C. D., 1950, *Proc. Phys. Soc.* A, **63**, 922 ; 1951, *Thesis*, Nottingham.
Néel, L., 1944, *J. Phys. Radium*, **5**, 241.
Williams, H. J., Bozorth, R. M., and Shockley, W., 1949, *Phys. Rev.*, **75**, 155.
Williams, H. J., and Shockley, W., 1949, *Phys. Rev.*, **75**, 179.
Yamamoto, M., and Iwata, T., 1951, *Phys. Rev.*, **81**, 887.

A Study of Surface Closure Domains by the Powder Pattern Technique

By L. F. BATES and C. D. MEE*
University of Nottingham

MS. received 9th *August* 1951

ABSTRACT. The powder patterns in the neighbourhood of cavities and inclusions on the surfaces of single crystals of silicon–iron have been studied, and the photographs obtained are evidence for the essential correctness of current views on closure domain structures.

§ 1. INTRODUCTION

In a series of important papers, Williams, Bozorth and Shockley (1949) and Williams and Shockley (1949) have described the 'dagger' and 'tree' patterns which may be formed by the Bitter powder technique on the carefully polished surface of a single crystal of silicon–iron, and have given convincing explanations of the modes of formation of special patterns in terms of ferromagnetic domain theory. We have in the course of recent researches made many similar observations and have confirmed the essential correctness of these explanations. In addition, we have made a careful study of the closure domains found in the neighbourhood of cavities or inclusions in the crystal surface, and of the way in which such closure domains are modified by the presence of a main 180° boundary wall in the neighbourhood of the imperfections. A full description of the colloid or powder technique and references to other work will be found in papers by Bates and Neale (1950), Bates (1950), and Bozorth (1951).

---

* Now with The Steel Company of Wales Ltd., Lysaght Works, Newport.

§2. A STUDY OF DOMAIN MOVEMENTS

In fig. 1 (Plate I) is reproduced an interesting series of pictures of powder patterns formed on the (100) plane of a 3% silicon–iron crystal specimen, some 13 mm long, 6 mm wide and 6 mm deep, which illustrate the domain formations around irregularly shaped cavities and the way in which they are modified as a main 180° boundary moves from one cavity to another. In fig. 1 (*a*) we see that a main boundary wall appears to be attached somewhere near the lower edge of the cavity system. The actual placing of this boundary was achieved by applying a small magnetic field parallel to the surface of the specimen and to the long edge of the paper. Two distinct types of closure structure are visible around the two main cavities, which appear as large irregular blobs in the picture. The structure around the cavity which is further to the left in the picture is of the type shown diagrammatically in that part of fig. 3 which lies to the left of the main domain wall, while that around the cavity to the right is of the type which lies to the right of the main domain wall in fig. 3. In both cases the possible directions of the domain magnetization vectors are given by the arrows.

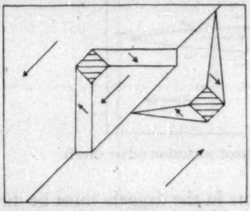

Fig. 3. Schematic representation of fig. 1 (*a*).

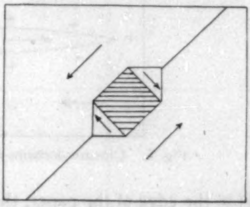

Fig. 4. Closure domains around an inclusion (after Néel).

On increasing the magnetic field the boundary moved slowly from the position shown in fig. 1 (*a*) to reach the positions successively shown in figs. 1 (*b*) and 1 (*c*). In fig. 1 (*b*) the closure structures to the left are extended and still attached to the boundary, but in 1 (*c*) they have broken away. In fig. 1 (*c*) the main boundary now attempts to pass through the cavity on the right, and the closure structure round this cavity changes from the earlier 'dagger' formation to a single type which was predicted by Néel (1944) and which is shown diagrammatically in fig. 4 (a very good example is seen in fig. 2 (*a*)). We note that the lower closure domain of the cavity on the left in fig. 1 (*c*) is still attached to the main domain wall, but is complicated by being joined to another closure domain system originating from a cavity somewhere on the left of the picture. On the upper side of the cavity the domain structure is now that really characteristic of a large cavity isolated within a large domain, and it bears a striking resemblance to the structure, shown diagrammatically in fig. 5, which was predicted by Néel for such a case. The twin-triangle structure is clearly pronounced in both figs. 1 (*c*) and 1 (*d*), to which we next refer.

Fig. 1 (*d*), shows what happened when a slight reduction in the applied field was made; the closure structure is seen to extend up to the main wall from the cavity on the right. On again increasing the field the wall moved across the cavity with the newly formed structure attached to it, as shown in fig. 1 (*e*). Finally, with still greater field, the wall moved away from both cavities as in fig. 1 (*f*), where we now see that the structure around the cavity on the left is definitely that of fig. 5, while the structure around that on the right is somewhat similar thereto.

Some experiments were also carried out on the (011) surface of the above specimen. In the demagnetized state the powder deposits showed that on this surface the domains were magnetized along the [100] and [$\bar{1}$00] directions. Some six 180° boundaries were irregularly spaced over the surface, and each domain was covered with striations of powder deposits perpendicular to the direction of domain magnetization.

In fig. 2 (*b*) are shown some dagger-shaped domains of reversed magnetization close to three comparatively large cavities. If we picture the magnetization vector of the main domain in which they are situated to be directed downwards parallel to the edge of the paper, then the vectors in the daggers must be directed upwards in order that a minimum of free poles shall occur on the boundaries of the shallow daggers. Such dagger domains must decrease the magnetostatic energy of the free poles which exist on the sides of the cavities. Hence, it is probable that the complete structure consists of dagger and small triangular closure domains similar to the system depicted in fig. 5. The total energy of the system is thus reduced, since the extra energy located in the walls of the daggers must be less than the change in magnetostatic energy which results from their formation.

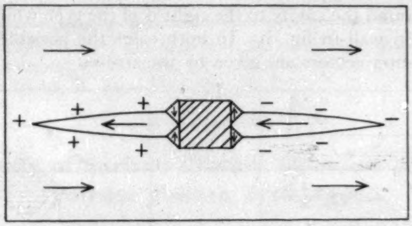

Fig. 5. Closure domains around an isolated inclusion (after Néel).

Applying a field of a few oersteds parallel to the direction of magnetization of a domain caused the crystal to become saturated, and it was found that the size of the daggers was independent of the field, thus indicating that the change in the energy associated with them in the presence of the field was small compared with the change in magnetostatic energy caused by their initial formation.

It is considered that daggers appeared on only one side of a cavity in fig. 2 (*b*) because the surface in this case was not a true (011) plane but was inclined slightly thereto. Thus only one of the daggers, which are orientated along the [100] direction, intersects the surface. Following upon much more accurate grinding of the surface, checked by orientation measurements, it was found that at an undulation in the surface dagger-shaped domains of reversed magnetization were obtained as in fig. 2 (*c*). The vertical line, about one-third of the width of the picture from the left, is a 180° boundary. To the left of this boundary a main domain may be considered magnetized in the direction from bottom to top of the printed plate; to the right of the boundary a main domain may be considered as magnetized from top to bottom. It is then reasonable to consider the lozenge-shaped daggers on the left of the boundary as magnetized in the top to bottom direction, and those on the right to be magnetized in the bottom to top direction. Again, on magnetizing the crystal along a [100] direction, the 180° boundary in fig. 2 (*c*) was displaced laterally across the picture, but no change in position or appearance of the daggers was observed.

Similar experiments were made on a 2·6% silicon–iron single crystal sheet specimen some 0·5 mm thick, with the (110) plane inclined at about 2° to the surface, and the edge of the surface parallel to a [1$\bar{1}$0] direction. Very regular deposits were observed on the demagnetized crystal as shown in fig. 2 (*d*). The black lines running parallel to the long edge of the plate are 180° boundaries between domains magnetized alternately in opposite directions parallel to that edge, for the powder striations perpendicular to such directions are clearly seen. In addition, there is an interesting arrow-head formation on the 180° walls.

.A
5
2

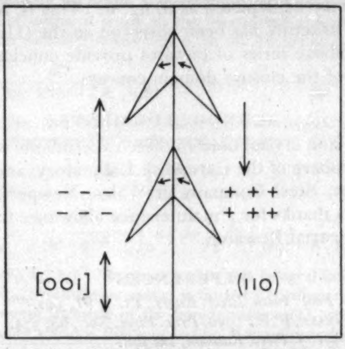

Fig. 6. Schematic explanation of arrow-head formations.

On applying a small field perpendicular to the surface the arrow-heads were more clearly manifested, since certain (alternate) domains collected colloid, whereas the arrow-heads situated in them did not, while in the adjacent, comparatively colloid-free, domains the arrow-heads collected colloid. This is clearly shown by figs. 2 (*e*) and 2 (*f*). The asymmetric distribution of colloid on the main domains is explained by the fact that the [001] direction does not lie exactly in the crystal surface, since that surface is inclined to the (110) plane about the [1$\bar{1}$0] direction. Hence, with no external applied field, the neighbouring domains have an even distribution of positive and negative free poles and the distribution of colloid is symmetrical. When a vertical field is applied, however, the domain vectors rotate slightly towards the field direction and the surface density of free poles is no longer uniform, successive domains now having greater or lesser free pole density. Moreover, the colloid particles are now polarized perpendicularly to the surface in such a way that they are repelled from domains of lesser free pole density and attracted to those of greater free pole density. This explanation also covers the colloid distributions on arrow-head formations.

Because the main domain structure consists of 180° domains, and because the specimen surface is slightly inclined to the easy direction along which the domains are magnetized, it is natural to think that the arrow-head formation represents some kind of closure structure similar to the 'trees' observed on the (100) plane of a silicon–iron crystal. Very similar arrow-head patterns have recently been observed on a ($\bar{1}$10) plane of a nickel crystal by Yamamoto and Iwata (1951) for which they give a 'tree' pattern explanation. But in the case of silicon–iron the [001] direction is the only direction of easy magnetization lying in the surface, and therefore the arrow-heads must be magnetized along a more difficult direction of magnetization. This direction can be estimated roughly by measuring the angle, α, between the sides of the arrow-heads and the [001] direction, since α must be half the angle between the magnetization vectors of the arrow-heads and the [001] direction if the condition of continuous magnetization over the boundary is obeyed. The mean value of α, as measured from the photographs, was 32°, so that the domain vectors in the arrow-heads must make an angle of about 64° with the [001] direction. Consequently, the domain structure for the arrow-heads may be depicted as in fig. 6. This is, in effect, a statement that a kind of 'tree' structure has been observed on the (110) plane.

In our view, the above series of pictures provide conclusive evidence of the essential correctness of the closure domain concept.

ACKNOWLEDGMENTS

The large silicon–iron crystal used in these experiments was kindly presented to us by Dr. D. Shoenberg of the Cavendish Laboratory, and the strip specimen by Mr. G. C. Richer, Steel Company of Wales, Newport, Mon. One of us (C. D. M.) records his thanks for a maintenance allowance from the Department of Scientific and Industrial Research.

REFERENCES

Bates, L. F., 1950, *Proc. Instn. Elect. Engrs.*, Pt. I, **97**, 340.
Bates, L. F., and Neale, F. E., 1950, *Proc. Phys. Soc.*, **63**, 374.
Bozorth, R. M., 1951, *J. Phys. Radium*, **12**, 308.
Néel, L., 1944, *Cah. de Phys.*, **25**, 21-44.
Williams, H. J., Bozorth, R. M., and Shockley, W., 1949, *Phys. Rev.*, **75**, 155.
Williams, H. J., and Shockley, W., 1949, *Phys. Rev.*, **75**, 179.
Yamamoto, M., and Iwata, T., 1951, *Phys. Rev.*, **81**, 887.

LETTERS TO THE EDITOR

On the Radiative Correction to the Coulomb Scattering of Electrons

The result obtained by Schwinger (1949) for the radiative correction to electron scattering by nuclei has been checked by the use of the method of Feynman (1949), and agreement with Schwinger's formula has been obtained. However, there is some doubt about the method of Schwinger's proof.

Using the Feynman approach we have to calculate the matrix elements corresponding to the first and second Born approximations and to the first radiative correction. The second Born approximation must be included as it is of the same order in $e^2/\hbar c$ as the first radiative correction. The inclusion of the latter leads to the well-known infra-red divergence which is exactly cancelled by the infra-red divergence arising from inelastic scattering. To obtain the correct cancellation it is important to use the same limiting process in both cases. This is easily achieved, if a vanishingly small photon rest-mass (the Feynman $\lambda_{\min}$) is used (Dalitz 1951 b), which is relativistically invariant. Schwinger uses a minimum photon momentum $k_{\min}$, but he applies the $k_{\min}$ cut-off in the radiative correction after first changing the origin in momentum space (Schwinger 1949, eqn. (1.88)), while no such change of origin is made in the bremsstrahlung calculation. In fact, the divergent integral in the radiative correction is, in the Feynman notation,

$$\int \frac{d^4k}{(\mathbf{k}^2-2\mathbf{p}_2\,.\,\mathbf{k})(\mathbf{k}^2-2\mathbf{p}_1\,.\,\mathbf{k})\mathbf{k}^2} = \int_0^1 2x\,dx \int_0^1 dy \int \frac{d^4k}{(\mathbf{k}^2-2\mathbf{p}\,.\,\mathbf{k})^3}, \quad \ldots\ldots(1)$$

where $\mathbf{p}=xy\mathbf{p}_1+x(1-y)\mathbf{p}_2$, and the change of origin (Schwinger's eqn. (1.88)) is equivalent to the transformation (Feynman 1949, after eqn. (11 *a*))

$$\mathbf{k}\rightarrow\mathbf{k}+\mathbf{p}, \quad \ldots\ldots(2)$$

which transforms (1) into

$$\int_0^1 2x\,dx \int_0^1 dy \int \frac{d^4k}{(\mathbf{k}^2-\mathbf{p}^2)^3} = \int_0^1 2x\,dx \int_0^1 dy \int \frac{d^4k}{(k_y{}^2-\mathbf{K}\,.\,\mathbf{K}-\mathbf{p}^2)^3}, \quad \ldots\ldots(3)$$

where the vector $\mathbf{K}$ is (k_1, k_2, k_3). Feynman makes this integral finite by giving the photon an infinitesimal mass $\lambda_{\min}$; Schwinger makes it finite by cutting off $|\mathbf{K}|$ at an infinitesimal momentum $k_{\min}$. However, because of the transformation (2), which is clearly a function of the integration variables x and y, this $k_{\min}$ has no direct physical meaning and is certainly not identical with the $k_{\min}$ employed in the corresponding bremsstrahlung integral, which is a cut-off on the true momentum. Thus different regions are cut out of the momentum space in the two cases. The infinite parts of the two cross sections still cancel, but the remaining finite part comes out quite incorrectly. The reason that Schwinger's final result is nevertheless correct is due to the fact that a second error exactly cancelling the first is introduced in his eqn. (2.89), the right-hand side of which should be zero (Ward, private communication).

Further, it can be shown that the $k_{\min}$ used in the radiative correction is, most unexpectedly, relativistically invariant. On comparing the result of integrating (3) which is, using Schwinger's method and Feynman's notation,

$$\frac{i}{4}\int_0^1 \frac{dy}{\mathbf{p}_y{}^2}\left(\log\frac{2k_{\min}}{|\mathbf{p}_y|}-1\right),$$

with the corresponding expression, using the $\lambda_{\min}$ process, which is (Feynman's eqn. (23 *a*))

$$\frac{i}{4}\int_0^1 \frac{dy}{\mathbf{p}_y{}^2}\log\frac{\lambda_{\min}}{|\mathbf{p}_y|},$$

we see that $\log \lambda_{\min} = \log 2k_{\min} - 1$ at all energies. In contrast with this, the relationship between $\lambda_{\min}$ and the $k_{\min}$ of the bremsstrahlung calculation is (Dalitz 1951 b)

$$\log \lambda_{\min} = \log 2k_{\min} - \frac{1}{1-2\phi \coth 2\phi} \times \left\{ \frac{1}{2\beta} \log \frac{1+\beta}{1-\beta} - \frac{1-\beta^2}{2} \cosh 2\phi \int_{\cos \theta/2}^{1} \frac{d\zeta}{\beta\zeta(1-\beta^2\zeta^2) \sin \frac{1}{2}\theta (\zeta^2 - \cos^2 \frac{1}{2}\theta)^{1/2}} \log \frac{1+\beta\zeta}{1-\beta\zeta} \right\},$$

which reduces in the non-relativistic limit to $\log \lambda_{\min} = \log 2k_{\min} - \frac{5}{6}$ so that this $k_{\min}$ is not relativistically invariant. Here $\sinh \phi = \beta(1-\beta^2)^{-1/2} \sin \frac{1}{2}\theta$, $\beta = v/c$ and θ is the scattering angle.

The cross section for essentially elastic scattering, i.e. scattering where the bremsstrahlung photon has an energy up to ΔE where $\Delta E \ll W$ the kinetic energy of the electron, is then

$$\frac{d\sigma}{d\Omega}(\theta, \Delta E) = \left(\frac{Ze^2}{2m\beta^2 \sin^2 \frac{1}{2}\theta} \right)^2 (1-\beta^2)(1-\beta^2 \sin^2 \tfrac{1}{2}\theta)(1+\delta_B - \delta_R),$$

where (McKinley and Feshbach 1948, Dalitz 1951 a)

$$\delta_B(\theta) = \pi Z e^2 \beta \sin \tfrac{1}{2}\theta \, (1 - \sin \tfrac{1}{2}\theta)(1-\beta^2 \sin^2 \tfrac{1}{2}\theta)^{-1}$$

and

$$\begin{aligned} \delta_R(\theta, \Delta E \ll W) = (e^2/\pi) \Big\{ & 2(1-2\phi \coth 2\phi)(1+\log 2\Delta E/m) + \phi \tanh \phi \\ & + 2(1-\phi \coth \phi)(1-\tfrac{1}{3}\coth^2 \phi) - \frac{2}{9} + \frac{1}{\beta} \log \frac{1-\beta}{1+\beta} + 2\phi \coth 2\phi \log \frac{4}{1-\beta^2} \\ & + \frac{2\beta^2 \sin^2 \frac{1}{2}\theta}{1-\beta^2 \sin^2 \frac{1}{2}\theta} \phi \operatorname{cosech} \phi \\ & - (1-\beta^2) \cosh 2\phi \int_{\cos \theta/2}^{1} \frac{d\zeta}{\beta \sin \frac{1}{2}\theta (\zeta^2 - \cos^2 \frac{1}{2}\theta)^{1/2}} \left(\frac{\log \frac{1}{2}(1-\beta\zeta)}{1+\beta\zeta} - \frac{\log \frac{1}{2}(1+\beta\zeta)}{1-\beta\zeta} \right) \Big\}. \end{aligned}$$

Here natural units have been used.

Lastly we consider the question of experimental verification. The second Born approximation gives correct results (MacKinley and Feshbach 1948) for Z less than approximately 15, so that we must restrict ourselves to light nuclei. For these, any deviation from pure Coulomb scattering due to the finite size of the nucleus is negligible at energies less than 10 MEV (Elton 1950, Acheson 1951). A further restriction is that δ_R must be small, as otherwise the next term in the perturbation series becomes important. The table of the radiative correction δ_R (as a percentage) for various energies W of the incident electron and ΔE for the bremsstrahlung photon has been worked out bearing these considerations in mind.

W (MEV)		2·5			4·0			9·5	
θ (deg.)	45	90	135	45	90	135	45	90	135
ΔE (kev)									
10	4·8	7·4	8·7	6·9	9·9	11·3	12·4	15·9	17·5
25	3·9	6·0	7·1	5·7	8·1	9·3	10·5	13·5	14·8
50	3·2	5·0	5·9	4·7	6·8	7·9	9·0	11·7	12·8
100	2·5	3·9	4·7	3·8	5·5	6·4	7·6	9·9	10·8

Our thanks are due to Professor H. S. W. Massey and Mr. L. Castillejo for many helpful discussions and to Dr. J. C. Ward for informing us of the error in Schwinger's eqn. (2.89), which started us on this investigation.

Wheatstone Physics Department,
King's College, London. L. R. B. ELTON.
University College, London. H. H. ROBERTSON.
9th November 1951.

ACHESON, L. K., 1951, *Phys. Rev.*, **82**, 488.
DALITZ, R. H., 1951 a, *Proc. Roy. Soc.* A, **206**, 509 ; 1951 b, *Ibid.*, 521.
ELTON, L. R. B., 1950, *Proc. Phys. Soc.* A, **63**, 1115.
FEYNMAN, R. P., 1949, *Phys. Rev.*, **76**, 769.
MCKINLEY, W. A., Jr., and FESHBACH, H., 1948, *Phys. Rev.*, **74**, 1759.
SCHWINGER, J., 1949, *Phys. Rev.*, **76**, 790.

Properties of Films of Non-Metallic Antimony

A recent investigation of photoconductivity in the elements (Moss 1951) has shown the elements B, C; Si, P, S; Ge, As, Se; Te and I to be photoconductive. It is now known that gray tin is a semiconductor (Busch, Weiland and Zoller 1951) and thus, presumably, should be photoconductive under appropriate conditions. Thus in the fourth row of the periodic table there is a gap between Te and Sn, and to retain an ordered progress in the table requires the filling of this gap by a semiconducting form of antimony.

From the behaviour of the other elements we are led to expect this semiconducting form to have an activation energy between those of Te (0·37 ev) and Sn (0·1 ev), and thus we might expect it to exhibit photoconductivity in the $8\,\mu$ region of the spectrum. It was to check this interesting speculation that the present work was carried out.

From experience with arsenic, which gives semiconducting layers if evaporated on to substrates not much hotter than room temperature, attempts were made to produce semiconducting antimony layers by evaporation (*in vacuo*) on to substrates at 195° K or 90° K. Semiconducting layers were obtained in this manner which changed irreversibly to the metallic form at temperatures near 0° C.

Measurements of the temperature dependence of resistance were repeatable provided the layer was not allowed to reach too high a temperature. Typical results are shown on the usual (log (resistance), reciprocal temperature) plot by curve A of the figure. Although the points do not all fall on one straight line, representative lines may be drawn through parts of the curve to obtain estimates of the activation energies. The values found are: low temperatures, 0·07 ev; high temperatures, 0·11 ev. Two other layers gave very similar values for the same temperature regions as the above.

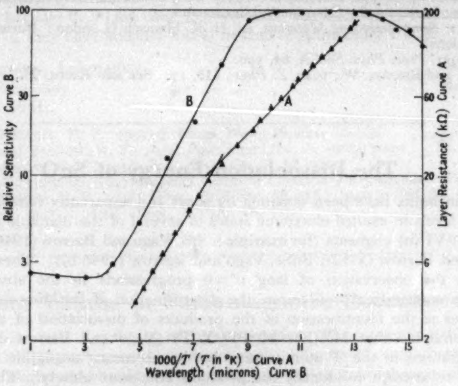

A. Resistance–temperature curve. B. Spectral sensitivity curve.

The resistance of the layers decreased on irradiation. Using a double monochromator with radiation interrupted at 33 c/s, it was possible to measure spectral sensitivity curves for some of the layers. With one cell fitted with a KRS5 window it was possible to extend the measurements to wavelengths greater than $15\,\mu$. The results for a layer temperature of 195° K are shown in curve B of the figure. The curve is characterized by a marked rise in sensitivity (~36 : 1) in the 4–$9\,\mu$ region. Similar behaviour was found in all cells measured, increases of 28 : 1, 33 : 1 and 37 : 1 being recorded for three other cells fitted with periclase, KRS5, and silver chloride windows.

For wavelengths greater than 9μ the sensitivity is relatively constant, with the possibility of a significant fall near the limit of measurements. As there is no well-defined drop of sensitivity at long wavelengths it is not possible to conclude from the spectral sensitivity curves whether the layer is acting as a photoconductor or bolometer.

Measurements of response times of layers gave values near 10^{-3} sec, which might equally apply to photoconductors or thin, backed bolometers. In one set of measurements the response time increased by 30% on cooling from 195° K to 90° K, in another set it decreased by 40% for the same cooling.

It is thus established that layers of antimony can be prepared which show semiconducting properties, thermal activation energies of 0·06 to 0·11 ev being indicated. A paper by Suhrmann and Berndt (1940), which has recently come to the notice of the author, gives values of 0·055–0·18 ev. Layers have been made which were sensitive to radiation of wavelengths as great as 15μ.

It is probable that with this investigation of non-metallic antimony (together with the elements mentioned above) *all* the possible photoconducting elements have now been investigated.

Acknowledgment is due to the Chief Scientist, Ministry of Supply, and to the Controller, H.M. Stationery Office, for permission to publish this letter.

Telecommunications Research Establishment, T. S. Moss
Gt. Malvern, Worcs.
11th October 1951.

Busch, G., Weiland, J., and Zoller, H., 1951, *Semi-conducting Materials*, ed. H. K. Henisch (London : Butterworths Scientific Publications).
Krebs, H., 1951, *Semi-conducting Materials*, ed. H. K. Henisch (London : Butterworths Scientific Publications).
Moss, T. S., 1951, *Proc. Phys. Soc.* A, **64**, 590.
Suhrmann, R., and Berndt, W., 1940, *Z. Phys.*, **115**, 17. See also Krebs, H., 1951.

The Dissociation Energy of SnO

Dissociation limits have been obtained by short and apparently reliable extrapolations of vibrational levels in excited electronic states of several of the diatomic molecules of the group IV (b)+VI (b) elements (for example : SiS, Vago and Barrow (1946 a); GeS, GeSe, Drummond and Barrow (1952); SnSe, Vago and Barrow (1946 b)). These extrapolations are based on the observation of long $v''=0$ progressions in the absorption systems $E \leftarrow X^1\Sigma$. The outstanding problem in the determination of the dissociation energies of these molecules is the identification of the products of dissociation of the states E. It seems most probable that $MX(E) \rightarrow M(^3P)+X(^3P)$ (Vago and Barrow 1946 a), but the multiplet separations in the ^3P atomic states are by no means negligible in all cases, and it is desirable to attempt to identify the products still more closely. The object of this note is to point out that, at least for SnO, a comparison of the thermo-chemical dissociation energy with the spectroscopic limit leads to a tolerably certain identification of the atomic products of dissociation of the state E.

The dissociation limit obtained from the E–X system of SnO corresponds to $D_0=131{\cdot}_9$ kcal (298° K) (Eisler and Barrow 1949). The thermo-chemical value is obtained from the heat of the reaction

$$Sn_c+SnO_{2c}=SnO_g \qquad \ldots\ldots(1)$$

for which Brewer and Mastick (1951), from an analysis of the data of Vesselovsky (1943) derive $\Delta H_{298}=136{\cdot}_9\pm0{\cdot}7$ kcal/mole, combined with the following values :

	ΔH_{298}, kcal/mole	Reference
$Sn_c+O_{2g}=SnO_{2c}$	−138·8	N.B.S. 1947
$Sn_c=Sn_g$	62	Baughan 1951 (private communication)
$O_{2g}=2O_g$	118·3	N.B.S. 1947

We obtain $D_0''(298)=122\cdot_2$ kcal/mole. The value derived for the excitation energy of the products of dissociation of the state E is thus $E_A=131\cdot_9-122\cdot_1=9\cdot_8$ kcal. The energies of the relevant atomic states are given below (values in kcal).

Sn				O			
$^1D_2$	$^3P_2$	$^3P_1$	$^3P_0$	$^1D_2$	$^3P_0$	$^3P_1$	$^3P_2$
24·6	9·8	4·8	0·0	45·4	0·65	0·45	0·0

The assumption that the products are Sn(^{3}P) + O(^{3}P) is strongly supported by these results. Moreover, the calculated value of E_A, $9\cdot_8$ kcal, fits very well with the excitation energy of Sn($^3P_2$), 9·8 kcal. (The multiplet separations of O(^{3}P) are of course far smaller than the experimental uncertainty in E_A.) The present evidence is therefore consistent with the process SnO(E) → Sn($^3P_2$) + O(^{3}P).

The validity of this argument depends primarily upon the accuracy of the values of the heat of sublimation of tin and of the vapour pressures of SnO used in the determination of the heat of reaction (1). The uncertainty in L_{Sn} is unlikely to be greater than ±2 kcal (Baughan, private communication); only the one set of observations on the vapour pressure of SnO is known to us ; the measurements are self-consistent, but there is no means of assessing the probable error in the value derived for ΔH of (1). We must therefore conclude that although the agreement between the thermo-chemical and spectroscopic values, on the basis that SnO(E) → Sn($^3P_2$) + O(^{3}P) is at the least highly suggestive, we cannot regard the present identification of the products of dissociation of the state E as more than tolerably certain.

The best value available for $D_0''(0°\,\mathrm{K})$ of SnO is then 121 kcal or $5\cdot 2_5$ ev.

Note added in proof:

Brewer and Mastick (1951) derive $D_0''(0°\mathrm{K})=131\cdot_6$ kcal/mole. The discrepancy between our values arises because they have used $L_{Sn}=70$ kcal, and because in correcting from D_0'' from 298° K to 0° K they have added 1·4 kcal instead of subtracting 1 kcal.

Physical Chemistry Laboratory,
Oxford University.
27th October 1951.

G. Drummond.
R. F. Barrow.

Brewer, L. and Mastick, D. F., 1951, *J. Chem. Phys.*, **19,** 841.
Drummond, G., and Barrow, R. F., 1952, *Proc. Phys. Soc.* A, in the press.
Eisler, B., and Barrow, R. F., 1949, *Proc. Phys. Soc.* A, **62,** 740.
National Bureau of Standards, 1947, *Selected Values of Chemical Thermodynamic Properties.*
Vago, E. E., and Barrow, R. F., 1946 a, *Proc. Phys. Soc.*, **58,** 538 ; 1946 b, *Ibid.*, **58,** 707.
Vesselovsky, B. K., 1943, *J. Appl. Chem., USSR.*, **16,** 397.

Line Widths in Ferromagnetic Resonance

In recent accounts of the theory of ferromagnetism (Bloembergen 1950, Kittel 1951, Van Vleck 1950, 1951) attention has been drawn to the difficulty of explaining the line widths. Various possible mechanisms have been proposed, and while some of these do give appreciable contributions, the different authors have come to the conclusion that the present known mechanisms are insufficient. It is the purpose of this letter to describe another possible mechanism.

It is probably best described by means of an example. Consider the case of nickel. The free atom has a ground state which, apart from inner shells, is built from $3d^8\,4s^2$. In the metal the wave functions of electrons on different lattice sites overlap and two different approaches, the Heisenberg and the collective electron models, have been used in attempts to describe the actual situation. Ferromagnetic resonance gives a *g*-value of 2·23 at 24° c, and it is usual to explain this as arising in some way from an electron which has nearly a free spin. On the other hand, measurement of the saturation magnetic moment gives an average magnetic moment of 0·606 Bohr magneton per nickel atom. This latter result is easily explained on the collective electron theory of ferromagnetism, while the former result has been shown to be a consequence of the Heisenberg approach. Suppose now that, instead of using the conventional collective electron model to explain the saturation magnetic moment, we postulate that 0·606 of the total lattice sites contain unpaired holes (i.e. are d^9)

and that the remainder are d^{10}. (The remaining electrons are paired off in a conduction band.) Then the saturation moment is given correctly and the resonance would arise from the d^{9} sites, giving $g \sim 2$. The arrangement of d^{9} and d^{10} sites will presumably fluctuate: an electron might move from a d^{10} site to a d^{9} or, alternatively, a d^{9} site might trap a conduction electron and become d^{10}. Thus one has a model in which magnetic and non-magnetic sites are continually interchanging, but in such a way that on the average 0·606 sites are magnetic. If the lifetime of a given magnetic site is long compared with a Larmor precession time, this model will give a width to the resonance line which will persist down to $T=0$, and will be of the order of the field set up at one lattice by a magnetic 'hole' at a neighbouring site. On the other hand, if the lifetime is short a very broad resonance might be expected.

The theoretical determination of the lifetime of a given magnetic site is not easy, but it is possible to devise an experiment to test the validity of the model. Suppose resonance measurements are made on an isotropic substance which has an integral number of Bohr magnetons per lattice site. There will not then be a fluctuation and the model would predict very narrow absorption lines. The choice of a suitable substance is very limited; gadolinium is the most obvious metal to use as it is known to have an integral number of electrons per lattice site, but so far no experiments have been made on it. If such a fluctuation does exist in the common ferromagnetic metals it is possible that a lower limit to the lifetime might be set by experiments on the scattering of neutrons by the magnetic sites.

Clarendon Laboratory,
Oxford.
29th November 1951.

K. W. H. Stevens.

Bloembergen, N., 1950, *Phys. Rev.*, **78**, 572.
Kittel, C., 1951, *J. Phys. Radium*, **12**, 291.
Van Vleck, J. H., 1950, *Phys. Rev.*, **78**, 266 ; 1951, *Physica*, **17**, 234.

Some Regularities in Nuclear Energy Levels

On several occasions nuclear energy levels have been found whose excitation energies bear integral ratios to each other. Guggenheimer (1943) carried out a general survey of the data then available and attempted, with some success, to explain low-lying nuclear levels in terms of a rotator model of the nucleus.

More recently the accuracy of the experimental results has very greatly increased, and a new survey of the data has been made to see whether or not there is now more trustworthy evidence for the general existence of simple numerical relations between nuclear excitation energies. Results obtained by β- and γ-ray absorption methods were rejected as being of too low accuracy to be useful; so also were 'continuum' levels of light nuclei since, although their spacing is generally known with considerable accuracy, their distance above the ground state is not.

The results of the survey may be summarized as follows:

(i) Out of 45 nuclei where the positions of two or more energy levels are known accurately (involving a total of 175 levels), 38 (involving 140 levels) obeyed the integer 'rule' to within 1 or 2%. The 'rule' was also obeyed in a further 16 nuclei out of 23 where γ-ray energies were known but not the positions of the levels.

After making allowance for the experimental errors, the probability of the random occurrence of all the observed integral sequences can be calculated approximately. The value obtained is 10^{-30}, within 2 or 3 orders of magnitude. Nuclear energy levels are probably not randomly distributed, so that this calculation is hardly a fair one; nevertheless the evidence for the physical significance of the integral ratios seems extremely strong.

The table gives as an example the experimental levels of ${}^{11}_{5}\mathrm{B}$ (van Patter, Beuchner and Sperduto 1951) together with the calculated levels, multiples of 0·1784 Mev, for comparison.

Experimental	2·138	4·459	5·034	6·758	6·808	7·298	8·568	8·926	9·190	9·276	Mev
Calculated	2·141	4·460	4·985	6·779		7·314	8·563	8·920	9·098	9·277	Mev

(ii) If the highest common factor of the nuclear excitation energies (e.g. 0·1784 Mev for ${}^{11}_{5}\mathrm{B}$) is plotted against the nuclear charge Z, then it is found that the majority of the points lie on or near two smooth curves, one for even–even nuclei and the other for nuclei having either odd Z or odd N.

This is especially striking in the case of even–even nuclei where, in addition, the nuclear shell structure (Mayer 1950) appears to influence the shape of the curve, since there are peaks in the region of nuclei having $N=50$ and $N=82$. This is shown in the figure. From this result it appears that the highest common factor of the excitation energies of the levels in a nucleus may have some physical significance as a nuclear constant.

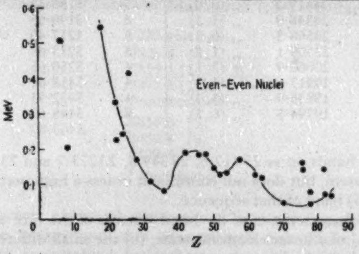

Department of Natural Philosophy, **P. J. Grant.**
The University, Glasgow.

20th November 1951.

Guggenheimer, K. M., 1943, *Proc. Roy. Soc.* A, **181**, 169.
Mayer, M. G., 1950, *Phys. Rev.*, **78**, 16.
van Patter, D., Beuchner, W., and Sperduto, A., 1951, *Phys. Rev.*, **82**, 248.

.A
5
2

The Spectrum of Lutecium Monoxide

An intense spectrogram of lutecium oxide was first obtained by Eder and Valenta (1911) from the sulphate burning in a carbon arc source. They recorded the approximate wavelengths of about 30 band heads. The prominent system of bands at λ4660 was later obtained at the Bureau of Standards on spectrograms of 5-amp d.c. arcs at 220 volts between silver electrodes tipped with LuO, and a vibrational analysis of that system was reported by Watson and Meggers (1938). Band heads at λ5170 and λ4093 were also measured by Meggers, but as a sufficient number of band heads did not develop in these regions (presumably due to the high excitation conditions of their 5-amp arcs) they were ignored. The three systems at λ5170, λ4660, λ4093 were obtained very clearly on 3-amp arc spectrograms taken in this laboratory using carbon electrodes soaked in a solution of lutecium oxide in HCl. The complete spectrogram as obtained later from the flame above a carbon rod steeped with the same solution and excited by a current of 600 amp at 15 volts is shown in the photograph.

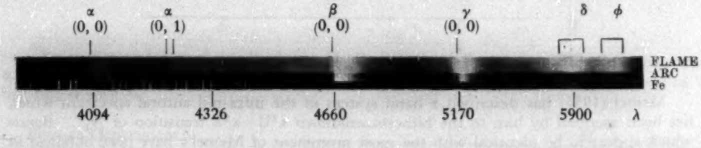

In addition to the above three systems named α, β, γ, the spectrum shows two continua δ and ϕ in the red region. On the original negative a hazy sequence of bands could be recognized in the feature at λ6000, but reliable measurements could not be made. The entire group of band systems and continua is attributable to lutecium oxide, as none of the features could be found on similar spectrograms taken with other rare earth oxides (Gatterer and Junkes 1945) free from lutecium impurity.

Watson and Meggers analysed system β. The vibrational analysis of the other two systems is presented in the table.

New Bands in Lutecium Oxide

Int.	λ	ν	$v'\,v''$	Int.	λ	ν	$v'\,v''$
2	3978·37	25128·8	α (2, 1)	10	5171·43	19331·6	γ (0, 0)
7	4094·00	24419·2	,, (0, 0)	7	5185·42	19279·5	,, (1, 1)
4	4105·81	24348·9	,, (1, 1)	4	5199·65	19226·7	,, (2, 2)
6	4241·80	23568·3	,, (0, 1)	8	5217·40	19161·3	,, (3, 3)
4	4252·49	23509·1	,, (1, 2)	5	5233·69	19101·7	,, (4, 4)
2	4983·83	20060·9	γ (2, 1)	4	5250·65	19040·0	,, (5, 5)
5	5019·28	19917·6	,, (4, 3)	4	5418·64	18449·7	,, (1, 2)
6	5034·64	19856·9	,, (5, 4)	4	5432·95	18401·1	,, (2, 3)
5	5050·52	19794·5	,, (6, 5)	8	5448·63	18348·2	,, (3, 4)
				7	5463·87	18297·0	,, (4, 5)

A short sequence of bands, at $\nu\nu$ 23 417·6, 23 349·3, 23 273·7 and 23 197·0, follows the (0, 1) sequence of the α-system, but does not continue it unless a high perturbation is supposed at the disappearing (2, 3) band of that sequence.

The well-known characteristics of the band systems of the rare earth oxides, viz. (i) the value 840 cm^{-1} for ω_e'' of a lower electronic state, (ii) the small difference in the values of the vibrational quanta of the lower and upper states, and (iii) the delimitation of the band systems to a few sequences round the (0, 0), are all observable in these systems too.

The spectrum of the oxide of lutecium with its 5d 6s^2 configuration may be expected to be similar to that of the oxide of lanthanum of the same electronic configuration if the effect of the completed 4f orbit in lutecium is negligible. Lanthanum oxide has a $^2\Sigma$ lowest electronic state, and transitions to this level from $\text{A}^2\Pi$, $\text{B}^2\Sigma$, $\text{C}^2\Pi$, and a D level are known. The $\text{A}^2\Pi-\text{X}^2\Sigma$ transition is in the red region and $\text{C}^2\Pi-\text{X}'^2\Sigma$ in the region λ4360−4415. The intense double system β and γ in the present spectrum appears on this analogy to be the $\text{C}^2\Pi-\text{X}^2\Sigma$ of lutecium oxide. The interval 2 114 cm^{-1} of the $\text{C}^2\Pi$ term of the molecular spectrum of the oxide is of the same order as the ^{2}D ground term interval 2 000 cm^{-1} (approx.) of Lu I. The CN band at λ4216 overlaps the α-system in the arc spectrograms and it is very brief in the flame spectrum shown in the photograph. The dispersion is too small, but from what could be judged from the use of the microscope, this system is of the simplest structure and may be a $^2\Sigma-{}^2\Sigma$ transition. It is believed that the continua too would develop recognizable band structure under lower excitation conditions.

Laboratorio Astrophysico,
Vatican City, Rome.
30th November 1951.

A. Gatterer.
S. G. Krishnamurty.

Eder, J. M., and Valenta, E., 1911, *Atlas typischer Spektren* (Vienna: Hof- und Staatsdruckerei).
Gatterer, A., and Junkes, J., 1945, *Spektren der seltenen Erden* (Rome: Vatican Observatory).
Watson, W. W., and Meggers, W. F., 1938, *Bur. Stand. J. Res. Wash.*, **20**, 125.

Meinel's Infra-Red Auroral Bands

Meinel (1951) has described a band system in the infra-red auroral spectrum which has been ascribed by him to the hitherto unknown $\text{A}^2\Pi-\text{X}^2\Sigma$ transition of N_2^+. Bands which appear to be identical with the most prominent of Meinel's have been obtained in this laboratory from two sources (see also Herman 1951). The first was an electron beam tube, similar to one used by Hanle and Schaffernicht (1930) for studying excitation functions. It contained nitrogen at a pressure of about 0·01 mm Hg. Accelerating potentials of about 200 volts were used. The spectrum was photographed with an instrument with dispersion 185 Å/mm at 8 000 Å. The second was a hollow cathode tube operated at 440 volts in nitrogen at a pressure of 0·2 mm Hg. The spectrum was photographed with a dispersion of 50 Å/mm at 8 000 Å. In both cases, hypersensitized Kodak II N plates were used. With the first source, the first positive bands were relatively weak, and isolated bands near the positions of Meinel's (1, 0) and (2, 1) bands were recorded.

There was also a very faint band near Meinel's (3, 2) band at *c.* 8 298 Å. With the second source, the new (1, 0) and (2, 1) bands were feebler relative to the first Positive bands, and largely obscured by the (7, 6) and (6, 5) heads of the latter. The wavelengths found for the maxima of intensity are given in the table, together with Meinel's data. The numbers in square brackets are rough estimates of intensity from densitometer records, after allowing for the background due to scattered light from the filament. The wavelengths found here are mostly a little shorter than Meinel's, but it is thought the differences may be due to different excitation conditions, and to a certain arbitrariness in locating intensity maxima. The figure is a photograph of the spectrum of a 220 volt beam, with an argon + neon reference spectrum. The spectrum of the beam shows a few Oɪ lines in addition to nitrogen bands and Nɪ lines; no spectra not due to nitrogen were found on the higher dispersion plate. The wavelengths and appearance of the bands are different from those of CN bands (Herzberg and Phillips 1948).

Wavelengths of Intensity Maxima of Infra-red Bands

Hollow cathode	220-volt beam	Aurora (Meinel)
7825·6	7826·[illegible] [8]	7828·2 (1, 0)
7859·4	7859·1 [11]	7861·9
7878·0	7877·8 [13]	7879·6
(7915)*	(not recorded)	7912·2
8053·0	8054·0 [5]	8056·8 (2, 1)
8090·8	8089·4 [9]	8094·0
8106·9	8109·8 [10]	8107·0

* Very feeble.

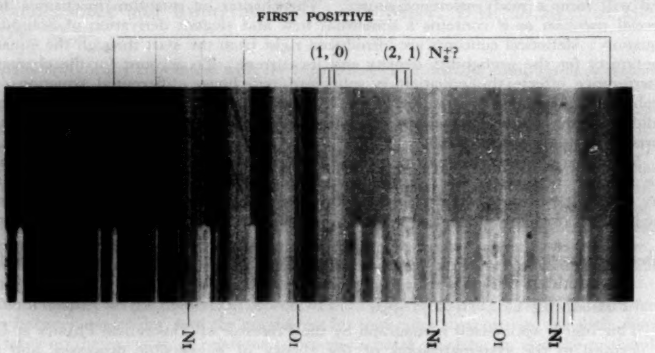

The writer wishes to thank Professor D. R. Bates and Professor K. G. Emeléus for suggesting the use of the two sources, and Dr. O. White and Mr. L. W. Kerr for help in building the tubes.

N. D. Sayers.

Physics Department,
Queen's University, Belfast.
11th December 1951.

Hanle, W., and Schaffernicht, W., 1930, *Ann. Phys., Lpz.*, **6**, 905.
Herman, R., 1951, *C.R. Acad. Sci., Paris*, **233**, 926.
Herzberg, G., and Phillips, J. G., 1948, *Astrophys. J.*, **108**, 163.
Meinel, A. B., 1951, *Astrophys. J.*, **113**, 583.

REVIEWS OF BOOKS

Die Mathematischen Hilfsmittel des Physikers, by E. MADELUNG. Pp. xx + 531. 4th Edition. (Berlin, Göttingen, Heidelberg: Springer Verlag, 1950.) DM. 49.70.

Madelung's book was very popular with German students of mathematical physics right from its first publication in 1922, and was doubtless also widely appreciated among physicists outside Germany. That the present fourth edition is about twice the size of the first corresponds with the great increase in the required mathematical equipment of the physicist, which has resulted mainly from the development of quantum mechanics.

One of the many attractive features of the present edition is that it combines a systematic compilation of mathematical results and formulae with the connected treatment of a textbook. Within the compass of 531 pages the author covers a wide range of mathematical topics, and the incorporation of adequate introductory and explanatory remarks much facilitates the use of the book. Throughout, the needs of the practising physicist are placed first. A resulting sacrifice of some mathematical rigour, which will be regretted only by the purist, is obviously necessary to avoid unwieldiness.

The book is divided into two main parts. The first entitled *Mathematics* contains thirteen sections dealing with almost every aspect of mathematics which is of use to present-day physicists. The main subjects discussed are: higher algebra, transformations and invariants, vector and tensor analysis, group theory, differential and integral equations, variational calculus and statistics. The second part is entitled *Physics* and constitutes a highly condensed treatment of modern theoretical physics. It is extremely well presented and will form a ready reference source. The chapter on quantum mechanics deserves special mention as it contains a somewhat new and elegant derivation of Schrödinger's equation: statistical concepts are introduced right from the start through the equation of continuity for the probability density and its current. To account for the characteristic interference effects the equation is split into two linear differential equations in the probability amplitude and its conjugate. The derivation is finally based on the exact validity of the classical equations of motion for the expectation value of any dynamical variable in its time dependence.

Madelung's book in its new edition will continue to be of excellent service to all who are engaged in physical research and teaching and it should make a valuable addition to any physicist's library. The publishers deserve congratulation for their share in making the book so attractive.

J. AHARONI.

Thermodynamics of Irreversible Processes, by S. R. DE GROOT. (Selected Topics in Modern Physics III.) Pp. xvi + 242. (Amsterdam: North Holland Publishing Co., 1951.) 35*s*.

This highly specialized monograph by the Professor of Theoretical Physics at Utrecht is devoted to the systematization of the theory of irreversible processes, and to the formulation of the general theory on a logical basis. The treatment is made to depend to a very great extent on a theorem due to Onsager which in its turn depends on a hypothesis, of a plausible character, about the nature of the fluctuations which can occur in a statistical-mechanical ensemble.

The book is clearly written and contains a number of very useful results in its chapters on the application of the theory to heat conduction, diffusion, thermal diffusion and thermo-electricity.

J. H. A.

Universal Mechanics and Hamilton's Quaternions, by O. F. FISCHER. Pp. vi + 356. (Stockholm: Axion Institute, 1951) $10.

This book describes itself in its preface as "a book written by a civil engineer on universal mechanics with an attempt to introduce a certain order in its mathematical structure by means of the calculus of Hamilton's quaternions". By universal mechanics is meant ordinary mechanics, elasticity, hydrodynamics, aerodynamics, electromagnetism, relativity and quantum theory. The description is a just one.

After summarizing vector analysis, quaternions are introduced and applied to mechanics and electromagnetism. The algebra is treated from a naive point of view which resembles the original one of Hamilton, and this is probably an advantage. In the course of these applications certain electro-mechanical analogies are discussed. The treatment is by no means confined to quaternion methods; for instance, theories of earth magnetism and Blackett's empirical relation are described. Special and general relativity are summarized, and Einstein's 1950 theory is described in 3½ pages. Clifford's numbers, or *E*-numbers, are considered as ' double quaternions ', and some of Eddington's ' fundamental theory ' is discussed. This discussion is uncritical of the physical aspects, but wisely remarks that, instead of rejection, ' It would be more useful to science to give careful thought . . . And then attempt to clear up what is dubious '. Some description is also given of H. G. Küssner's *Principia Physica* (Göttingen 1948). This includes a short account of his combinatorial theory of arithmetical invariants of mechanical systems, and its applications to fundamental physics.

The notations employed are not always such as to show the power and simplicity of quaternions; in the opinion of the reviewer it is a mistake to depart from Hamilton's use of simple juxtaposition to denote the quaternion product. On the other hand, the book contains a great deal of information drawn from a wide field; the bibliography lists references to 124 papers and books. This makes the work of some value to anyone using quaternions in physical applications. There has been no previous attempt to fill such a need. It is printed by a lithographic method in a rather small print. There is a very satisfactory index.

C. W. KILMISTER.

Fluoreszenz organischer Verbindungen, by TH. FÖRSTER. Pp. 312. (Göttingen : Vandenhoeck and Ruprecht, 1951.) In paper, DM. 29.50 ; in cloth, DM. 32.50.

A book specifically concerned with the luminescence of organic compounds is welcome at the present time. Recent developments in this field have already been reviewed by Professor Förster (*Naturwissenschaften*, 1947, **6**, 166), but his book provides a much more comprehensive and up-to-date appraisal. It includes all aspects of the subject, from experimental methods to the modern theories of the various phenomena involved. The book begins with a short introductory chapter containing necessary definitions of terms and a brief historical survey. Chapter II reviews the experimental techniques involved in luminescence studies, such as measurements of fluorescence intensities, degree of polarization of fluorescence, decay of emission and fluorescence spectra. Chapter III introduces the reader to the general properties of organic compounds, with particular reference to the aromatic hydrocarbons and dyestuffs. Their structural chemistry and the physical conditions necessary for fluorescence are discussed.

After a chapter on the theoretical aspects of light absorption and emission, the transfer of energy between molecules, and the conditions for molecular dissociation, the fifth chapter again takes up the question of relations between chemical constitution and the probability of fluorescence emission, dealing in detail with the aromatic hydrocarbons, with and without substituted groups, heterocyclic compounds and dyestuffs. After describing the older phenomenological theory which involved the assumption of chromophoric and fluorphoric groups, the later physical theory of fluorescence based on wave mechanical ideas is discussed. The emission and absorption spectra of organic compounds in vapour phase and in solution are next considered with respect to their electronic and vibrational energy states.

In chapter VII we find a discussion of the absolute yield of fluorescence and its dependence on the wavelength of exciting radiation, temperature and nature of the solvent, while the next chapter, a very brief one, deals with the decay of fluorescence. It is natural that a large space should be given to the important studies of polarization and quenching of fluorescence in solution, with which chapter IX and chapters X and XI are concerned respectively. Measurements of fluorescence polarization and its dependence on solution viscosity, temperature and concentration of the fluorescent compound furnish important information on molecular structure. A knowledge of the dependence of quenching of fluorescence by solvent impurities on similar factors to those affecting polarization indicates the nature of energy transfer in molecular systems and the relation of fluorescence to other phenomena such as photochemical dissociation and the state of molecular aggregation. With respect to the latter it is gratifying to see a section of chapter XI devoted to a discussion of the Scheibe polymers (pseudoisocyanin polymer threads), which show such remarkable fluorescence characteristics.

The text concludes with a chapter on phosphorescence of long duration in organic molecules, being particularly concerned with studies by Lewis and his collaborators of fluorescein in boric acid and the various theoretical interpretations of phosphorescence in condensed systems.

There are 28 pages of references, including a special list of recent literature on fluorescence which, however, is not quite complete. A short, but apparently quite adequate, subject index is provided.

It is apparent from the references in the text that the author is conversant with almost all of the recent and past studies in the field by workers in all countries. He has given adequate indications of the important contributions made during the last decade by Wawilow and other Russian workers, which are, perhaps, not so well known because of their relative inaccessibility.

Although the author lays stress on the theoretical aspects of his subject, he preserves a reasonable balance between them and experimental studies. It is valuable to have the recent and more detailed theoretical treatment of such phenomena as quenching and polarization of fluorescence since these have not been given collectively elsewhere. G. F. J. GARLICK.

Ferromagnétisme et Antiferromagnétisme (Colloques Internationaux du Centre National de la Recherche Scientifique, XXVII). Pp. 360. (Paris: CNRS, 1951.)

The present volume of the series of reports issued by the C.N.R.S. contains the 49 papers, in French or English, read at the international conference at Grenoble in July 1950. Its contents reflect the marked advances made in the field of ferromagnetism and antiferromagnetism since the last conference was held, under the chairmanship of the late Prof. Pierre Weiss, at Strasbourg in 1939. At the same time it is most noticeable what wide gaps still exist between well-established experimental facts relating to the magnetic properties of even the simplest solids, and a fully satisfying theoretical coordination of these facts.

On the credit side must be placed the enormously increased understanding of the domain structure and hysteretic properties of ferromagnetic metals and alloys. This advance is due in no small measure to the recent powder pattern experiments, yielding such fascinating results, described here by Dr. R. M. Bozorth (p. 160) and Prof. L. F. Bates (pp. 174, 356). Theoretical work on coercivity and related properties is described in an admirable review article by Dr. L. Weil (p. 289). The corresponding enormous recent advances in the performance of permanent magnets are described by Dr. K. Hoselitz (p. 300). An almost completely new, and already flourishing field of research, ferromagnetic resonance, is covered by Prof. C. Kittel (p. 143). The novelty of this field may be judged from the fact that spectroscopic splitting factors g which are considerably larger than 2 are here the rule. The long way theory has yet to advance, on the other hand, is exemplified by the results of precision measurements of the gyromagnetic ratio g' described by Dr. A. J. P. Meyer (p. 156), who finds $g'=2{\cdot}00$ for iron and nickel, in disagreement with Kittel's simple rule $g-2=2-g'$. Further, as stressed in discussion, present ideas as to the interpretation of ferromagnetic anisotropy seem to be invalidated by Meyer's results. The realization of the fundamental importance of anisotropy makes one regret that the theoretical aspects of this subject were not discussed more fully at the conference. The two main reviews of the present status of the basic atomic theory of ferromagnetism in metals and alloys, by Prof. E. C. Stoner (p. 224) and Prof. R. Forrer (p. 254), indicate that differences of viewpoint still exist between the various schools of thought, roughly described as the 'collective electron' school and the 'discrete levels' school. An international conference of this sort may do much to bring these viewpoints closer together and to help in overcoming old-established prejudices.

Perhaps even more spectacular advances, fully described in this volume, have recently been made in the field of antiferromagnetism and 'ferrimagnetism'; the latter term is one coined by Prof. L. Néel, the organizer and chairman of the conference and the present distinguished doyen of French magnetism. Prof. J. H. Van Vleck (p. 114), in a comprehensive review, states the theoretical position regarding antiferromagnetism, but ends on a note of caution by saying "the remarkable thing is that . . . idealized and over-simplified descriptions work as well as they do". In this connection it is to be regretted that the recently developed neutron diffraction technique was not described more fully in a separate article. Related to Van Vleck's review are the various accounts of the present state of experiment, by Prof. H. Bizette (p. 13), Prof. F. Trombe (p. 22) and others. Ferrimagnetism is best exhibited by the non-metallic solids grouped under the name ferrites. Their properties are described by the late Dr. J. L. Snoek (p. 80), Dr. C. Guillaud (p. 91), Dr. E. F. Bertaut (p. 104) and others. The fact that the properties of these substances may be understood by regarding them as arising from incomplete antiferromagnetism was first stated by Néel; his already classical papers on this subject underlie the discussion to a marked extent.

It is not possible to mention here more than a few of the papers included in the volume under review. Many of the accounts of which no mention is made deal with particular properties of particular solids in some detail, and frequently fail to consider these properties against the wider background afforded by the excellent more general review articles. Such specialized articles could have been more appropriately published as research papers in the scientific journals. Indeed, some of them are no more than slightly amended reprints of papers which have, in fact, already been published elsewhere. The space saved by their omission from the present volume might have been more profitably filled by further detailed reviews. On the other hand, a formal presentation of papers read at a scientific conference can never reproduce the more informal atmosphere usually prevailing on such occasions, and, in particular, from all accounts, on the occasion of the Grenoble conference during the hot French summer of 1950. E. P. WOHLFARTH.

Semi-Conducting Materials—Proceedings of the Reading Conference, 10–15th July 1950. Ed. H. K. HENISCH. (London: Butterworths Scientific Publications, 1951.) 40*s*.

The sub-title and the foreword of 14 lines are the only indication that this collection of twenty-eight papers on semiconducting materials is, in fact, the Proceedings of an International Conference on the subject, and, of the foreword, only four lines specifically refer to the Proceedings here presented:

> 'The Reading Conference 10–15th July 1950, of which this volume constitutes the Proceedings, provided research workers from this country and abroad with an opportunity for discussion of the most recent progress. Over 200 physicists and engineers took part, among whom it was a pleasure to welcome 80 visitors from other countries.'

As no discussions of the papers are reproduced, the book appears at first sight as an issue of a scientific periodical in which, by some chance, all papers deal with semiconductors. Its real significance however, consists in its representing the nearest thing to what used to be called a treatise on a scientific subject, i.e. a complete, up-to-date, concise but understandable review. It is to the credit of the organisers that by the selection of the speakers this book provides, in fact, a reasonably complete cross section of contemporary semiconductor physics, and to the credit of the authors that they have given well-readable accounts with a satisfactory selection of references.

It is obviously impossible to refer here to each of the 28 papers, and it would be an invidious task to refer to a few in particular. The reader will get a good idea of the theoretical problems involved, of the classification of materials, of measuring techniques, absorption spectra, of some recent ideas and experiments concerning carrier injection, transistors and surface phenomena, of the effect of nucleon bombardment, of motion of electrons in single crystals and in polycrystalline materials, of the influence of lattice defects and, of course, of the results obtained in measurements on a large number of particular materials. Further, there are papers on a particular class of semiconductors which have recently been called oxidic semiconductors and on some properties of thin metallic films.

The most serious omission (not the organisers' fault) is the lack of reference to recent Russian attempts to revise the theoretical basis of conduction in solids, for instance, by the introduction of polarons, electron pairs, etc.

The fact remains that this book will be studied and consulted again and again by everybody working on semiconductors or on allied fields, and it should be on the shelves of any physics library keeping a representative collection of periodicals. W. E.

Calcul Conceptuel ou Qualitatif, by RENÉ CORDEBAS. Pp. 38. (Paris: René Cordebas, 1951.)

Graphical methods of research of ideas and laws in the physical sciences. Tables of 'Idéogrammes'.

CONTENTS FOR SECTION B

PAGE

Dr. R. LATHAM, Mr. M. J. PENTZ and Dr. M. BLACKMAN. A Coil System for an Air-cored Betatron 89

Dr. G. LIEBMANN. Magnetic Electron Microscope Projector Lenses 94

Mr. W. G. STANDRING and Mr. J. S. T. LOOMS. The Electrical and Luminous Characteristics of Short Air Sparks suitable for High Speed Photography . 108

Dr. R. S. LONGHURST. A Note on the Calculation of Principal Ray Aberration . 116

Mr. A. N. GENT and Mr. R. S. RIVLIN. Experiments on the Mechanics of Rubber: I—Eversion of a Tube 118

Mr. W. P. OSMOND. An Interpretation of the Magnetic Properties of some Iron-Oxide Powders 121

Mr. D. A. WRIGHT and Dr. J. WOODS. The Emission from Oxide-coated Cathodes in an Accelerating Field 134

Dr. H. K. HENISCH and Mr. E. W. SAKER. The Effect of Mercury on Selenium . 149

Dr. E. W. J. MITCHELL. Impurity Scattering in Oxide Semiconductors . . . 154

Letters to the Editor:

Prof. P. SELÉNYI. Some Further Observations on the Effect of Bending on Selenium Rectifier Discs 161

Mr. E. W. LEE. The Approach to Saturation Magnetostriction of Nickel . 162

Reviews of Books 163

Contents for Section A 166

Abstracts for Section A 167

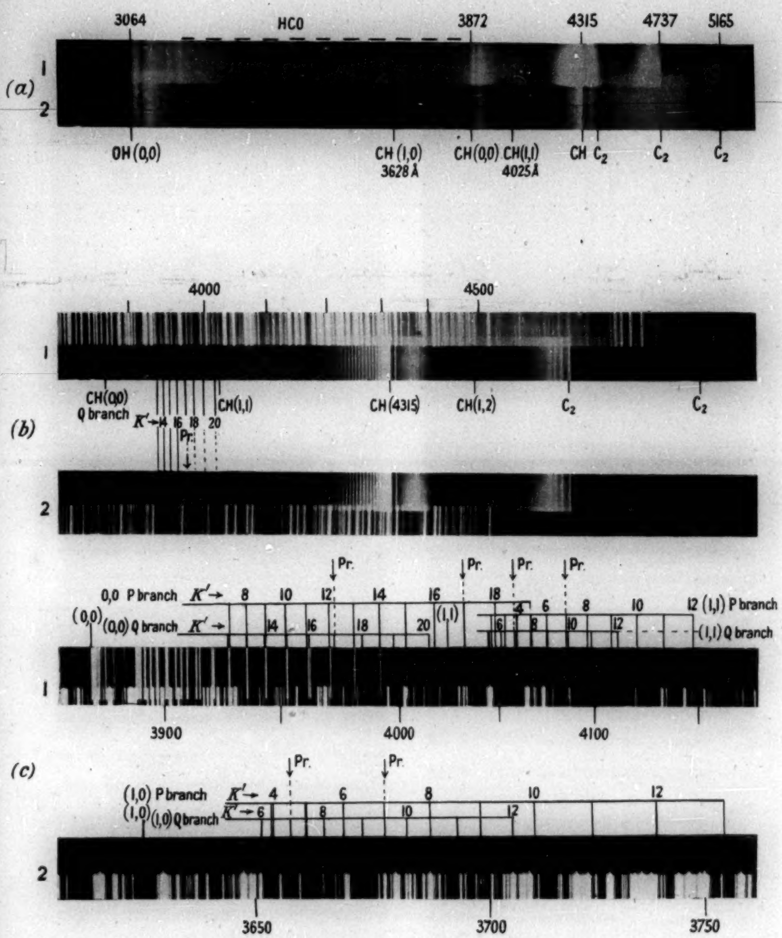

(*a*) Comparison of 1, an ethylene–air flame and 2, a hydrogen–air flame containing a small amount of perfluoro-methyl cyclo-hexane (C_7F_{14})—note strong CH (1, 0) and (1, 1) bands in the latter. (Raman quartz spectrograph, Ilford Zenith plate, exposure (1) 30 sec., (2) 10 min.)

(*b*) Comparison of 1, a hydrogen–air flame containing ethylene (1·2% ethylene and $\lambda=0{\cdot}36$) and 2, an ethylene–air flame. Note the suppression of the predissociation in the Q branch in (1). (Raman glass spectrograph, Zenith plate, exposure (1) 1 hour, (2) 15 sec.)

(*c*) 1. Large dispersion plate of CH (0, 0) and (1, 1) bands in a hydrogen–oxygen flame containing acetylene (2·5% acetylene, $\lambda=0{\cdot}43$).

2. CH (1, 0) band in the same flame.

Note the suppression of the predissociation in all three bands—Pr marks the line where predissociation usually sets in. (Quartz Littrow spectrograph, Zenith plate, exposure 4 hours.)

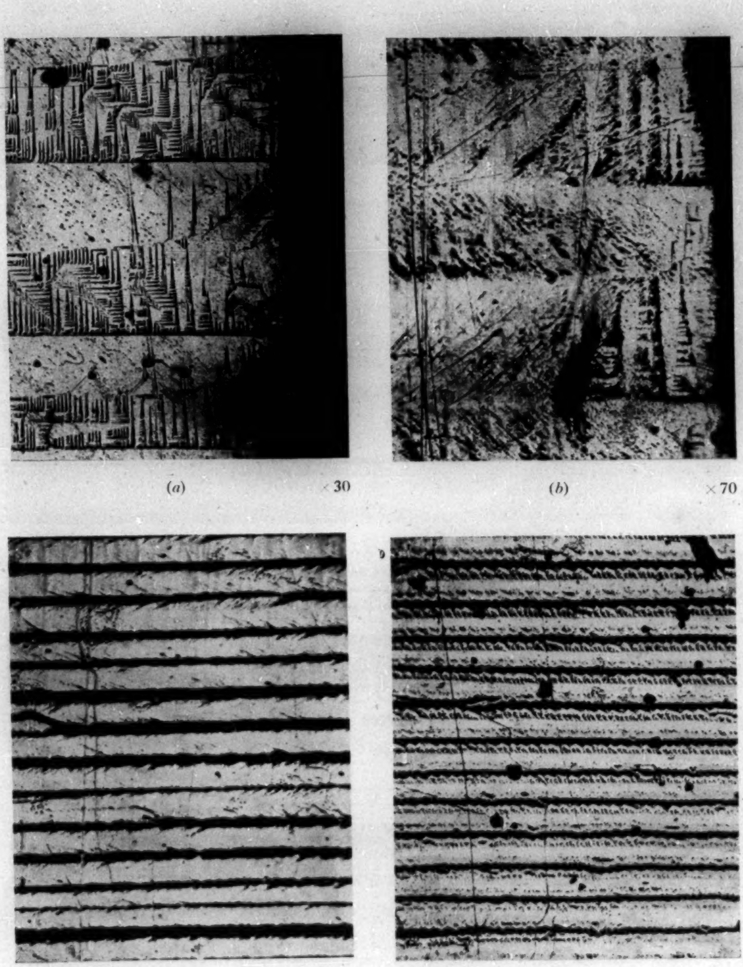

(*a*) ×30 (*b*) ×70

(*c*) ×45 (*d*) ×45

$H \uparrow . [0\bar{1}1] \updownarrow$

Fig. 2 (*a*), (*b*), (*c*): (100) patterns for 8, 20, 250 oersteds respectively; (*d*): (011) pattern for field of 50 oersteds

PLATE I.

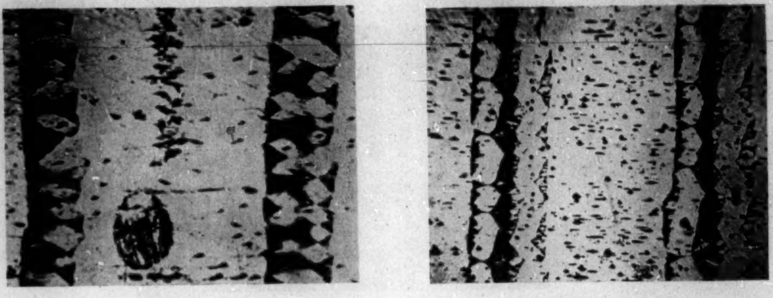

(*a*) $H=13$ Oe ×112 (*b*) $H=17$ Oe ×112

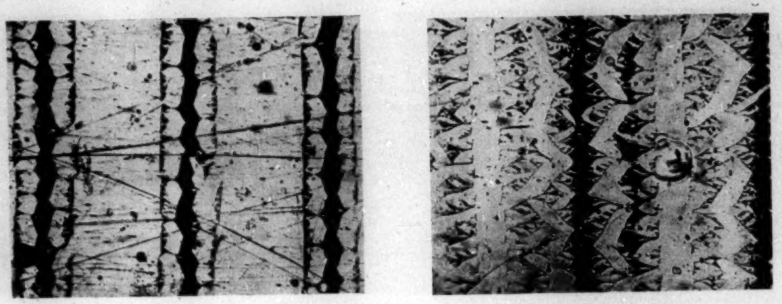

(*c*) $H=17$ Oe ×150 (*d*) $H=27$ Oe ×150

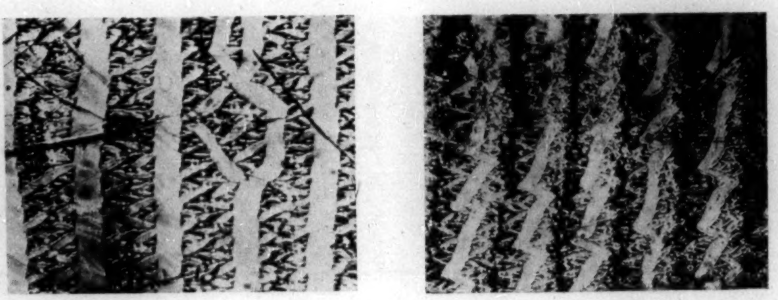

(*e*) $H=74$ Oe ×180 (*f*) $H=110$ Oe ×180

$H \rightarrow \updownarrow$ [100]

Fig. 3. Detailed form of (011) plane patterns.

PLATE II.

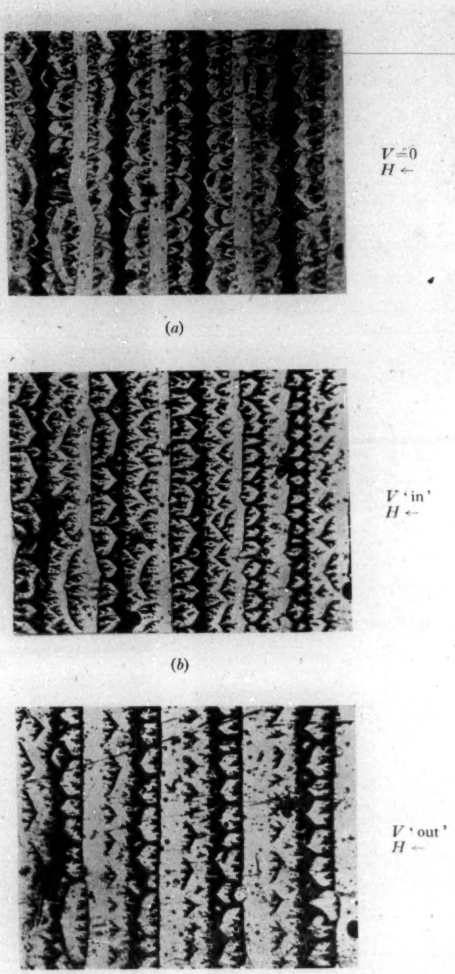
$V=0$
$H \leftarrow$
V 'in'
$H \leftarrow$
V 'out'
$H \leftarrow$

(*a*)

(*b*)

(*c*)

Fig. 4. Effect of small normal field V on (011) patterns.
Magnification = 75 ×

PLATE III.

.A
5
2

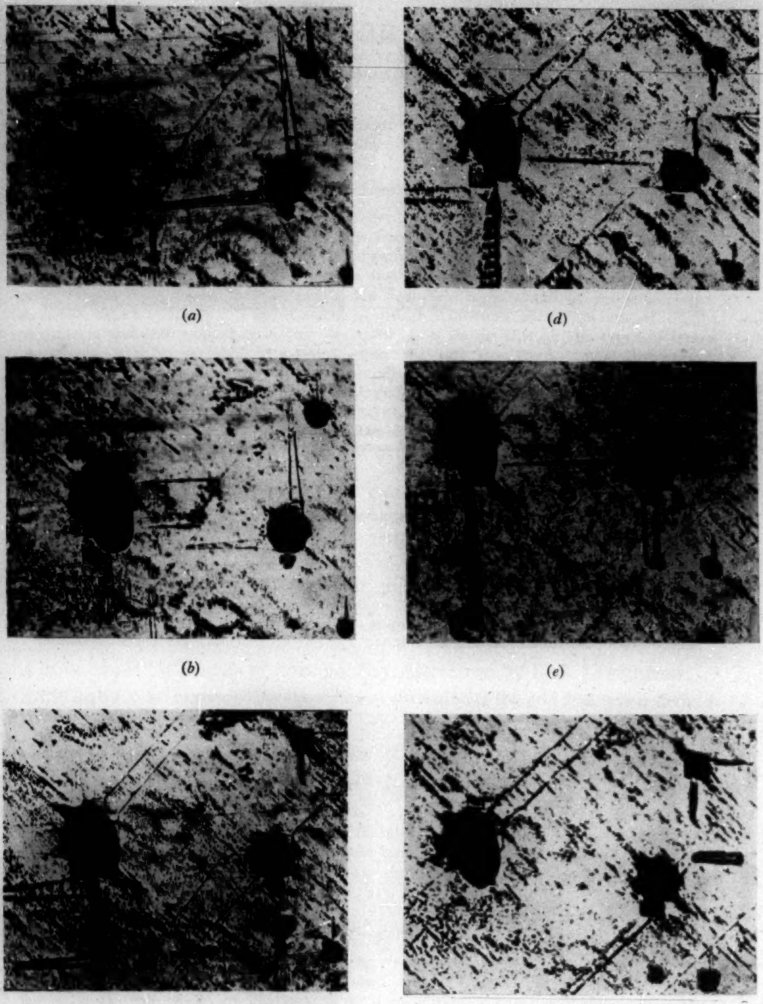

(*a*) (*d*)

(*b*) (*e*)

(*c*) (*f*)

Crystal axes X Magnification × 92

Fig. 1. Effect of cavities on the movement of a 180° boundary.

PLATE I.

PROC. PHYS. SOC. VOL. 65, PT. 2—A (L. F. BATES AND C. D. MEE, *Surface Closure Domains*)

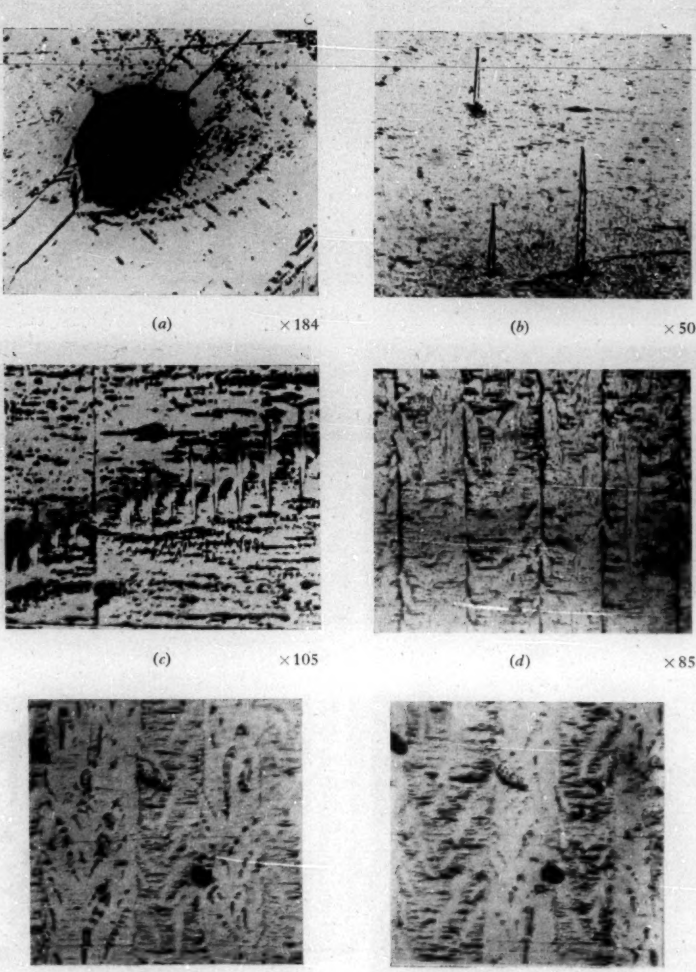

(*a*) ×184

(*b*) ×50

(*c*) ×105

(*d*) ×85

(*e*) ×96

(*f*) ×96

Fig. 2. Surface closure structures on silicon–iron.

Plate II.

ABSTRACTS FOR SECTION B

A Coil System for an Air-cored Betatron, by R. LATHAM, M. J. PENTZ and M. BLACKMAN.

ABSTRACT. The paper describes the design of an air-cored coil system for a small betatron and measurements of the field configuration produced by this system.

Magnetic Electron Microscope Projector Lenses, by G. LIEBMANN.

ABSTRACT. The results of an earlier paper are extended to the special case of the electron microscope projector and similar type lenses. It is shown that the focal properties of symmetrical projector lenses with different ratios of gap width S to lens bore D can be represented by a single curve. This is then applied to the discussion of various cases of practical interest. The calculated results are found to be in excellent agreement with measurements by Ruska. The question of image distortion as a function of design parameters and lens excitation is then discussed; it is shown that all the types of lenses investigated can be operated at a point where they are free from ' radial distortion '. A consideration of scaling operations shows that there is little difference between the optimum performance of lenses of different geometry, but equal focal length. Certain results of use in practical lens design are combined in a design chart from which the relevant design or operational parameters can be read directly. In conclusion, design rules are given for the optimum design of projector lenses covering a wide range of magnifications.

The Electrical and Luminous Characteristics of Short Air Sparks suitable for High Speed Photography, by W. G. STANDRING and J. S. T. LOOMS.

ABSTRACT. The light emitted by various forms of spark gap is examined, and the factors affecting maximum value and variation with time are discussed. Measurements of the voltage drop across the spark help to explain the effects on light output of spark duration and form of spark gap. A rough spectral analysis is given for an open gap.

A Note on the Calculation of Principal Ray Aberration, by R. S. LONGHURST.

ABSTRACT. An expression for the spherical aberration of the principal rays is derived. If the primary aberrations are calculated the principal ray aberration may be found with very little additional effort.

Experiments on the Mechanics of Rubber: I—Eversion of a Tube, by A. N. GENT and R. S. RIVLIN.

ABSTRACT. Measurements are made of the changes which take place in the dimensions of rubber tubes when they are turned inside out. These are compared with the values predicted from the theory of large elastic deformations of incompressible isotropic materials.

An Interpretation of the Magnetic Properties of Some Iron-Oxide Powders, by W. P. OSMOND.

ABSTRACT. The observed magnetic properties of fine dispersed powders of the ferromagnetic iron oxides are discussed in the light of modern theories of the magnetization of ferrites and of ferromagnetics containing non-magnetic inclusions. The individual powder particles are shown to be probably of single-domain size, and the relative coercivities of γ-ferric oxide powders of nearly spherical and of markedly acicular grains are qualitatively in agreement with theory, on the grounds of shape anisotropy. After allowance is made for volume concentration and small departures from stoichiometric composition, the ratio of the coercivities of apparently identical acicular powders of

γ-ferric oxide and of magnetite is found to be approximately that of the saturation magnetization per ferric ion rather than that of the value per unit volume, and both coercivities are lower than theory would predict. It is concluded that magneto-crystalline anisotropy is also involved. In contrast, relative and actual values of intrinsic induction at the beginning of the approach to saturation are in satisfactory agreement with theory, as are the relative values at remanence although the actual values here are rather low. It is hoped to extend the study to larger departures from stoichiometric composition involving partial transformation to the antiferromagnetic iron oxides α-Fe_2O_3 and FeO.

The Emission from Oxide-coated Cathodes in an Accelerating Field, by D. A. Wright and J. Woods.

ABSTRACT. It is shown that the steep rise of current with accelerating field in a diode with an oxide-coated cathode cannot be fully explained either by surface roughness or by patch effect. This leads to a theoretical treatment, based on the existence of a space-charge zone immediately inside the coating. The charge in this zone is shown to vary with applied field and with current density, and with certain coating parameters. The variation in the charge leads to a variation in work function, and thereby to a dependence of emission on field strength, which is to be combined with the normal Schottky effect. The effects of partial space charge on the relationship between field and anode voltage are discussed, and the diode characteristics of oxide cathodes can then be calculated for accelerating fields as a function of the coating parameters. The results are shown to be in agreement with experiment, and to confirm values of coating conductivity, electron density and mobility as determined directly by conductivity and Hall effect measurements.

The Effect of Mercury on Selenium, by H. K. Henisch and E. W. Saker.

ABSTRACT. It is shown that the interaction between crystalline selenium and liquid mercury or mercury vapour results in the formation of mercuric selenide. When produced in this form, this material is an excess semiconductor of high conductivity. The associated volume and surface diffusion have been investigated using radioactive ^{203}Hg. Mercury added to selenium *before* the crystallization process results in material of high resistivity. This is ascribed to a reduction of the positive hole mobility.

Impurity Scattering in Oxide Semiconductors, by E. W. J. Mitchell.

ABSTRACT. The oxide semiconductors are characterized by relatively high concentrations of impurity centres and low electron mobility. It is suggested that electron scattering by neutral impurity centres makes an important contribution to the resistivity of these materials. The familiar relation $\log \sigma_0 = \alpha + \beta\epsilon$ together with the theory given by Busch are discussed and an alternative explanation involving impurity scattering and a dependence of ϵ on N is given. This is compared with experimental results for several oxides, including measurements by the author on the $Fe_2(Ti)O_3$ system.